VOLUME 92, NO. [illegible]

APRIL 1966

PART I

JOURNAL OF THE

Engineering Mechanics Division

PROCEEDINGS OF THE

AMERICAN SOCIETY

OF CIVIL ENGINEERS

BASIC REQUIREMENTS FOR MANUSCRIPTS

Original papers and discussions of previously published papers should be submitted to the Manager of Technical Publications, ASCE. Authors should indicate the technical division to which the paper is referred. The final date on which a discussion should reach the Society is given as a footnote with each paper. Those who are planning to submit material will expedite the review and publication procedures by complying with the following basic requirements:

1. Titles must have a length not exceeding 50 characters and spaces.

2. A summary of approximately 50 words must accompany the paper, a 300-word abstract must precede it, and a set of conclusions must end it.

3. The manuscript (an original ribbon copy and two duplicate copies) should be double-spaced on one side of 8½-inch by 11-inch paper. Three copies of all illustrations, tables, etc., must be included.

4. The author's full name, Society membership grade, and footnote reference giving present employment must appear on the first page of the paper.

5. Math matter are recomposed from the copy that is submitted. Because of this, it is necessary that letters be drawn carefully, and that special symbols be properly identified. The letter symbols used should be defined where they first appear, in the illustrations or in the text, and arranged alphabetically, in an Appendix.

6. Tables should be typed (an original ribbon copy and two duplicate copies) on one side of 8½-inch by 11-inch paper. Specific illustrations and explanation must be made in the text for each table.

7. Illustrations must be drawn in black ink on one side of 8½-inch by 11-inch paper. Because illustrations will be reproduced with a width of between 3 inches and 4½ inches, the lettering must be large enough to be legible at this width. Photographs should be submitted as glossy prints. Explanations and descriptions must be made within the text for each illustration.

8. The desirable average length of a paper is about 12,000 words and the absolute maximum is 18,000 words. As an approximation, each full page of typed text, table, or illustration is the equivalent of 600 words.

9. Technical papers intended for publication must be written in the third person.

10. The author should distinguish between a list of "Reading References" and a "Bibliography," which would encompass the subject of his paper.

Reprints from this Journal may be made on condition that the full title of the paper, name of author, page reference, and date of publication by the Society are given. The Society is not responsible for any statement made or opinion expressed in its publications.

This Journal is published bi-monthly by the American Society of Civil Engineers. Publication office is at 2500 South State Street, Ann Arbor, Michigan. Editorial and General Offices are at 33 West 39 Street, New York 18, New York. $4.00 of annual dues are applied as a subscription to this Journal. Second-class postage paid at Ann Arbor, Michigan.

The index for 1959 was published as ASCE Publication 1960-10 (list price $3.00); indexes for previous years are also available.

PRINTED IN U.S.A.

Journal of the

ENGINEERING MECHANICS DIVISION

Proceedings of the American Society of Civil Engineers

ENGINEERING MECHANICS DIVISION
EXECUTIVE COMMITTEE
Egor P. Popov, Chairman; Bruce G. Johnston, Vice Chairman;
John W. Clark; Merit P. White; Edward Wenk, Jr., Secretary
Elmer K. Timby, Board Contact Member

COMMITTEE ON PUBLICATIONS
Bruce G. Johnston, Chairman; Hans H. Bleich; Jack E. Cermak;
Donald L. Dean; John E. Goldberg; William J. Hall; John D. Haltiwanger;
Herbert S. Suer; Joseph F. Throop

CONTENTS

April, 1961

Papers

Page

Response of Multi-Story Structures to Earthquake
by Glen V. Berg 1

Two-Dimensional Flow with Corner Eddies
by Aris C. Spengos 17

Brittle Fractures Explained by Negative Residuals
by L. E. Grinter 25

Bending of Beams Resting on Isotropic Elastic Solid
by Aleksandar B. Vesić 35

Continuous Beam-Columns on Elastic Foundation
by S. L. Lee, T. M. Wang, and J. S. Kao 55

(over)

Copyright 1961 by the American Society of Civil Engineers.

Note.--Part 2 of this Journal is the 1961-14 Newsletter of the Engineering Mechanics Division.

DISCUSSION

Page

Analysis of Frames with Non-Linear Behavior, by Alfredo H.-S. Ang. (June, 1960. Prior discussion: December, 1960. Discussion closed.)
by Alfredo H.-S. Ang (closure) 73

Wind Stresses in Domes, by P. Gondikas and M. G. Salvadori. (October, 1960. Prior discussion: None. Discussion closed.)
by Gerrit H. Toebes 75

Bearing Capacity of Floating Ice Sheets, by G. G. Meyerhof. (October, 1960. Prior discussion: February, 1961. Discussion closed.)
by L. W. Gold 83
by R. H. Wood 86
by N. C. Lind and D. T. Wright 87

Elasto-Plastic Analysis by Numerical Procedures, by Annabel L. Tong. (December, 1960. Prior discussion: None. Discussion closed.)
by Daniel Frederick 89

Journal of the
ENGINEERING MECHANICS DIVISION
Proceedings of the American Society of Civil Engineers

RESPONSE OF MULTI-STORY STRUCTURES TO EARTHQUAKE

By Glen V. Berg,[1] F. ASCE

SYNOPSIS

The behavior of multi-story buildings responding to strong earthquake ground motion has been computed by a high-speed digital computer. Response curves and tables are presented, and the effects of certain structural parameters on the response are studied.

INTRODUCTION

A multi-story building in vibration is an extremely complicated dynamic system. It has infinitely many degrees of freedom and is far from linear. Many of its components are erratic in their behavior, even in carefully controlled laboratory specimens. Finding precisely the motion of such a system except by actual measurement is beyond accomplishment. The system can be simplified by means of reasonable approximations to reduce it to a solvable mathematical model. However, in doing this, bear in mind that the solution, no matter how precise it may be mathematically, is only the response of a model.

In an earthquake, the ground shakes irregularly and sometimes violently in all directions. This induces structural response in six components of motion, three translational and three rotational.[2] This study is limited to a single

Note.—Discussion open until September 1, 1961. To extend the closing date one month, a written request must be filed with the Executive Secretary, ASCE. This paper is part of the copyrighted Journal of the Engineering Mechanics Division, Proceedings of the American Society of Civil Engineers, Vol. 87, No. EM 2, April, 1961.

[1] Assoc. Prof. of Civ. Engrg., Univ. of Michigan, Ann Arbor, Mich.

[2] "Methods for Calculating the Earthquake Response of Shear Buildings," by Robert S. Ayre, Proceedings, First World Conf. on Earthquake Engrg., Berkeley, Calif., June, 1956.

translational component of ground motion and a single translational component of structural response. A single translational component of ground motion may induce all six components of structural motion. Even if rocking of the structure is prevented or ignored, rotation about a vertical axis will occur unless the structure is dynamically symmetric about a plane parallel to the ground motion or about two perpendicular planes. If the structure has a plane of symmetry parallel to the direction of ground motion, and if rocking is prevented, the response will have a single translational component. This is the case considered herein.

The mass of an actual structure is distributed over the entire structure. In most cases, the actual system can be approximated reasonably well by assuming that its entire mass is concentrated at several discrete points. Thus a lumped mass system is obtained. If the system consists of n point masses, it has 3 n degrees of freedom in a general motion, and n degrees of freedom in the one-directional translation considered herein. A multi-story building does in fact have most of its mass situated at the floor levels. It can be considered a lumped mass system, taking the mass of each floor and half the mass of the walls and columns in the stories immediately above and below as a point mass located at floor level. The error introduced in this approximation can be expected to be small in the lower modes of vibration,[3] which are the modes of primary importance in structural response to earthquake.

METHOD OF SOLUTION

Three components of resistance to motion were considered, namely, flexural resistance of the frame, shear resistance of the walls, and viscous damping resistance. It was assumed that the joints of the rectangular building frame were rigid, that is, there could be no relative rotation between the ends of the members at a joint. In reality, this assumption is not strictly true except perhaps in a frame in which each member at a joint is welded to develop the full moment capacity of the member. It was further assumed that all members in the frame, columns, and girders alike, had ideal elastic-plastic moment-rotation characteristics.

A process for solving the differential equations of motion for such a structure by high-speed digital computer has been presented in detail elsewhere.[4]

The walls in a multi-story building may have a sizable influence on the response of the building to an earthquake. However, the exact behavior of walls is difficult to evaluate. In experimental work on determining the periods of vibration of the fifteen-story Alexander Building in San Francisco, Calif., John A. Blume, F. ASCE, found that the tile partitions offered little or no contribution to the rigidity of the building at small amplitudes of vibration.[5,6] The brickwork participated in the rigidity, but not to the extent that its modulus of

---

3 "On the Fundamental Frequencies of Vibration of Rigid Frames," by E. F. Masur, Proceedings, First Midwestern Conf. on Solid Mechanics, Urbana, Ill., April, 1953.

4 "Dynamic Analysis of Elasto-Plastic Structures," by G. V. Berg and D. A. DaDeppo, Proceedings, ASCE, Vol. 86, No. EM 2, April, 1960.

5 "Period Determinations and Other Earthquake Studies of a Fifteen-Story Building," by John A. Blume, Proceedings, First World Conf. on Earthquake Engrg., Berkeley, Calif., June, 1956.

6 "Structural Dynamics in Earthquake-Resistant Design," by John A. Blume, Proceedings, ASCE, Vol. 84, No. ST 4, July, 1958.

elasticity would imply. A greater participation might be expected at the greater amplitudes which would be experienced in a strong motion earthquake.

G. W. Housner, M. ASCE, has pointed out that a large share of the effect of masonry walls on large amplitude vibrations is because of the energy dissipated by the masonry units cracking and grinding together.[7] Even plaster partitions may be able to dissipate appreciable amounts of energy.

Experiments conducted at Stanford University on brick and concrete shear walls[8] suggest that the load-deflection characteristics of such walls can be reasonably described by a tri-linear elastic-semielastic-plastic curve. Tests involving strain reversal in masonry shear walls have not been reported, to the writer's knowledge. For reasons of mathematical convenience, an elastic-plastic type load-deflection curve, with hysteresis on reversal of strain, was used to represent the overall behavior of a shear wall. This is admittedly a rough approximation. No claim is made that masonry has elastic-plastic properties in shear.

The evaluation of the shear resistance of the walls was accomplished by an incremental technique similar to that used for the elastic-plastic frame. Because of the absence of carry-over from one story to the next, the details of applying the technique were much simpler for shear walls.

STRUCTURES ANALYZED

Response computations were made for buildings of two different heights, and for two different earthquake components. The buildings chosen for the computations represent steel framed structures proportioned for the lateral wind loads specified in typical United States building codes. Framing diagrams are shown in Figs. 1 and 2. The frames were not designed for seismic forces, and they are more flexible than might be expected of seismically designed buildings of comparable size.

For the four-story building, computations were made using four different mathematical models to represent the structure. The first of these was an undamped elastic system in which the resistance was taken as that due to the elastic frame alone, with no allowance for damping forces, inelastic frame deformation, or the resistance of walls and partitions. Second was a damped elastic model in which a resistance due to inter-floor viscous damping was added to the elastic resistance. In the third model, the system was taken as the undamped elastic resistance of the bare frame, plus an elastic-plastic type component of resistance due to shear walls. For the fourth model, the system was taken as an elastic-plastic bare frame, without shear walls or viscous damping. For each of these systems, the elastic resistance of the bare frame was the dominant resistance component, and in the last three cases it was modified by one additional component. For the eight-story building, the analyses were limited to the elastic undamped case and the elastic frame with interfloor viscous damping.

The mathematical models used for the response computations were based on frames one bay wide, equivalent to the three-bay frames in the sense that the total flexural stiffness and ultimate flexural strength of all the columns in

---

[7] "Behavior of Structures During Earthquakes," by G. W. Housner, Proceedings, Vol. 85, No. EM 4, October, 1959.

[8] "Behavior of Reinforced Concrete Shear Walls," by J. R. Benjamin and H. A. Williams, Transactions, ASCE, Vol. 124, 1959, pp. 669-708.

each story were the same in the equivalent frame as in the original frame. The same equivalence applied to the beams in each floor. The reason for this substitution was that in the elastic-plastic case, computing the moments and hinge rotations for the original three-bay frames would have required more storage space for matrix elements and computed results than was available in the 2,000-word memory of the computer. Even though the original three-bay frames could have been used for all cases except the elastic-plastic case, the equivalent frames were used for all analyses in order to avoid introducing unwanted differences which might have invalidated comparison of the results for the different systems. It turned out that the equivalent frames were slightly stiffer than the original frames, the difference being of the order of 1%.

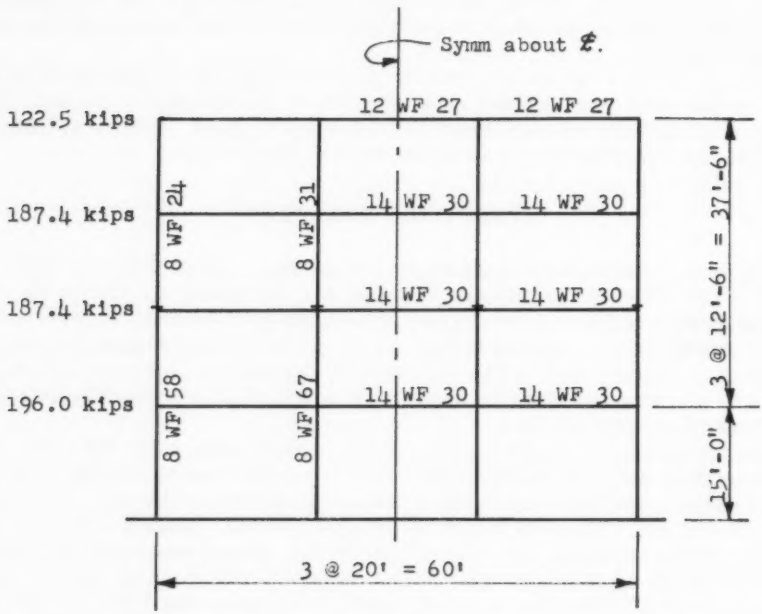

FIG. 1.—FRAMING DIAGRAM, FOUR-STORY BENT

It should be noted that equivalence in the aforementioned sense does not produce dynamic equivalence (or, for that matter, even static equivalence) in the elastic-plastic case. For example, in an elastic-plastic multi-bay frame it would be possible (indeed, almost certain) that at some stage of the response, part of the columns in a story would be in the elastic range while other columns in the same story contained plastic hinges. In the single bay frame, under the assumptions used herein, plastic hinges occur simultaneously in symmetric pairs, and all columns in a story reach plasticity at the same time.

It was assumed for the viscous damped models that interfloor viscous damping forces of a magnitude of 3 kip sec/in. were effective in each story. This type of damping is shown symbolically in Fig. 3.

For the four-story building with shear walls, the same elastic-plastic type resistance function was used for the shear walls in each story. The shear stiffness in each story was taken as 30 kips per in. and the ultimate shear strength in each story was taken as 20 kips. The shear wall stiffness was pur-

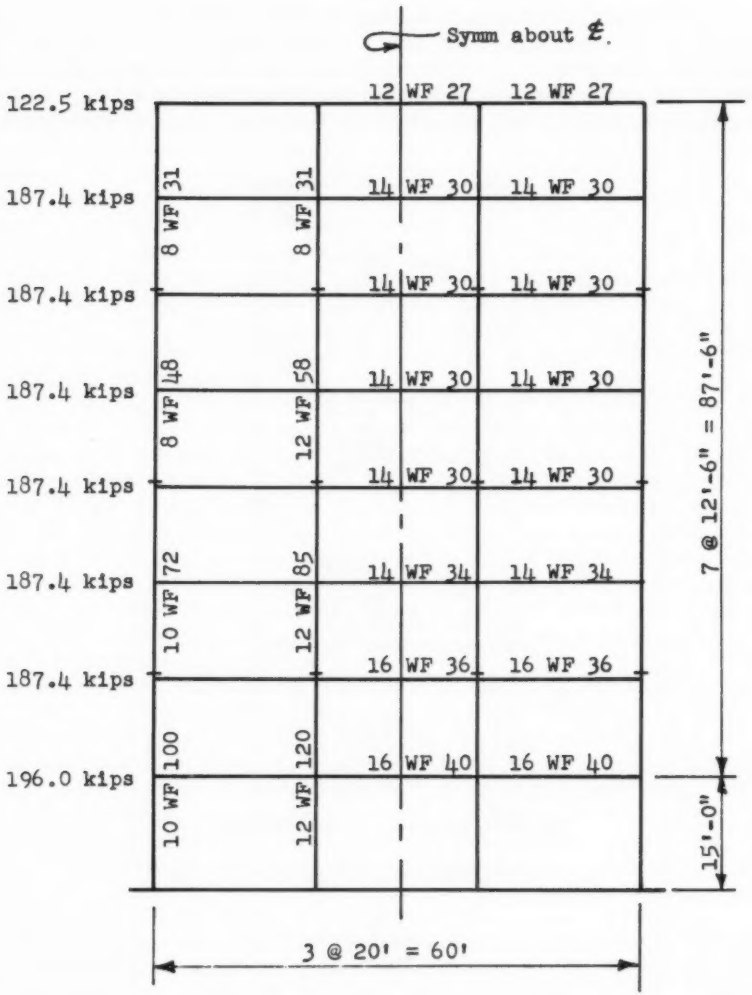

FIG. 2.—FRAMING DIAGRAM, EIGHT-STORY BENT

posely taken to be less than the stiffness of the elastic frame, and the shear wall strength was taken to be quite low. This was done to obtain an idea of how the response is affected by adding a small amount of shear wall resistance to

the structure. Had the shear walls been assumed to be very stiff and strong, shear wall component of resistance would have dominated the response.

GROUND MOTION

Two earthquake accelerograms were used in the analyses; namely, the E-W component of the earthquake recorded in Helena, Mont., on October 31, 1935, and the N-S component of the earthquake recorded at El Centro, Calif., on May 18, 1940. The accelerograms were assumed to be true records of the actual ground accelerations. It was found that the recorded accelerograms could be

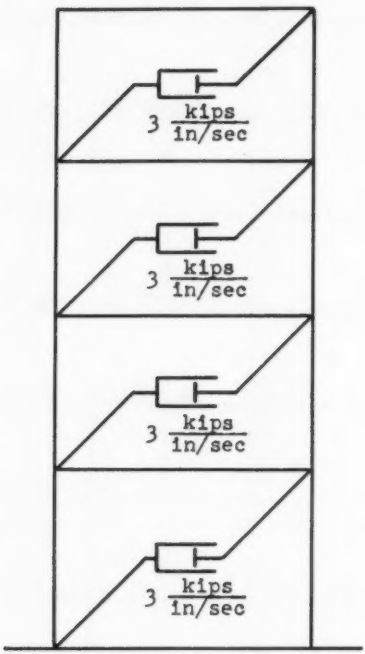

FIG. 3.—INTERFLOOR VISCOUS DAMPING

approximated quite closely by piecewise linear functions, which are also convenient for use in the computer. The time-acceleration coordinates of the intersection points of successive line segments were put in punched card form for machine input data. Fig. 4 shows an enlarged portion of an accelerogram record and a plot of the same portion of the punched card accelerogram.

There is no zero axis on the accelerogram record and the true axis cannot be located with certainty. For these studies the axis was selected parallel to the horizontal baseline appearing on the record and located such that if zero initial velocity were assumed, the computed ground velocity at the end of the punched card accelerogram would also be zero. Subsequent investigations of

computed ground displacements have led to better methods of locating the axis.[9] Differences are slight, however, being of the order of 0.003 g. While the effect of such differences on computed ground motion may be substantial, their effect on structural response is negligible.

COMPUTED RESULTS

The response of the four-story undamped elastic system to the Helena ground motion is shown in Fig. 5. After the first 2.5 sec, the response tends to be nearly periodic, with a period of 2.0 sec. The natural period for the fundamental mode of this system is in fact 2.01 sec. The irregularities in the deflection curves are evidence of vibration in the higher modes.

The response of the four-story viscous damped system to the Helena ground motion is shown in Fig. 6. As might be expected, there is a marked difference between this and the undamped system. Here the deflections build up to a peak at about 2.9 sec, which is about the end of the most severe portion of the ground shock. Thereafter, the structure oscillates with a period of about 2 sec, and with steadily decreasing amplitudes. The irregularities in the deflection curves are not as pronounced here, indicating that the higher modes of vibration are damped out rapidly.

Since the viscous damped system can be solved by the method of normal modes, it is of interest to evaluate the first mode of response and compare it with the total response obtained by direct numerical integration. The fraction of critical damping is 0.148 in this mode. The first mode response is shown in Fig. 7. It compares favorably with the total response shown in Fig. 6. However, the comparison cannot be expected to be this good in all cases.

Fig. 8 shows a plot of the response to the Helena quake for the four-story undamped structure with shear walls added. The shear walls act as conservative elements when they are in the elastic range, and become dissipative elements when the elastic range is exceeded. One effect of the shear walls appears as a shortening of the period of vibration of the structure. After the structure reaches its extreme amplitude, it oscillates with a period of 1.45 sec, or about three quarters of what the period was when the shear walls were not present. The fundamental period of the system is 1.45 sec when the shear walls are in the elastic range. The effect of the dissipative forces due to shear walls appears as a decay in the amplitude of oscillation with time. However, the amplitude does not approach zero as it did in the case of the viscous damped system, but rather diminishes to the point where the oscillations have an amplitude sufficiently small to permit the shear walls to remain in the elastic range and, thereafter, the system behaves as an undamped system. The dissipative forces do not tend to damp out the higher modes of vibration.

No response is given for the elastic-plastic frame to the Helena ground motion, because the ground motion was not severe enough to induce plasticity in the structure.

Fig. 9 shows the deflection-time curves for the four-story undamped elastic structure responding to the El Centro ground motion. The El Centro earthquake was considerably more intense and of longer duration than the Helena earthquake. Only the first 10 sec of response is shown in Fig. 9. The characteristics of the response are much the same as appeared in Fig. 5 for the

[9] "Integrated Velocity and Displacement of Strong Earthquake Ground Motion," by G. V. Berg and G. W. Housner, Bulletin, Seismological Soc. of America (to be published).

same system and the Helena ground motion. The amplitude of oscillation increases steadily during the time shown. The computations were actually carried further, and it was found that the maximum amplitude was about 10% greater than that shown in Fig. 9. The response shown here was computed on the assumption that the system would remain elastic regardless of the amplitude of the deflections. This would be the case if the frame members were built of

(a) Original Accelerogram

(b) Plot of Punched Card Data

FIG. 4.—PORTION OF TYPICAL STRONG-MOTION RECORD

steel having an extremely high elastic limit. ASTM-A7 steel has an average yield strength of approximately 42,000 psi under dynamic load conditions, and would be strained well into the inelastic range by the oscillations shown in Fig. 9.

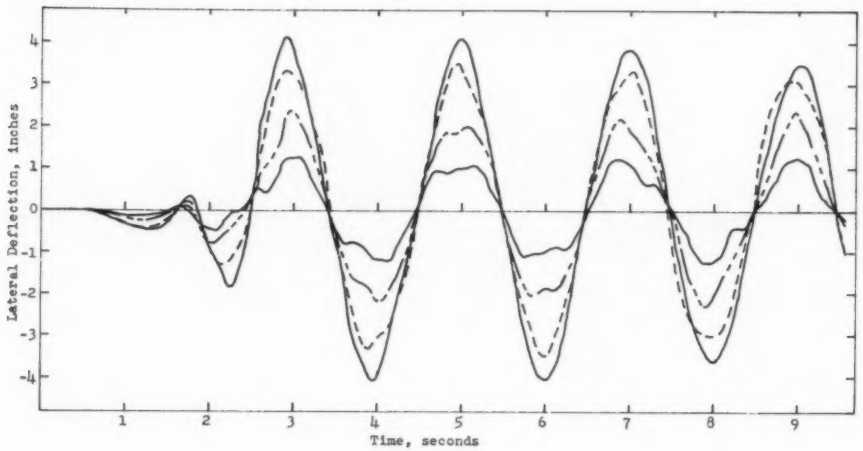

FIG. 5.—RESPONSE OF FOUR-STORY UNDAMPED ELASTIC FRAME, HELENA EARTHQUAKE

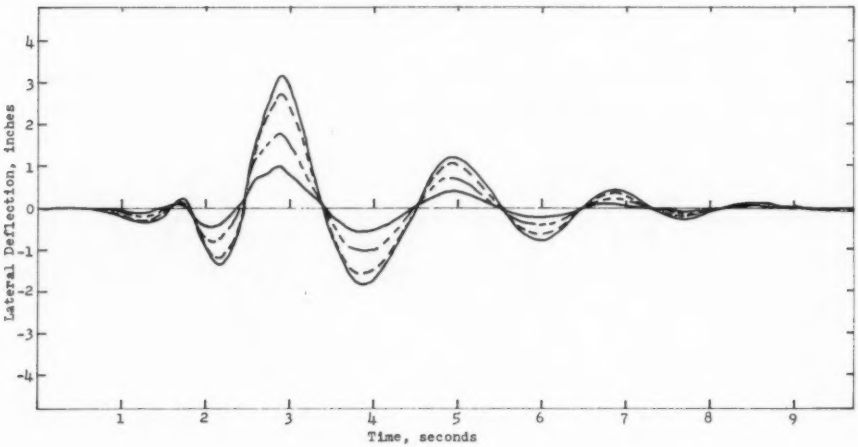

FIG. 6.—RESPONSE OF FOUR-STORY VISCOUS DAMPED FRAME, HELENA EARTHQUAKE

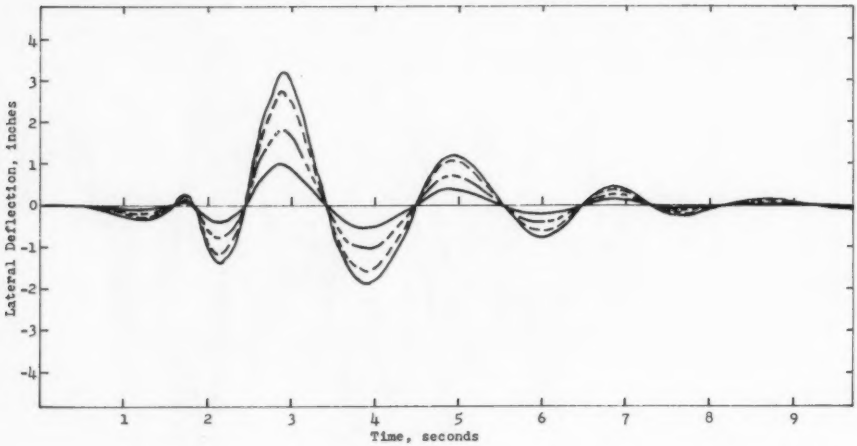

FIG. 7.—FIRST MODE RESPONSE, FOUR-STORY VISCOUS DAMPED FRAME, HELENA EARTHQUAKE

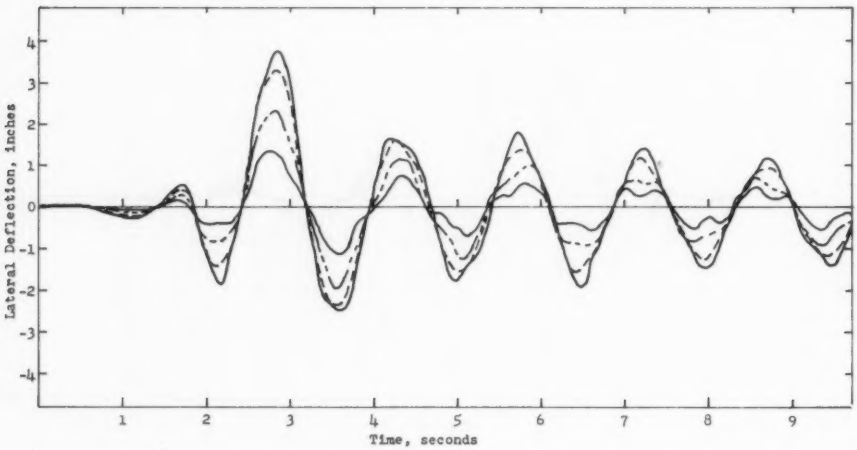

FIG. 8.—RESPONSE OF FOUR-STORY UNDAMPED FRAME WITH SHEAR WALLS, HELENA EARTHQUAKE

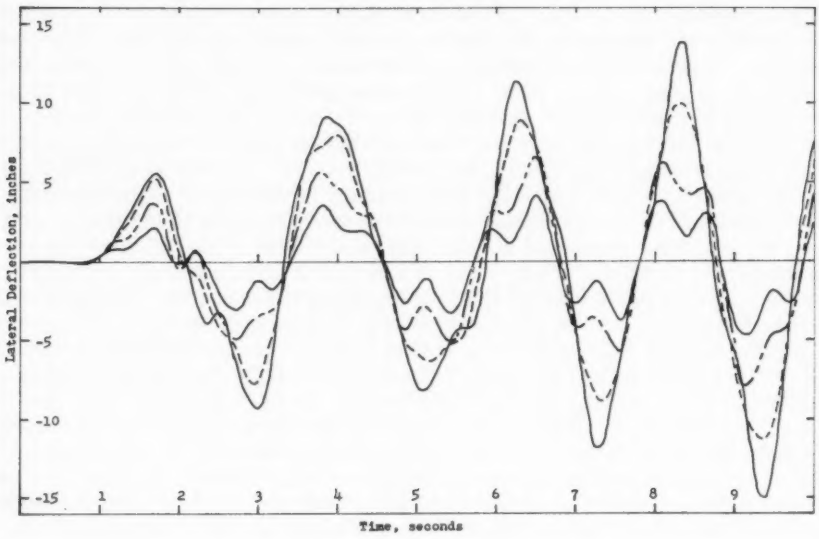

FIG. 9.—RESPONSE OF FOUR-STORY UNDAMPED ELASTIC FRAME, EL CENTRO EARTHQUAKE

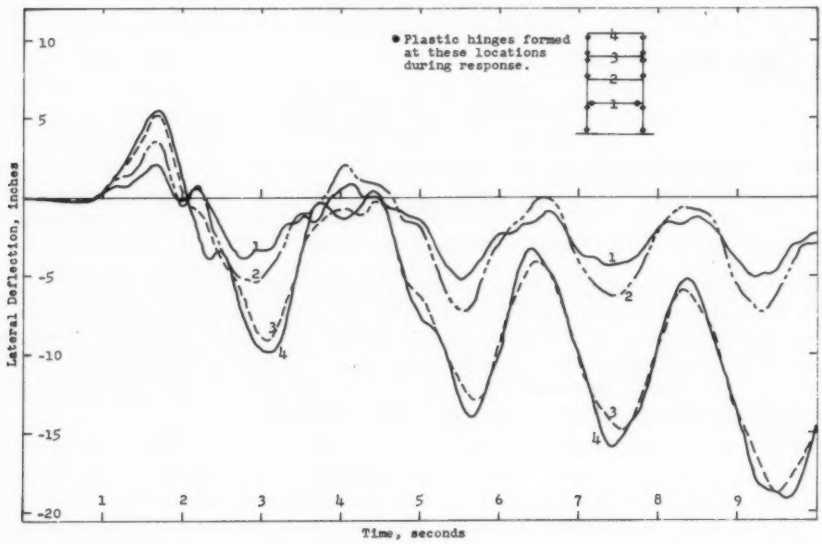

FIG. 10.—RESPONSE OF FOUR-STORY ELASTIC-PLASTIC FRAME, EL CENTRO EARTHQUAKE

For the same framework with elastic-plastic frame members of 42,000 psi yield strength, the response to the El Centro ground motion is plotted as deflection versus time in Fig. 10. At first glance, these curves appear almost unrelated to the curves for the elastic system, except for the first 2.5 sec of response. However, a close inspection reveals a great deal of similarity. The periodicity of the oscillation is nearly the same as for the elastic system. However, in the elastic-plastic system, the oscillation occurs about a position of equilibrium which shifts away from the zero position and keeps changing as inelastic deformation progresses. Moreover, the shift in equilibrium position is not the same for all floors. Also, the amplitude of oscillation about this shifting equilibrium position remains nearly constant, whereas in the elastic system, the amplitude increased steadily during the first 10 sec of the response. Although the total deflections, measured from the zero position, are greater for the elastic-plastic system than for the elastic system, the amplitudes of the oscillation are only about half the elastic amplitudes. Here, as in the earlier case where shear walls were considered, the system behaves as a conservative system during the part of its response when the system is elastic, and behaves as a dissipative system when plasticity is present. The occurrence of plasticity induces a decrease in stiffness of the structure, which amounts for the increase in maximum deflection measured from the zero position. Plastic deformation also dissipates energy that would otherwise be stored in the structure as recoverable strain energy, and thus acts to reduce the amplitude of oscillation. The locations at which plastic hinges formed during the response are shown in Fig. 10.

The maximum values obtained for various parameters in the analyses are summarized in Table 1. The important parameters are the maximum deflections at each floor; the shear coefficient for each story S_i;

$$S_i = \frac{\text{Maximum shear in } i^{th} \text{ story}}{\text{Weight of structure}} \quad \ldots\ldots\ldots\ldots\ldots\ldots (1)$$

the shear distribution D_i;

$$D_i = \frac{\text{Maximum shear in } i^{th} \text{ story}}{\text{Maximum shear in first story}} \quad \ldots\ldots\ldots\ldots\ldots\ldots (2)$$

and the seismic coefficient for each story C_i.

$$C_i = \frac{\text{Maximum shear in } i^{th} \text{ story}}{\text{Weight of structure above } i^{th} \text{ story}} \quad \ldots\ldots\ldots\ldots (3)$$

These parameters are shown in Table 1(a) for the Helena ground motion for the four-story building. Table 1(b) shows the same parameters for the four-story building and the El Centro ground motion, and Table 1(c) shows the parameters for the eight-story building and the Helena ground motion. For comparison, the design parameters computed in accordance with the Los Angles and San Francisco building codes are also tabulated.

CONCLUSIONS

In the analyses reported in this paper, the displacement response of a damped linear system is approximated reasonably well by the response of the first mode alone. For each of the analyses, the maximum displacement in the first

mode differs from the total maximum displacement by about 10% at most. For the same system, the deviation is greater for the more intense earthquake. However, there is no reason to believe that this would be true in general. For the same earthquake, the deviation is greater for the taller structure. The modes beyond the first would be expected to be more important for a taller structure, simply because there are more of them.

In terms of seismic coefficients, which are the parameters of the first significance, the first mode approximation is less attractive, especially in the upper stories. For the four-story structure, the deviation of the first mode response from the total response in terms of seismic coefficients is 11% at most. For the eight-story structure, the deviation ranges from practically zero in the bottom three stories to 44% in the top story.

Any form of energy dissipation in the system tends to reduce the amplitude of oscillation below that which would prevail if the dissipative forces were not there. This is true even for the case in which the energy dissipation occurs through the deformation of plastic hinges in the structural member. The frame becomes less stiff when the plastic hinges are present, but the plastic deformation still results in a decreased amplitude of oscillation. The decrease in amplitude is accompanied by a decrease in the shears and seismic coefficients, as can be seen clearly from Table 1(b). The results here partially substantiate a thesis proposed by Housner for limit design of structures.[7] In brief, Housner's thesis is that if a structure can be built in such a way that inelastic deformation progresses far enough to dissipate a substantial amount of energy, then the structure can be designed on the basis of lower seismic coefficients than would have to be considered for a comparable elastic structure. This is because the energy dissipation will act to reduce the magnitude of the maximum shears in the structure.

Information now available (1961) is not sufficient to enable the determination of the value of equivalent viscous damping to be assigned to any given structure. More information is needed in this regard. Certainly no one can question the desirability of treating a structural system as a viscous damped system, if that can be accomplished. Damping forces in a building are present in both the structural and non-structural elements, and in many buildings the non-structural elements are apt to be the greater contributors. It would seem that the damping forces in the structure, if they are to be considered as viscous damping forces, might be reasonably well represented by interfloor damping forces, or symbolically by interfloor dashpots.

It is interesting to note that the same system of interfloor damping forces produced 14.8% of critical damping in the first mode of the four-story structure, but only 6.25% of critical damping for the eight-story structure. Since the damping forces are produced in large part by non-structural elements, they might not be significantly different for similar buildings of different heights. If this is so, it can be expected that tall buildings are less effectively damped than short buildings of similar type.

The actual damping forces in a structure are, of course, not truly viscous. For the most part they are attributed to internal friction within the components of the structure. L. S. Jacobsen has shown[10] that a single degree system with non-viscous damping, subjected to a sinusoidal input force, can be treated as a viscous damped system without any appreciable loss in accuracy,

[10] "Steady Forced Vibration as Influenced by Damping," by L. S. Jacobsen, Transactions, ASME, Paper APM-54-15, 1930.

TABLE 1.—MAXIMUM MAGNITUDES OF RESPONSE PARAMETERS

Parameter		Undamped elastic frame	Undamped elastic-plastic frame	Elastic frame and shear walls	Viscous Damped Frame		1959 Los Angeles Code	1958 San Francisco Code
					Total response	First mode[a]		
(a) Helena ground motion, 4-story structure								
Deflection, in inches	x_4	4.13		3.76	3.13	3.11		
	x_3	3.50		3.30	2.70	2.70		
	x_2	2.39		2.32	1.78	1.78		
	x_1	1.28		2.32	.97	.97		
Shear coefficinet	S_4	.032		.019	.014	.013	.024	.018
	S_3	.062		.038	.032	.031	.049	.038
	S_2	.074		.059	.046	.045	.066	.052
	S_1	.073		.074	.053	.053	.080	.060
Shear distribution	D_4	.44		.25	.27	.25	.29	.29
	D_3	.85		.51	.61	.60	.61	.63
	D_2	1.01		.80	.88	.86	.83	.87
	D_1	1.00		1.00	1.00	1.00	1.00	1.00
Seismic coefficient	C_4	.181		.106	.080	.074	.133	.099
	C_3	.139		.084	.072	.070	.109	.085
	C_2	.103		.082	.065	.063	.092	.073
	C_1	.073		.074	.053	.053	.080	.060
(b) First 10 Sec of El Centro ground motion, 4-story structure								
Deflection, in inches	x_4	15.01	19.06	6.35	6.68	6.79		
	x_3	11.26	17.65	5.57	5.88	5.88		
	x_2	7.96	7.25	3.49	4.06	3.85		
	x_1	4.75	5.20	1.86	2.29	2.09		
Shear coefficient	S_4	.133	.071	.037	.029	.029	.024	.018
	S_3	.219	.082	.097	.068	.069	.049	.038
	S_2	.180	.118	.112	.102	.098	.066	.052
	S_1	.268	.127	.109	.127	.113	.080	.060
Shear distribution	D_4	.50	.56	.34	.23	.26	.29	.29
	D_3	.82	.65	.89	.54	.61	.61	.63
	D_2	.67	.93	1.03	.80	.86	.83	.87
	D_1	1.00	1.00	1.00	1.00	1.00	1.00	1.00
Seismic	C_4	.754	.403	.207	.161	.166	.133	.099

coefficient	C_3	.490	.184	.217	.153	.155	.109	.085
	C_2	.251	.164	.156	.142	.136	.092	.073
	C_1	.268	.127	.109	.127	.113	.080	.060
(c) Helena ground motion, 8-story structure								
Deflection, in inches	x_8	7.35			4.78	4.28		
	x_7	6.09			4.36	4.03		
	x_6	5.00			3.47	3.46		
	x_5	4.81			2.74	2.92		
	x_4	4.25			2.06	2.23		
	x_3	3.35			1.44	1.57		
	x_2	2.11			0.88	0.94		
	x_1	1.04			0.40	0.42		
Shear coefficient	S_8	.026			.007	.004	.011	.005
	S_7	.037			.017	.010	.023	.013
	S_6	.055			.023	.015	.032	.019
	S_5	.046			.026	.020	.038	.024
	S_4	.039			.027	.023	.043	.028
	S_3	.057			.026	.026	.046	.032
	S_2	.064			.027	.027	.049	.034
	S_1	.073			.030	.028	.052	.035
Shear distribution	D_8	.36			.24	.15	.22	.15
	D_7	.51			.56	.36	.45	.36
	D_6	.75			.77	.55	.61	.54
	D_5	.63			.88	.71	.73	.69
	D_4	.54			.90	.84	.82	.81
	D_3	.78			.87	.92	.89	.90
	D_2	.88			.90	.98	.94	.96
	D_1	1.00			1.00	1.00	1.00	1.00
Seismic coefficient	C_8	.312			.086	.048	.133	.063
	C_7	.174			.077	.047	.109	.059
	C_6	.158			.067	.045	.092	.055
	C_5	.097			.055	.042	.080	.051
	C_4	.065			.044	.039	.071	.047
	C_3	.078			.035	.035	.063	.043
	C_2	.074			.031	.031	.057	.039
	C_1	.073			.030	.028	.052	.035

[a] Fraction of critical damping = 0.148 for (a) and (b), and 0.0625 for (c).

provided the damping coefficient is chosen so that the energy dissipation in each cycle of oscillation is the same for the viscous damping forces as for the actual damping forces. But in the earthquake problem an additional difficulty appears, for the fraction of critical damping for equal energy dissipation must vary as the amplitude of the motion varies. This is easily demonstrated for the single degree oscillatory system by considering the energy dissipated per cycle of oscillation.[11] The same tendency exhibits itself in the effect of the inelastic deformation of the shear walls. When elastic-plastic shear walls were added to the undamped system, the reduction in maximum response was much more pronounced in the more intense earthquake. If the energy dissipation by the action of the shear walls were to be represented as equivalent viscous damping, a greater fraction of critical damping would need to be assigned for more intense ground motion. This agrees with the results of large amplitude vibration tests reported by T. Hisada and K. Nakagawa,[12] which indicate that the fraction of critical damping as determined experimentally tends to increase with an increase in amplitude.

A good reason for the desirability of reducing a structure to an equivalent viscous damped system is that this puts the structure in a condition to be analyzed by response spectrum techniques.[7] Recent efforts to extend spectrum concepts to non-linear systems show great promise, but are not yet ready for general use on multi-story structures.[13]

The reader is cautioned against drawing too-broad conclusions from the limited studies presented herein. Some of the computed results might be substantially altered if the properties of the structures were changed. In the elastic-plastic case, the single bay frame used in the computations is not dynamically equivalent to the three-bay frame from which it was derived. And in any case, the solution can be no truer than the mathematical model used in it.

The primary function of dynamic analysis in earthquake engineering is to lead to a better understanding of response phenomena, to an improved evaluation of the structural parameters, and to a more complete knowledge of the effects of load parameters and structural parameters on the response. These in turn lead to better design procedures.

ACKNOWLEDGMENTS

The computations for this paper were executed on an IBM 650 computer at the University of Michigan Computing Center. Some of the matrices used in the analyses were evaluated on the computer by D. A. DaDeppo, A. M. ASCE. The studies were taken from the writer's doctoral dissertation.

---

11 "Frictional Effects in Composite Structures Subjected to Earthquake Vibrations," by L. S. Jacobsen, Stanford Univ., March, 1959.

12 "Vibration Tests on Various Types of Building Structures Up to Failure," by T. Hisada and K. Nakagawa, Proceedings, First World Conf. on Earthquake Engrg., Berkeley, Calif., June, 1956.

13 "Effect of Inelastic Behavior on the Response of Simple Systems to Earthquake Motions," by A. S. Veletsos and N. M. Newmark, Proceedings, Second World Conf. on Earthquake Engrg., Tokyo, July, 1960.

Journal of the
ENGINEERING MECHANICS DIVISION
Proceedings of the American Society of Civil Engineers

TWO-DIMENSIONAL FLOW WITH CORNER EDDIES

By Aris C. Spengos,[1] M. ASCE

SYNOPSIS

Flow in a two-dimensional channel with an asymmetrical abrupt contraction is treated. It is assumed that the flow is steady and rotational and the fluid inviscid. The velocity distribution far upstream from the contraction is approximated by a sine curve. The solution of the governing differential system shows the streamline pattern at the region immediately preceding the contraction.

INTRODUCTION

The separation of flow and formation of eddies at the corners immediately preceding an abrupt contraction in a conduit, in which a homogeneous viscous fluid is flowing, can be attributed to the rotationality of the flow far upstream and the subsequent action of viscosity. To demonstrate the effect of upstream rotationality on eddy formation, C. S. Yih[2] obtained the exact solutions of the governing differential equation for the cases (a) of the two-dimensional flow with a line sink symmetrically located with respect to the longitudinal boundary, and (b) of an axis-symmetric flow with a point sink located on the axis of symmetry. In these solutions, viscosity was considered only as far as its effect in producing rotationality of the flow is concerned, and it was neglected in setting up the differential system.

Note.—Discussion open until September 1, 1961. To extend the closing date one month, a written request must be filed with the Executive Secretary, ASCE. This paper is part of the copyrighted Journal of the Engineering Mechanics Division, Proceedings of the American Society of Civil Engineers, Vol. 87, No. EM 2, April, 1961.

[1] Engrg. Research Div., Scott Paper Co., Chester, Pa.

[2] "Two Solutions for Inviscid Rotational Flow with Corner Eddies," by C. S. Yih, Journal of Fluid Mechanics, Vol. 5, Part 1, January, 1959, p. 36.

The differential system, and its solution, for the flow in a two-dimensional conduit with an asymmetric contraction are presented herein. The asymmetric contraction first is approximated by a line sink, and second by a finite slot opening. In both cases the streamline pattern obtained from the solution of the differential system shows the separation zone (corner eddy) at the region immediately preceding the contraction. A comparison of the two solutions indicates that for large contraction ratios, small slot openings compared to channel width, the contraction can be approximated by a sink without changing the flow pattern appreciably.

FLOW INTO AN ASYMMETRIC LINE SINK

The flow under consideration is a steady two-dimensional flow in a long channel of width equal to unity and terminating in a wall with a line sink located asymmetrically at the corner. Such an arrangement approximates that

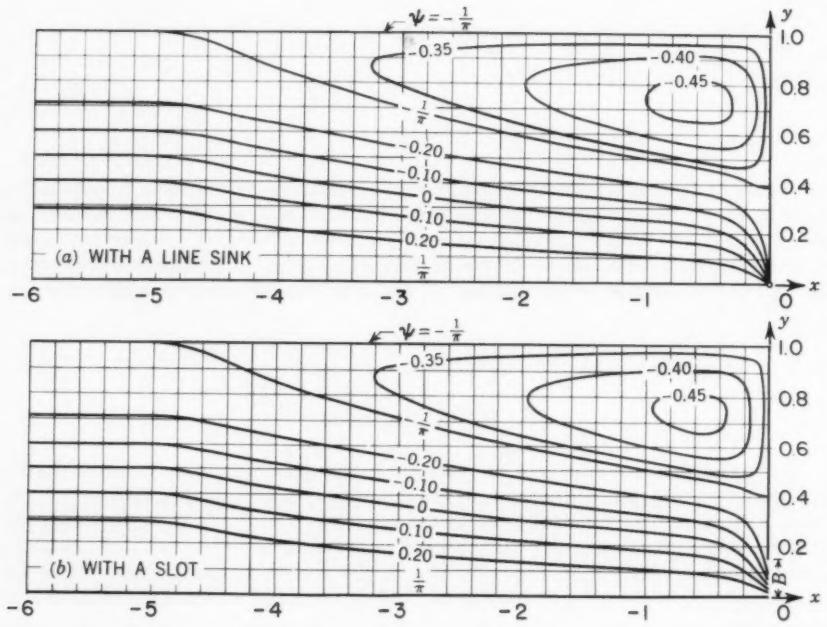

FIG. 1.—CORNER EDDIES

of the flow under a sluice gate, located at the end of a closed conduit, with the gate opening replaced by a line sink. The trace of the line sink is taken as the origin of a Cartesian system of coordinates, with the y-axis extending along the lower boundary of the conduit (Fig. 1).

Making the same assumptions as those mentioned previously, that is, rotational flow of an inviscid fluid, and if ψ is Lagrange's stream function, the

equation[3] governing the steady two-dimensional flow is

$$\nabla^2 \psi = \frac{\partial^2 \psi}{\partial x^2} + \frac{\partial^2 \psi}{\partial y^2} = f(\psi) \quad \ldots\ldots\ldots\ldots\ldots (1)$$

Eq. 1 shows that the z-component of the vorticity along a streamline is constant and is therefore a function of ψ only.

If the flow of a viscous fluid is considered, the velocity distribution far upstream from the sink should be parabolic or that for turbulent flow. But either of these distributions would make Eq. 1 non-linear and, consequently, rather difficult to obtain a simple solution. Instead the velocity distribution far upstream is approximated by a sine distribution which is nearly parabolic. This approximation makes Eq. 1 linear. Such an assumption can be tolerated since the effect of non-uniformity of the upstream velocity on the flow pattern in the vicinity of the line sink is sought. If U_{max} is the velocity at the center line of the channel, that is, at half-width, the dimensionless upstream velocity is then

$$u = \frac{U}{U_{max}} = \sin(\pi y) \quad \ldots\ldots\ldots\ldots\ldots (2)$$

which vanishes at y = 0 and y = 1. The corresponding dimensionless stream function upstream is then

$$\psi = \int_0^y -\sin(\pi y)\, dy = \frac{1}{\pi}\cos(\pi y) - \frac{1}{\pi} \quad \ldots\ldots\ldots\ldots (3)$$

The absolute value of ψ is immaterial and, hence, the additive term $-1/\pi$ may be neglected. Substituting Eq. 3 in Eq. 1, for a section far upstream,

$$\nabla^2 \psi = -\pi \cos(\pi y) \quad \ldots\ldots\ldots\ldots\ldots (4)$$

But $\cos(\pi y) = \pi \psi$ from Eq. 3, thus

$$f(\psi) = -\pi^2 \psi \quad \ldots\ldots\ldots\ldots\ldots (5)$$

which is valid not only far upstream but also everywhere downstream, since the vorticity remains constant along a stream line, and viscous forces are neglected. Eq. 1 then becomes

$$\nabla^2 \psi = -\pi^2 \psi \quad \ldots\ldots\ldots\ldots\ldots (6)$$

and is valid for the whole field of flow, far upstream as well as near the line sink.

If ψ is dimensionless, and L is the length of the channel, the boundary conditions for ψ are

(i)	$\psi \to -\frac{1}{\pi}\cos(\pi y)$	as $x \to -L$	and $0 \le y \le 1$,
(ii)	$\psi = -\frac{1}{\pi}$	for $x \le 0$	and $y = 1$,
(iii)	$\psi = \frac{1}{\pi}$	for $x < 0$	and $y = 0$,
(iv)	$\psi = -\frac{1}{\pi}$	for $x = 0$	and $0 < y \le 1$.

3 "Hydrodynamics," by H. Lamb, Dover Publications, New York, 1945, p. 244.

To take care of the conditions near the line sink assume that

$$\psi = \frac{1}{\pi}\cos(\pi y) + \psi_1 \quad \ldots\ldots\ldots\ldots\ldots\ldots \quad (7)$$

Substitution of Eq. 7 in Eq. 1 yields

$$\nabla^2 \psi_1 = -\pi^2 \psi_1 \quad \ldots\ldots\ldots\ldots\ldots\ldots\ldots \quad (8)$$

and the boundary conditions for ψ_1 are

(i)	$\psi_1 \to 0$	for $x \to -L$	and $0 \le y \le 1$,
(ii)	$\psi_1 = 0$	for $x \le 0$	and $y = 1$,
(iii)	$\psi_1 = 0$	for $x < 0$	and $y = 0$,
(iv)	$\psi_1 = -\frac{1}{\pi} - \frac{1}{\pi}\cos(\pi y)$	for $x = 0$	and $0 < y \le 1$.

The boundary conditions for ψ_1 were obtained by consideration of Eq. 7 and the boundary conditions for ψ.

Solution of Eq. 8 by the method of separation of variables[4] yields

$$\psi_1 = C_1\left(1+\frac{x}{L}\right)\sin(\pi y) + \sum_{n=2}^{\infty} C_n\left[e^{\pi\left(n^2-1\right)^{1/2}x} - e^{-\pi\left(n^2-1\right)^{1/2}(2L+x)}\right]\sin(n\pi y) \quad \ldots \quad (9)$$

and is valid for $0 \ge x \ge -L$. This limitation on the values of x was found necessary in order to obtain a Fourier series type of solution. Eq. 9 satisfies Eq. 8 and the boundary conditions (i), (ii), and (iii) for ψ_1. The coefficients C_1 and C_n are determined from the boundary condition (iv) for ψ_1 in the following manner

$$C_1 = 2\int_0^1 -\frac{1}{\pi}\left[1+\cos(\pi y)\right]\sin(\pi y)\,dy = -\frac{4}{\pi^2} \quad \ldots\ldots\ldots \quad (10)$$

and

$$C_n = 2\int_0^1 -\frac{1}{\pi}\left[1+\cos(\pi y)\right]\left[1-e^{-2\pi L\left(n^2-1\right)^{1/2}}\right]\sin(n\pi y)\,dy$$

$$= \frac{-2}{n\pi^2\left(n^2-1\right)}\left[2n^2+\cos(n\pi)-1\right]\left[1-e^{-2\pi L\left(n^2-1\right)^{1/2}}\right] \quad \ldots\ldots\ldots \quad (11)$$

for $n = 2, 3, 4, \ldots\ldots$

Thus, the stream function ψ defining the flow pattern in a channel of length L is

$$\psi = \frac{1}{\pi}\cos(\pi y) - \frac{4}{\pi^2}\left(1+\frac{x}{L}\right)\sin(\pi y) + \sum_{n=2}^{\infty} C_n\left[e^{\pi\left(n^2-1\right)^{1/2}x} - e^{-\pi\left(n^2-1\right)^{1/2}(2L+x)}\right]\sin(n\pi y) \quad \ldots\ldots \quad (12)$$

---

[4] "Fourier Series and Boundary Valve Problems," by R. V. Churchill, McGraw-Hill Book Co., Inc., New York, 1941.

The flow pattern for an assumed L of 5 is shown in Fig. 1(a), in which the separation of the flow and the formation of the corner eddy are evident. The point of separation is at x =-5, because at this section the velocity has been assumed to have a sine distribution.

FLOW INTO AN ASYMMETRIC FINITE SLOT

The geometry of the flow considered herein is the same as that in the previous case except that the line sink at the origin has been replaced by a two-dimensional finite slot opening of width B.

The velocity far upstream is again assumed to have a sine distribution, while the dimensionless horizontal component of the velocity at the slot, u_h, is assumed to have the cosine distribution

$$u_h = C \cos \frac{\pi y}{2B} \quad \ldots\ldots\ldots\ldots\ldots\ldots \quad (13)$$

and vanishes at y = B, while it has the value C at y = 0. If ψ' is Lagrange's stream function, the value of C is determined with the use of the continuity equation in the following manner

$$\psi'_{y=0} - \psi'_{y=1} = C \int_0^B \cos \frac{\pi y}{2B} dy = \frac{2BC}{\pi} \quad \ldots\ldots\ldots \quad (14)$$

in which the stream function values are taken at x =-L. From the previous section, for a sine distribution of the velocity far upstream, the value of ψ' is

$$\psi' = \frac{1}{\pi} \cos(\pi y) \quad \ldots\ldots\ldots\ldots\ldots\ldots \quad (15)$$

therefore

$$\frac{2}{\pi} = \frac{2BC}{\pi} \quad \ldots\ldots\ldots\ldots\ldots\ldots \quad (16)$$

or

$$C = \frac{1}{B} \quad \ldots\ldots\ldots\ldots\ldots\ldots \quad (17)$$

and

$$u_h = \frac{1}{B} \cos \frac{\pi y}{2B} \quad \ldots\ldots\ldots\ldots\ldots\ldots \quad (18)$$

The boundary conditions for ψ' are

(i) $\psi' \rightarrow \frac{1}{\pi} \cos(\pi y)$ as $x \rightarrow -L$ and $0 \leq y \leq 1$,

(ii) $\psi' = -\frac{1}{\pi}$ for $x \leq 0$ and $y = 1$,

(iii) $\psi' = \frac{1}{\pi}$ for $x < 0$ and $y = 0$,

(iv) $\psi' = -\frac{1}{\pi}$ for $x = 0$ and $B \leq y \leq 1$.

Again, in order to take care of the conditions near the slot opening, assume that

$$\psi' = \frac{1}{\pi} \cos(\pi y) + \psi'_1 \quad \ldots\ldots\ldots\ldots\ldots\ldots \quad (19)$$

and consequently

$$\nabla^2 \psi_1' = -\pi^2 \psi_1' \quad \ldots\ldots\ldots\ldots\ldots\ldots \quad (20)$$

The boundary conditions for ψ_1' in this case are

(i) $\psi_1' \to 0$	as $x \to -L$	and $0 \le y \le 1$,
(ii) $\psi_1' = 0$	for $x \le 0$	and $y = 1$,
(iii) $\psi_1' = 0$	for $x < 0$	and $y = 0$,
(iv) $\psi_1' = -\frac{1}{\pi} - \frac{1}{\pi}\cos(\pi y)$	for $x = 0$	and $B \le y \le 1$.

and for $x = 0$ and $0 \le y \le B$, ψ_1' is obtained from the assumed distribution of the horizontal component of the velocity at the slot and the boundary condition of ψ' at this section. Therefore, this yields

$$\psi_1' = \int_0^y -C \cos\left(\frac{\pi y}{2B}\right) dy + \frac{1}{\pi} - \frac{1}{\pi}\cos(\pi y) \quad \ldots\ldots\ldots \quad (21)$$

The last boundary condition (v) is

$$\psi_1' = -\frac{2}{\pi}\sin\frac{\pi y}{2B} + \frac{1}{\pi} - \frac{1}{\pi}\cos(\pi y)$$

for $x = 0$ and $0 \le y \le B$.

Solution of Eq. 20 by the method of separation of variables[4] yields

$$\psi_1' = C_1'\left(1 + \frac{x}{L}\right)\sin(\pi y) + \sum_{n=2}^{\infty} C_n' \left[e^{\pi\left(n^2-1\right)^{1/2} x} - e^{-\pi\left(n^2-1\right)^{1/2}(2L+x)}\right]\sin(n\pi y) \quad \ldots\ldots \quad (22)$$

which is the same as Eq. 9 and satisfies Eq. 20 and the preceding boundary conditions for ψ_1'.

The coefficients C_1' and C_n' are determined from the boundary conditions (iv) and (v) for ψ_1' in the following manner

$$C_1' = 2\int_B^1 -\frac{1}{\pi}\left[1+\cos(\pi y)\right]\sin(\pi y)\, dy + 2\int_0^B -\frac{1}{\pi}\left[2\sin\frac{\pi y}{2B} - 1 + \cos(\pi y)\right]\sin(\pi y)\, dy \quad \ldots\ldots\ldots\ldots \quad (23a)$$

$$C_1' = -\frac{4\cos(\pi B)}{\pi^2\left(1-4B^2\right)} \quad \ldots\ldots\ldots\ldots\ldots\ldots \quad (23b)$$

and

$$C_n' = 2\int_B^1 -\frac{1}{\pi}\left[1+\cos(\pi y)\right]\left[1-e^{-2\pi L\left(n^2-1\right)^{1/2}}\right]\sin(n\pi y)\, dy + 2\int_0^B -\frac{1}{\pi}\left[2\sin\frac{\pi y}{2B} - 1 + \cos(\pi y)\right]\left[1-e^{-2\pi L\left(n^2-1\right)^{1/2}}\right]\sin(n\pi y)\, dy \quad \ldots \quad (24a)$$

$$C'_n = \left[\frac{2+2\cos(n\pi)}{n\pi^2(n^2-1)} - \frac{4\cos(n\pi B)}{n\pi^2(1-4B^2n^2)}\right]\left[1-e^{-2\pi L(n^2-1)^{1/2}}\right] \quad \ldots\ldots (24b)$$

for n = 2, 3, 4, ...

Thus, the stream function ψ' defining the flow pattern in a channel with a slot opening of width B is

$$\psi' = \frac{1}{\pi}\cos(\pi y) - \frac{4\cos(\pi B)}{\pi^2(1-4B^2)}\left(1+\frac{x}{L}\right)\sin(\pi y)$$
$$+ \sum_{n=2}^{\infty} C'_n \left[e^{\pi(n^2-1)^{1/2}x} - e^{-\pi(n^2-1)^{1/2}(2L+x)}\right]\sin(n\pi y) \quad \ldots\ldots (25)$$

The flow pattern for an assumed L of 5 and B = 0.15 is shown in Fig. 1(b), in which the corner eddy is again evident.

CONCLUSIONS

The analyses presented clearly indicate that the formation of corner eddies immediately preceding an abrupt contraction can be attributed to the rotationality of the flow. The theory of irrotational flow[5] does not predict the existence of corner eddies for flows with similar contractions.

A comparison of the two flow patterns in Fig. 1, indicates that for B = 0.15, or B → 0, there is small difference in the size of the corner eddies. Therefore, the use of a line sink is justified for approximating contractions, or discharge openings, of width small compared to the channel width. For large discharge openings it is expected that the corner eddy will be smaller.

The asymmetric location of the line sink, or slot opening, made it necessary to specify a finite value of x at which the velocity has the assumed distribution, if a simple Fourier series type of solution is desirable. Similar limitations are necessary in the solution of some problems of mathematical physics. This limitation, however, was not necessary in the cases considered by Yih[2] because the sink was symmetrically located with respect to the flow.

The solution of the basic differential equation, Eq. 1, for actual velocity distributions, that is, when Eq. 1 is non-linear, can be accomplished with the use of computing machines, or by the method of relaxation. It should be kept in mind that solutions of Eq. 1 do not represent the flow pattern[6] inside the eddies, because this flow does not originate far upstream. Consequently, these solutions are likely to be valid only for the regions outside the corner eddies and for flows of viscous fluids at high Reynolds numbers. These limitations

---

5 "Theoretical Hydrodynamics," by L. M. Milne-Thomson, The Macmillan Co., New York, 1957, p. 268.

6 "On Steady Laminar Flow with Closed Streamlines at Large Reynolds Number," by G. K. Batchelor, Journal of Fluid Mechanics, Vol. 1, 1956, p. 117.

on the solutions are imposed because viscous effects have been taken into account only partially, that is, in producing rotationality of the flow only.

ACKNOWLEDGMENT

The writer expresses his sincere appreciation and indebtedness to C. S. Yih, of the University of Michigan, for his numerous suggestions in carrying out the analyses presented in this note.

Journal of the
ENGINEERING MECHANICS DIVISION
Proceedings of the American Society of Civil Engineers

BRITTLE FRACTURES EXPLAINED BY NEGATIVE RESIDUALS

By L. E. Grinter,[1] F. ASCE

SYNOPSIS

The hypothesis presented is that residual lateral compressive stresses may suppress ductility across a notch and permit cleavage fracture to occur. A theoretical explanation is given. Tests made at Brown University on precompressed notched plates tested in tension (and on comparable cylinders) are used to check this principle. They provide substantiation within the range of specimen geometry used.

INTRODUCTION

Ultimate load design of structural steel has developed sufficient acceptance to make a lack of understanding of brittle fracture a factor of critical importance. Any clarification of the subject, particularly by use of the simple concepts of mechanics used by structural designers, will have a strong influence toward improved design. Hence, the writer has attempted to explain the only static tests of brittle fracture that have been widely circulated and discussed through use of the elementary concepts of stress and strain, both elastic and plastic.

The principle established is that lateral compressive residual stresses, introduced by precompression across a notch, crack or flaw, under load reversal may suppress necessary ductility across the notch and thus permit a cleavage fracture to occur.

Note.—Discussion open until September 1, 1961. To extend the closing date one month, a written request must be filed with the Executive Secretary, ASCE. This paper is part of the copyrighted Journal of the Engineering Mechanics Division, Proceedings of the American Society of Civil Engineers, Vol. 87, No. EM 2, April, 1961.

[1] Dean, Graduate School, Univ. of Florida, Gainesville, Fla.

It will not be necessary to review the acceptance of a simplified stress-strain diagram for structural steel representing perfect elasticity followed by ideal plasticity. Nor will it be useful to review the unquestioned effect of the initiation of plasticity in eliminating residual stresses of either sign when they are aligned with the primary stresses due to the loading. It is not clear that slight plastic flow in the x direction will as readily eliminate residual stresses perpendicular thereto in the y and z directions. However, because this argument is not essential here it will not be emphasized.

MODES OF FRACTURE OF STEEL

Steel will fracture in two distinctly different modes, that is, by shear flow and by tensile cleavage. Shear slip leads to the ductile mode of fracture. However, temperature is also a factor. The 1.0 shear-tension ratio of pure torsion may be compared with the 0.5 shear-tension ratio for uniaxial tension. The former permits a ductile fracture at temperatures far below the brittle fracture temperature range for simple tensile specimens.

As the shear-tension ratio reduces, the temperature at which a cleavage fracture may occur increases until at a zero shear-tension ratio (equal triaxial tensions) only a cleavage fracture is possible. A sufficiently low shear-tension ratio to initiate a brittle fracture may occur at a notch because tension applied across a notch induces lateral tensions along and perpendicular to the notch. Fractures always initiate at a notch or at a notch-like flaw.

PLASTIC FLOW INCREASES TRIAXIAL TENSIONS AT END OF CRACK

A plate may resist tensile loads perpendicular to each other that produce a biaxial stress field. At an internal crack or microscopic flaw a condition similar to that shown in Fig. 1 will then exist. The stresses acting on the microscopic particles A and B located at the end of the crack or flaw must be considered. This problem has been analyzed by elementary elastic concepts on the assumption that the particles A and B must remain of the same thickness.[2] The conclusion reached was that there is an induced tension perpendicular to the plate at its mid-depth at particle A equal to $\mu\,\sigma_{yield}$, that is, the product of Poisson's ratio and the yield stress of the material when the σ_y stress at the exact end of the crack in Fig. 1 approaches the yield stress. No distinction will be made herein between the numerical values of yield stress and elastic limit stress.

For σ_y = 37,000 psi and μ = 0.3, the particle A in Fig. 1 may resist tensile stresses of 37,000 psi in two directions and 11,100 psi in the third perpendicular direction. Such a particle will have its range of possible ductility restricted but not totally suppressed. Tests have shown that a specimen such as Fig. 1 must be subjected to a relatively low temperature before the ductility may be sufficiently reduced to permit the flaw or microscopic crack to extend without evidence of plastic flow.

Close inspection of brittle fractures in large structures confirms the fact that some slight plastic flow had taken place before the brittle fracture occurred. The stress concentration at the end of the crack in the vertical direction in Fig. 1 as n σ_y when n may reach a factor of ten or more. When n σ_y

[2] "How Does Propagation of a Small Crack Take Place in a Thin Plate?," by L. E. Grinter, Welding Journal Research Supplement, 1945, p. 319-s.

reaches σ_{yield} the deformation ϵ_y at the exact end of the crack will grow relatively large. Therefore, because plastic flow takes place without change in volume of the plastic material, particle A must reduce its thickness rather sharply perpendicular to the plate in order to elongate in the vertical or y direction. Particle B does not undergo the plastic strain ϵ_y. Nevertheless, because B is attached to A it must also reduce in thickness while resisting the action of A. Again, as for elastic deformation, it is evident that plastic deformation at the

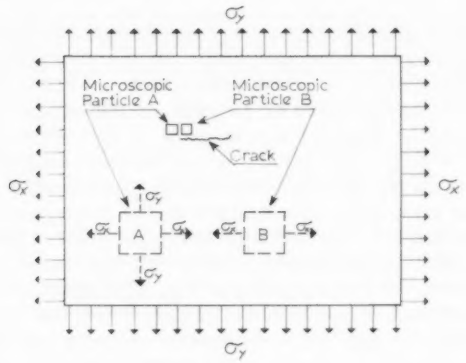

FIG. 1.—TRIAXIALITY OF STRESS AT END OF CRACK IN PLATE ACTING UNDER BIAXIAL LOADING

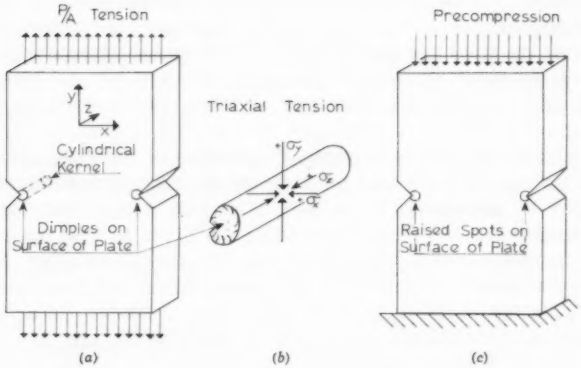

FIG. 2.—DRUCKER-MYLONAS NOTCHED SPECIMEN FOR FRACTURE TESTS

end of the crack will force particle A to develop tension and B compression, perpendicular to the plate. Because plastic deformation is much greater than elastic deformation, it is concluded that the tensile stress developed perpendicularly to the plate at the end of a crack (Fig. 1) should considerably exceed the elastically induced stress of $\mu\,\sigma_{yield}$ or 11,100 psi, as soon as plastic deformation is initiated in the y direction. In fact, the stress perpendicular to

the plate due to the initiation of plastic flow across the crack may conceivably approach σ_{yield}, thus producing nearly equal triaxial tensions. This would help explain the observed suppression of ductility that accompanies a running crack in a large plate-type structure. There are of course dynamic factors also to be considered. These were analyzed by J. M. Frankland.[3]

MECHANICS OF BRITTLE FRACTURE OF NOTCHED PLATE AT YIELD TENSION P/A

The notched plate, Fig. 2(a), is a convenient specimen for testing the typical effects of a stress raiser on the action of a plate under uniaxial loading. Tensile tests of notched plates have repeatedly produced brittle fractures when the nominal P/A stress has reached or slightly exceeded the virgin yield stress of unnotched material. The test specimen of D. C. Drucker, F. ASCE and C. Mylonas[4] shown in Fig. 2(a) usually fractured by such cleavage at -10° F when P/A reached yield tension. The fractured specimen developed a small depressed area or dimple on each surface of the plate surrounding the notch. This surface indication of a cylindrical kernel of plastic material leads to an understanding of the internal mechanism of embrittlement.

Long before the tensile P/A loading in Fig. 2(a) approached the initial yield stress across the throat of the plate between notches, the stress concentration σ_y at the notch had reached the yield stress. Plastic deformation across the notch must occur without change in volume of the plastic material. Hence, in order for the plastic cylindrical kernel of Fig. 2(b) to increase in diameter in the y direction it should reduce in diameter in the x direction. This lateral deformation induces a tension σ_x at the level of the notch resisted by compressive reaction stresses in the x direction above and below the cylindrical kernel. The stress arrows, in Fig. 2(b) indicate action of the notch kernel upon the surrounding material, that is, tensile forces pull inward. However, the appearance of dimples on the surface of the plate shows that the internal area of the plate must be very resistant to flow toward the notch in the x direction and that considerable flow inward along the notch occurs in the z direction.

The complexity of tension and shear variation in and around the cylindrical kernel of Fig. 2(a) is such that only the crudest computations of the internal tensile stress σ_z necessary to produce a surface dimple can be made. However, the assumption that shear flow will take place around the surface of the cylindrical kernel due to tensile force on its central circular cross-section, which is comparable to the initiation of an indentation under the action of a rivet punch, provides the relation $\sigma_z\, d = 2\, \tau\, t$. Here, t is the plate thickness, d is the diameter of the cylindrical kernel or surface dimple, and τ is the unit shear that produces shear flow. For $\tau = 0.5\, \sigma_z = 0.5\, \sigma_{yield}$, as in plastic flow under uniaxial tension, d = t is obtained. Therefore, the diameter of the dimple would need to be equal to the thickness of the plate for a surface dimple to be produced by a yield point tension σ_z at the mid-depth of the plate. Because the diameter of the dimple in a structural plate is usually less than the

---

[3] "Triaxial Tension at the Head of a Rapidly Running Crack in a Plate," by J. M. Frankland, Journal of Applied Mechanics, December, 1959, p. 570.

[4] "Static Brittle Fracture Initiation at Net Stress 40% of Yield," by C. Mylonas, D. C. Drucker, and J. D. Brunton, Welding Journal Research Supplement, 1958, 473-s.

thickness, it appears that the value of σ_z not only equals σ_{yield} but that it occurs from the mid-depth of the plate outward to within a depth from the surface about equal to the radius of the dimple. In contrast, the compressive reaction stresses surrounding the kernel will be mainly elastic because the cross-sectional area of reactive material is much larger than the cross-sectional area of the kernel.

For a thin sheet (in which $d > t$) the stress σ_z would doubtless be far below σ_{yield}. Accordingly, there would be a sufficient difference between the principal stresses to produce internal shears that should initiate plastic flow in the y direction. Only as the thickness increases to structural dimensions, above 1/4 in., will the lateral resistance to deformation in the z direction become sufficient for σ_z to approach σ_{yield}, with resulting possibility of brittle fracture.

TESTS DEMONSTRATE EMBRITTLEMENT DUE TO PLASTIC PRECOMPRESSION

Through extensive tests Drucker and Mylonas have shown that both the notched plate and the simple cylindrical bar without a notch, when precompressed plastically as indicated in Fig. 2(c), may later fracture by cleavage if loaded lightly in tension.[5,6] The precompressive deformation in Fig. 3(a) was from 1% to 3% measured across the notch. The precompressive deformation of the cylinder in Fig. 3(b) was 40% to 50% longitudinally. This was thought to represent the maximum possible unit strain at the root of the notch in Fig. 3(a) due to stress concentration. Precompressed specimens of both types tested in tension at -10° F fractured by cleavage at a low tensile P/A stress. However, only a few of the cylinders cracked below the yield tension while a large proportion of the notched and precompressed plates fractured at a P/A stress well below yield. Hence, the embrittlement due to precompression was much more severe in the notched plate specimens than in the cylindrical specimens. The residual stress pattern in each type of specimen will be developed to determine whether the brittle fractures observed can be explained by the action of negative residual stresses in suppressing plastic deformation. Note in Fig. 3 that the direction of arrows represent action of the notch kernel on the surrounding material, that is, compressive residual forces act outward and tensile forces inward.

RESIDUAL STRESSES IN NOTCHED PRECOMPRESSED PLATE

The notched plate of Fig. 3(a) when precompressed about 3% across the notch by a compressive force in the y direction developed small raised pimples on each surface at the notch. Accordingly, compressive plastic flow at the notch took place along both y and z axes. It may be assumed without much chance of error that some plastic flow also took place outward from the notch along the x axis. This action is represented in Fig. 3(a) by flattening or increasing the horizontal axis of the imaginary plastic cylindrical kernel at the notch. Hence, under the compressive loading, triaxial compressive stresses

5 "On the Exhaustion of Ductility of E-Steel in Tension Following Compressive Prestrain," by D. C. Drucker, C. Mylonas, and G. Lianis, Report, Div. of Engrg., Brown Univ., 1959.

6 "Prestrain, Sizes and Residual Stresses in Static Brittle Fracture Initiation," by C. Mylonas, Welding Journal Research Supplement, 1959, p. 414-s.

exist at the mid-point of the notch with each axial stress equal to the yield stress in compression. When the compressive load is removed, the cylindrical plastic kernel will tend to increase its vertical diameter, its horizontal diameter, and its length by elastic recovery.

Expansion of the kernel cannot occur freely because it is surrounded by a much larger volume of elastic material. For example, as the cylindrical kernel increases in length from outward plastic flow in the z direction its motion is resisted by surface shears that in turn develop tension in the surrounding material equal in total magnitude to the total compressive stress of the kernel in the z direction. Of course, the average unit tensile stress σ_z' developed may be only a fraction of σ_z, the compressive stress, (Fig. 3(a)) because the

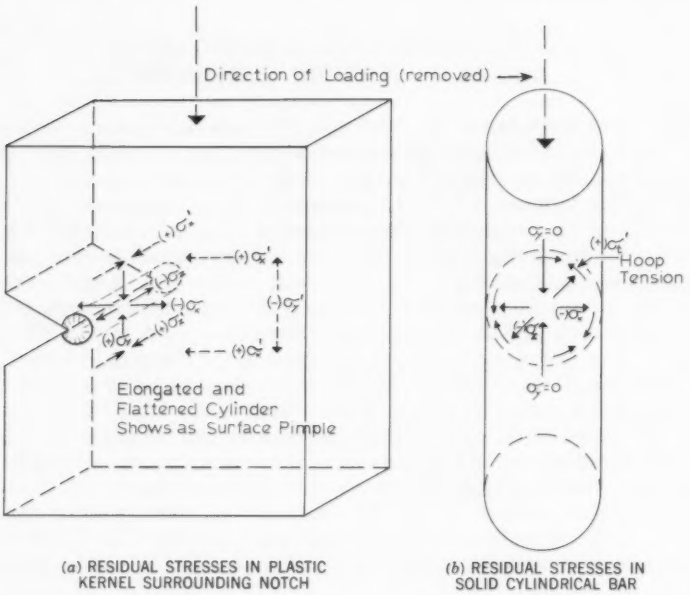

(a) RESIDUAL STRESSES IN PLASTIC KERNEL SURROUNDING NOTCH

(b) RESIDUAL STRESSES IN SOLID CYLINDRICAL BAR

FIG. 3.—RESIDUAL STRESSES LEFT BY PLASTIC PRECOMPRESSION

resistive material surrounding the kernel may have several times its volume. Note particularly that the compressive and tensile lateral forces are in dynamic equilibrium during plastic flow and will remain in static equilibrium when flow is terminated. Hence, there is little opportunity for release of residual lateral compression in the cylindrical kernel in the z direction. Although the situation in the x direction is much less readily visualized, there will be a residual compressive stress σ_x at the level of the notch that will be in equilibrium with residual tensions σ_x' above and below the notch. The important conclusion is that the residual lateral compressive stresses of yield value required for lateral plastic flow are essentially frozen into the plate at the level of the notch by a condition of stress equilibrium. It is not evident how appreciable

relaxation of stress or recovery of elastic deformation may occur. Hence, the biaxial residual compressions must represent large fractions of the yield stress, probably 0.75 σ_{yield} or greater.

In the vertical or y direction the entire plate will recover elastically due to removal of the compressive loading. The plate will elongate in the vertical direction. The only resistance to this motion is from the plastically shortened material across the root of the notch that must be stretched by a residual tension of considerable magnitude. As required by statics ($\Sigma F_y = 0$) the high residual tension σ_y at the notch (Fig. 3(a)) must be balanced by a low residual compression σ_y' across the major part of the throat of the plate between the notches. Hence, the residual stress pattern at the mid-point of the notch, as shown in Fig. 3(a), is that of compressive stresses equal to at least 0.75 σ_{yield} for σ_x and σ_z with perhaps an equal tension σ_y across the notch.

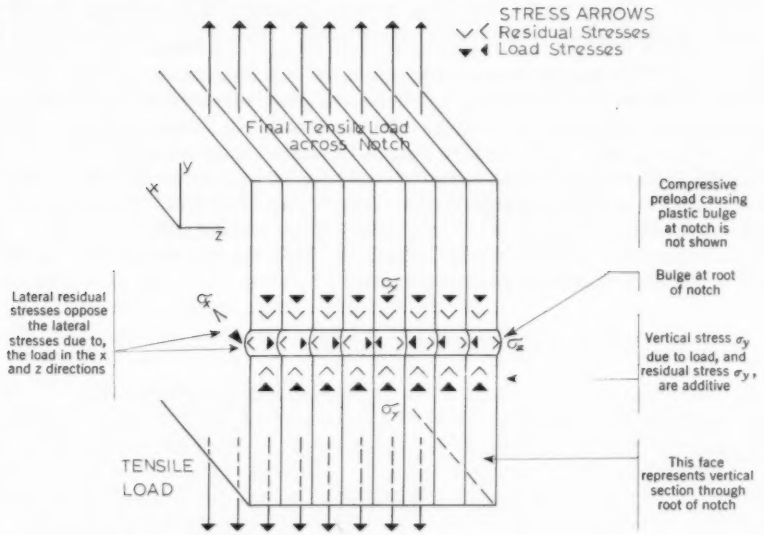
STRESS ARROWS
Residual Stresses
Load Stresses
Final Tensile Load across Notch
y
x
z
Compressive preload causing plastic bulge at notch is not shown
Bulge at root of notch
Lateral residual stresses oppose the lateral stresses due to, the load in the x and z directions
Vertical stress σ_y due to load, and residual stress σ_y, are additive
TENSILE LOAD
This face represents vertical section through root of notch

FIG. 4.—PLATE WITH IMAGINARY SLICES ACROSS THE NOTCH ILLUSTRATING STRESS ADDITION IN DIRECTION OF LOADING AND LATERAL STRESS REDUCTION

A study of the precompressed cylinder Fig. 3(b) establishes the existence of high residual internal lateral compressions in equilibrium with a residual hoop tension. The residual stress σ_y is zero.

BIAXIAL RESIDUAL COMPRESSIONS SUPPRESS DUCTILE DEFORMATION

Fig. 4 shows the superposition of the residual stresses left by precompression and the triaxial tensions at the notch produced by a final tensile load applied across the notch. For clarity only the stress arrows showing the action of the cylindrical kernel on its surrounding material are included. It can be

observed that the residual stress and the stress concentration due to vertical load tend to add numerically in the y direction because they are of the same sense. Laterally, in either the x or z direction, the load stress is of opposite sense to that of the residual stress. Because the stress concentration factor for the notch in the y direction in Fig. 4 is several times P/A, and because a large residual stress of the same sense and direction already exists due to elastic recovery of the plate after precompressive plastic flow, it is clear that a very low average P/A stress of perhaps 10% of σ_{yield} will be likely to produce a resultant yield stress in the y direction at the notch. At the same time the lateral residual compressions and their accompanying shears are reduced, perhaps to zero, by the lateral tensions and shears developed by the vertical yield stress acting under the restriction that plastic flow does not increase the volume of the plastic material. The cancellation or reduction of lateral stresses and their accompanying shears by opposite residuals suppresses ductility.

Perhaps a better way to describe this phenomenon is to note that the lateral stresses must change elastically from about $-0.75\ \sigma_{yield}$ to $+1.00\ \sigma_{yield}$, a variation of $1.75\ \sigma_{yield}$. During the same instant of time the cross-notch tension can only increase elastically. If its range of stress is comparable to that of the lateral stresses, it should instantaneously reach $2.5\ \sigma_{yield}$ if the residual tension σ_y was equal to $0.75\ \sigma_{yield}$. Evidently, the cleavage stress under these conditions may be less than the instantaneous elastic tensile stress with the result that a brittle fracture is initiated. Whether the fracture crack terminates quickly or progresses is dependent on the magnitude of the overall stress field at the time of crack initiation. This may be expressed as the energy available for crack propagation.

FURTHER EXPLANATION OF TEST RESULTS

In tension tests on notched plates, after an initial precompression, it has been reported that nearly all specimens develop at least a short brittle fracture crack at low load that may be heard even if not observed on the surface. It is understandable from the preceding explanation that these brittle tensile cracks develop at a P/A stress of but 1/10 of yield. As pointed out by Drucker and Mylonas a short crack at the notch may then permit the remainder of the plate to stretch plastically. The reason, following the concept previously explained, is that the crack extends beyond the area of residual compressive stresses so that the material at the end of the crack does not have its ductility suppressed by residual biaxial compressions perpendicular to the direction of the applied load.

For a perfect precompressed cylinder (Fig. 3(b)) a P/A tensile stress equal to σ_{yield} would have to be applied to develop a brittle fracture, because there is no notch stress concentration nor any residual tension in the vertical direction. However, there are flaws in all materials. An occasional specimen will have a flaw within the central core that would produce a stress concentration both under precompression and later under an applied tensile load. Accordingly, in agreement with tests, some cylindrical specimens might be expected to fracture at a final P/A loading well below σ_{yield}. It appears there-

fore that the principle of suppression of ductility by lateral compressive residual stresses explains adequately the brittle fractures observed in tests of steel under precompression followed by load reversal.

CONCLUSIONS

Notch Embrittlement and Structural Fractures.—Tests have shown that notches or other severe stress raisers will produce brittle fractures under an application of a single tensile stress equal to the yield P/A stress. For members not subject to stress reversal, having determinable stresses well below the elastic limit, notches should not endanger the structure because their stress concentrations will be reduced sharply by the initiation of plastic flow.

For material subject to stress reversal, such as ship plates and certain members of bridge trusses, a sharp notch may produce a high compressive stress concentration that will upset or thicken the notch material by plastic deformation even under a normal P/A compressive stress. On release of the load there may remain lateral residual compressive stresses at right angles to each other and to the direction of the load. Such residual stresses may be expected to approach the yield stress. Then, when the load is reversed, the lateral tensile stresses must first eliminate the lateral residual compressions before they can induce the shear stresses necessary for plastic flow. The delay or suppression of plastic flow under tension across the notch even for an instant may permit the tensile stress at the root of the notch to reach the ultimate cleavage strength of the steel so that a brittle fracture will result.

A comparable upsetting action followed by stress reversal can occur from welding. The weld heat, by expanding a restrained plate locally, may upset material at a notch or flaw that may remain below an annealing temperature. Then on cooling, the main force at the notch will automatically be reversed to tension with the possibility of brittle fracture.

It must be recognized that the phenomena of plastic flow and cleavage fracture are subject to many variables within the material itself. It is therefore expected that geometrically similar test specimens or comparable structures will show considerable variation in method of fracture and in the fracture loading. Occurrence of a significant percentage of brittle fractures, however, is evidence that ductility is being suppressed.

An inspection of visible notches should make it possible to locate upset or thickened material in a structure. In some cases it may be possible to drill out such material leaving a circular hole that produces a much lower stress concentration and eliminates residual compressions produced by plastic flow at the notch. Doubtless expert use of a torch could be made to release the residual compressions and thus eliminate the immediate danger of brittle fracture. However, the existence of the notch remains as a threat if stress reversal can reoccur.

Tests are needed to determine whether stress reversals repeated many times at a low P/A compression along with a high stress concentration factor may eventually suppress ductility in the same manner as occurred for the tests considered herein.

Journal of the
ENGINEERING MECHANICS DIVISION
Proceedings of the American Society of Civil Engineers

BENDING OF BEAMS RESTING ON ISOTROPIC ELASTIC SOLID

By Aleksandar B. Vesić,[1] M. ASCE

SYNOPSIS

In the first part of this paper, Biot's solution for bending, under a concentrated load, of an infinite beam resting on an isotropic elastic solid is brought to a complete form and extended to the case of loading by a couple. Integrals appearing in both solutions are evaluated numerically and approximated by analytical functions.

The second part of the paper contains a thorough investigation of the reliability of the conventional approach to the problem by means of the coefficient of subgrade reaction k. For the first time the realm of validity of the well-known Winkler's hypothesis, and the amount of error induced by its application, are determined.

It is shown that this hypothesis is practically satisfied for beams of infinite length. Concerning beams of finite length a criterion is given for distinction of cases where the conventional analysis may give reasonably accurate results. An expression is derived for evaluation of the coefficient k in appropriate cases.

INTRODUCTION

Notation.—The letter symbols adopted for use in this paper are defined where they first appear, in the illustrations or in the text, and are arranged alphabetically, for convenience of reference, in Appendix II.

Note.—Discussion open until September 1, 1961. To extend the closing date one month, a written request must be filed with the Executive Secretary, ASCE. This paper is part of the copyrighted Journal of the Engineering Mechanics Division, Proceedings of the American Society of Civil Engineers, Vol. 87, No. EM 2, April, 1961.

[1] Assoc. Prof. of Civ. Engrg., Georgia Inst. of Tech., Atlanta, Ga.

The problem of bending of beams resting on an isotropic elastic solid characterized by a Young's modulus E_s and a Poisson's ratio μ_s has been treated by several authors. M. A. Biot[2] derived a rigorous solution for a beam of infinite length acted upon by a concentrated load. E. E. De Beer,[3,4] A. Habel,[5] J. Ohde,[6] De Beer and D. Krsmanovitch,[7] M. Kany,[8] and others presented approximate solutions for particular cases of beams of finite length loaded by one or several concentrated loads.

Biot considered the problem of bending, under a concentrated load P (Fig. 1) of a flexible beam of infinite length on a semi-infinite homogeneous, elastic,

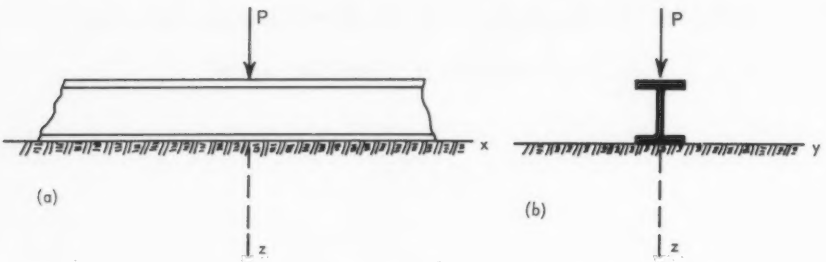

FIG. 1.—AN INFINITE BEAM ACTED UPON BY A CONCENTRATED LOAD

and isotropic solid. For the bending moment M at any point x of the beam Biot found the expression

$$M(x) = \frac{P\,c}{\pi} \int_0^\infty \frac{\alpha \cos(\alpha\, x/c)\, d\alpha}{\alpha^3 + \psi(\beta)} \quad \ldots\ldots\ldots\ldots\ldots\ldots (1)$$

in which α denotes a dimensionless parameter; b is the half-width of the beam; c denotes $\left[C\left(1-\mu_s^2\right)\frac{E_b I}{E_s}\right]^{1/3}$, the fundamental length of the beam; C refers to a function of $b\alpha/c$ (C = 1.00 if the distribution of pressures across the width

---

2 "Bending of an Infinite Beam on an Elastic Foundation," by M. A. Biot, Journal of Applied Mechanics, Transactions, Amer. Soc. of Mech. Engrs., Vol. 59, 1937, pp. A1-A7.

3 "Le calcul de poutres reposant sur le sol," by E. E. De Beer, Annales des Travaux Publics de Belgique, Vol. 51, 1948, pp. 393-418, 525-552, 653-691, 721-749.

4 "Computation of Beams Resting on Soil," by E. E. De Beer, Proceedings, Second Internatl. Conf. on Soil Mech. and Foundation Engrg., Vol. 1, Rotterdam, 1948, pp. 119-121.

5 "Näherungsberechnung des auf dem elastisch-isotropen Halbraum aufliegenden elastischen Balkens," by A. Habel, Der Bauingenieur, Vol. 19, 1938, pp. 76-78.

6 "Die Berechnung der Sohldruckverteilung unter Gründungskörpern," by J. Ohde, Der Bauingenieur, Vol. 23, 1942, pp. 99-107, 122-127.

7 "Calcul de poutres reposant sur le sol," by E. E. De Beer and D. Krsmanovitch, Annales des Travaux Publics de Belgique, Vol. 52, 1951, pp. 981-1018; Vol. 53, 1952, pp. 9-56.

8 "Berechnung von Flächengründungen," by M. Kany, Ernst, Berlin, 1959.

of the beam is uniform; $1.00 < C < 1.13$ if the deflection across the width of the beam is uniform); E_bI denotes the stiffness of the beam (E_b being Young's modulus and I the moment of inertia of the beam); E_s, μ_s are Young's modulus and Poisson's ratio of the subgrade respectively; $\beta = b\alpha/c$ refers to a dimensionless parameter; $\psi(\beta)$ is a function tabulated for $\beta > 0.1$ and given by an assympotic expression for $\beta < 0.1$; and P denotes the concentrated load. Having computed the approximate value of bending moment under the load, that is, for x = 0, he found that, in the interval $0.01 < b/c < 1$, with an error of the order of 2% to 3%

$$M_{max} = 0.332\ P\ b \left[C\left(1 - \mu_s^2\right)\frac{E_b I}{E_s b^4} \right]^{0.277} \quad \ldots\ldots\ (2)$$

After comparing Eq. 2 with the expression obtained by means of the conventional analysis using the modulus of subgrade reaction $K = 2\ k\ b = k\ B$

$$M_{max} = 0.353\ P\ b \left[\frac{E_b\ I}{K\ b^4} \right]^{0.250} \quad \ldots\ldots\ (3)$$

Biot found that, taking for the modulus K the value

$$K = 1.23 \left[\frac{E_s b^4}{C\left(1-\mu_s^2\right) E_b\ I} \right]^{0.11} \frac{E_s}{1 - \mu_s^2} \quad \ldots\ldots\ (4)$$

the maximum bending moment, as found by the conventional analysis (Eq. 3) will be the same as obtained by the more rigorous theory (Eq. 2). (The term "modulus of subgrade reaction" is sometimes used for the coefficient of subgrade reaction k which represents the constant ratio of contact pressures and deflections along the beam, and has a dimension of pounds per cubic inch. In this paper the term "modulus" is strictly reserved for K=kB, which is a quantity measured in pounds per square inch, having therefore the dimension of the Young's modulus E.) Biot also showed that the expression for deflections should give finite values in spite of the infinite value of the integrand for $\alpha = 0$.

However, bending moments other than the maximum one as well as other influences in the beam (deflections, shearing forces, contact pressures) were not evaluated by Biot. Also, no solution for the case of loading by a couple was presented.

The results which follow in the next three sections of this paper are obtained by extending Biot's solution.

BEAM ACTED UPON BY A CONCENTRATED LOAD

Eq. 1 is taken as a basis for complete solution of the considered problem. Using the well-known relationships between the bending moment M(x) on the one hand and the shearing force V(x), contact pressure p(x), as well as the

slope $\theta(x)$ and the deflection $w(x)$ of the beam on the other hand, the following expressions are obtained:

$$E_b I w(x) = \frac{P c^3}{\pi} \int_0^\infty \frac{\cos(\alpha x/c)\, d\alpha}{\alpha\left[\alpha^3 + \psi(\beta)\right]} = \frac{P c^3}{\pi} J_0(x) \quad \ldots\ldots\ldots (5)$$

$$E_b I\, \theta(x) = -\frac{P c^2}{\pi} \int_0^\infty \frac{\sin(\alpha x/c)\, d\alpha}{\alpha^3 + \psi(\beta)} = -\frac{P c^2}{\pi} J_1(x) \quad \ldots\ldots\ldots (6)$$

$$M(x) = \frac{Pc}{\pi} \int_0^\infty \frac{\alpha \cos(\alpha x/c)\, d\alpha}{\alpha^3 + \psi(\beta)} = \frac{P c}{\pi} J_2(x) \quad \ldots\ldots\ldots (7)$$

$$V(x) = -\frac{P}{\pi} \int_0^\infty \frac{\alpha^2 \sin(\alpha x/c)\, d\alpha}{\alpha^3 + \psi(\beta)} = -\frac{P}{\pi} J_3(x) \quad \ldots\ldots\ldots (8)$$

and

$$p(x) = \frac{P}{c\pi} \int_0^\infty \frac{\psi(\beta) \cos(\alpha x/c)\, d\alpha}{\alpha^3 + \psi(\beta)} = \frac{P}{c\pi} J_4(x) \quad \ldots\ldots\ldots (9)$$

In deriving Eq. 9 it should be noted that

$$J_4(x) = -\int_0^\infty \frac{\alpha^3 \cos(\alpha x/c)\, d\alpha}{\alpha^3 + \psi(\beta)} = -\int_0^\infty \cos(\alpha x/c)\, d\alpha + \int_0^\infty \frac{\psi(\beta) \cos(\alpha x/c)\, d\alpha}{\alpha^3 + \psi(\beta)}$$

and that the divergent part of the integral can be identified with zero.[9]

Eqs. 5 through 9 enable the computation of any of the influences in an infinite beam acted upon by any concentrated loads.

BEAM ACTED UPON BY A COUPLE

The extension of the solution for the case of loading by a concentrated couple **M** [Fig. 2(a)] can be obtained by using an approach similar to that used in the conventional theory of subgrade reaction.[10]

Consider a beam [Fig. 2(b)] under the action of two equal and opposite loads P at a distance Δx. Any influence Z will be

$$Z = P\left[Z_1(x + \Delta x) - Z_1(x)\right] \quad \ldots\ldots\ldots (10)$$

---

[9] "Grillage Beams on Elastic Foundation," by B. Drapkin, Proceedings, ASCE, Proceedings-Separate No. 771, Vol. 81, August, 1955.

[10] "Beams on Elastic Foundations," by M. Hetényi, Univ. of Michigan Press, Ann Arbor, 1946.

in which Z_1 is the influence for P=1. The loading by a couple **M** may be considered as a limiting case of the loading shown in Fig. 2(b), provided that

$$\lim P \Delta x = \mathbf{M} \quad \ldots\ldots\ldots\ldots\ldots\ldots \quad (11)$$

Thus, multiplying and dividing the right side of Eq. 11 by Δx and passing to the limit

$$Z = \mathbf{M} \frac{dZ_1}{dx} \quad \ldots\ldots\ldots\ldots\ldots\ldots (12)$$

Applying this relation the following expressions are derived from Eqs. 5 to 9:

$$E_b I w(x) = \frac{\mathbf{M} c^2}{\pi} \int_0^\infty \frac{\sin(\alpha\, x/c)\, d\alpha}{\alpha^3 + \psi(\beta)} = \frac{\mathbf{M} c^2}{\pi} J_1(x) \quad \ldots\ldots\ldots\ldots \quad (13)$$

$$E_b I \theta(x) = \frac{\mathbf{M} c}{\pi} \int_0^\infty \frac{\alpha \cos(\alpha\, x/c)\, d\alpha}{\alpha^3 + \psi(\beta)} = \frac{\mathbf{M} c}{\pi} J_2(x) \quad \ldots\ldots\ldots\ldots \quad (14)$$

$$M(x) = \frac{\mathbf{M}}{\pi} \int_0^\infty \frac{\alpha^2 \sin(\alpha\, x/c)\, d\alpha}{\alpha^3 + \psi(\beta)} = \frac{\mathbf{M}}{\pi} J_3(x) \quad \ldots\ldots\ldots\ldots (15)$$

$$V(x) = -\frac{\mathbf{M}}{c\,\pi} \int_0^\infty \frac{\psi(\beta) \cos(\alpha\, x/c)\, d\alpha}{\alpha^3 + \psi(\beta)} = -\frac{\mathbf{M}}{c\,\pi} J_4(x) \quad \ldots\ldots\ldots \quad (16)$$

and

$$p(x) = \frac{\mathbf{M}}{c^2\,\pi} \int_0^\infty \frac{\alpha\, \psi(\beta) \sin(\alpha\, x/c)\, d\alpha}{\alpha^3 + \psi(\beta)} = \frac{\mathbf{M}}{c^2\,\pi} J_5(x) \quad \ldots\ldots\ldots \quad (17)$$

These expressions, together with Eqs. 5 through 9 represent a complete general solution of the problem of bending of infinite flexible beams on a semi-infinite elastic-isotropic solid.

EVALUATION OF INTEGRALS

In view of application of derived expressions one of the six integrals $J_n(x)$ must be evaluated numerically for different abscissas $x/c = \xi$. The remaining five integrals may then be found by integration or differentiation of J_n, provided their value in one point (such as at $x = 0$) is also computed. For complete evaluation the integral $J_2(x)$ (Eqs. 7 or 14) was chosen.

The numerical integration of this type of integral evidently presents some difficulties which can be overcome in different ways. In this case an integration by interpolation was found to be suitable up to a certain point M (Fig. 3) from which point on the integrand could have been replaced with sufficient ac-

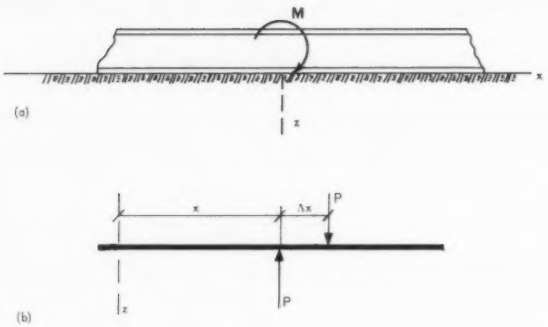

FIG. 2.—AN INFINITE BEAM ACTED UPON BY A COUPLE

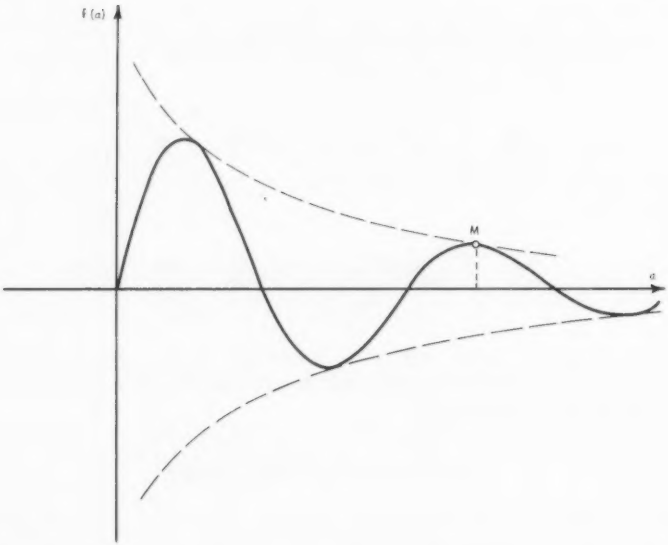

FIG. 3.—EVALUATION OF THE INTEGRAL $J_2(x) = \int_0^\infty F(x,\alpha)d\alpha$

curacy, by a simpler analytical function, representing its upper limit in the considered interval. Thus, the integral was divided into two parts;

$$\left|J_2\right|_0^\infty = \left|J_2\right|_0^M + \left|J_2\right|_M^\infty \quad \ldots\ldots\ldots\ldots\ldots\ldots \quad (18)$$

The first part ($0 < \alpha < M$) was integrated by interpolation using Simpson's rule, whereas for the second part the following approximation was applied:

$$\left|J_2\right|_M^\infty = \int_M^\infty \frac{\alpha \cos(\alpha\, x/c)\, d\alpha}{\alpha^3 + \psi(\beta)} \approx \int_M^\infty \frac{\cos \xi\, \alpha\, d\alpha}{\alpha^2} \quad \ldots\ldots\ldots \quad (19)$$

in which $\xi = x/c$. The latter expression was then integrated analytically, so that

$$\left|J_2\right|_M^\infty \approx \frac{\cos \xi M}{M} - \frac{\pi \xi}{2} + \xi\, \mathrm{Si}(\xi M) \quad \ldots\ldots\ldots\ldots\ldots \quad (20)$$

The position of the point M as well as the number of points for interpolation after Simpson were chosen so as to assure an accuracy of 2% in the final value

TABLE 1.—VALUES OF INTEGRAL $J_2 = \int_0^\infty \frac{\alpha \cos(\alpha x/c)}{\alpha^3 + \psi(\beta)}\, d\alpha$

ξ \ b/c	0.01	0.05	0.20	1.00
0	+0.46348	+0.64115	+0.81400	+1.03166
0.25	+0.15016	+0.29768	+0.45101	+0.66837
0.50	-0.01439	+0.09057	+0.21966	+0.40546
0.75	-0.08041	-0.03704	+0.05006	+0.20586
1	-0.09217	-0.08960	-0.05947	+0.05110
1.50	-0.05077	-0.11983	-0.14779	-0.11980
2	-0.01269	-0.07870	-0.13826	-0.17587
3	+0.00193	-0.01218	-0.05811	-0.14021
4	-0.00183	+0.00193	-0.01366	-0.07273

of the integral. The results of the computation are given in Table 1 and also shown graphically on Fig. 4.

ANALYTICAL EXPRESSIONS FOR INTEGRALS

A study of the shape of curves shown in Fig. 4 revealed their great similarity with the curves of damped wave type. After some investigations it was found that the computed numerical values of the integral J_2 fit the analytical expression

$$J_2(x) = J_2(0)\, e^{-\lambda' x} [\cos \lambda' x - \sin \lambda' x] \quad \ldots\ldots \quad (21)$$

in which $J_2(0)$ represents the value of the integral for x=0:

$$J_2(0) = 0.332\left(\frac{b}{c}\right)^{0.169} \quad \ldots\ldots\ldots\ldots\ldots\ldots \quad (22)$$

and λ' a parameter having the dimension $(\text{length})^{-1}$ and defined by

$$\lambda' = \frac{\pi}{4\,x_0} \quad \ldots\ldots\ldots\ldots\ldots\ldots\ldots\ldots \quad (23)$$

in which x_0 is the abscissa of the first zero of the integral.

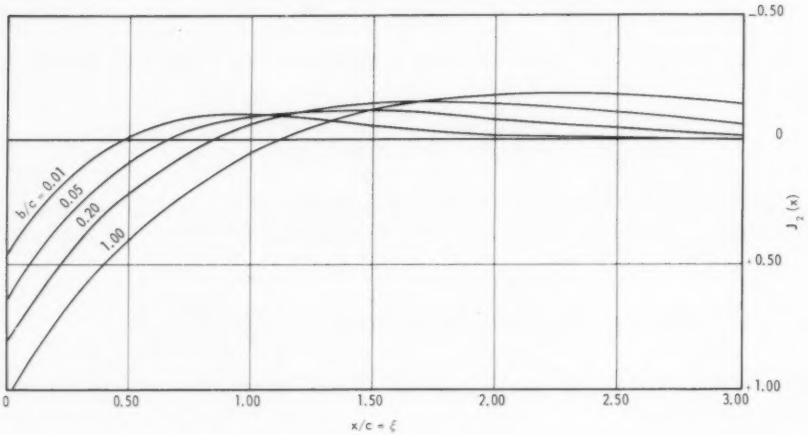

FIG. 4.—VALUES OF THE INTEGRAL $J_2(x)$

It was found that the value of this abscissa can be approximated, with a maximum error of the order of 2% in the interval $0.01 < b/c < 1$, by the expression

$$x_0 = 1.140\,c\left(\frac{b}{c}\right)^{0.187} \quad \ldots\ldots\ldots\ldots\ldots\ldots \quad (24)$$

so that the final expression for λ' was obtained as

$$\lambda' = \frac{0.689}{b}\left(\frac{b}{c}\right)^{0.813} \quad \ldots\ldots\ldots\ldots\ldots\ldots \quad (25)$$

As λ' is a function of b/c only, it can easily be proven that the remaining five integrals $J_0(x)$ to $J_5(x)$ may be found from the expressions:

$$J_0(x) = J_0(0)\,e^{-\lambda' x}\,(\cos \lambda' x \sin \lambda' x) \quad \ldots\ldots\ldots \quad (26)$$

$$J_1(x) = J_1\left(\frac{\pi}{2\lambda'}\right) e^{-\lambda' x} \sin \lambda' x \quad \ldots\ldots\ldots\ldots\ldots \quad (27)$$

$$J_3(x) = J_3(0)\, e^{-\lambda' x} \cos \lambda' x \quad \ldots\ldots\ldots\ldots\ldots \quad (28)$$

$$J_4(x) = J_4(0)\, e^{-\lambda' x} (\cos \lambda' x + \sin \lambda' x) \quad \ldots\ldots \quad (29)$$

and

$$J_5(x) = J_5\left(\frac{\pi}{2\lambda'}\right) e^{-\lambda' x} \sin \lambda' x \quad \ldots\ldots\ldots\ldots \quad (30)$$

Here $J(0)$ and $J\left(\frac{\pi}{2\lambda'}\right)$ are the values of the integrals for $x = 0$ and $x = \frac{\pi}{2\lambda'}$ respectively. One of these integrals is already known:

$$J_3(0) = \frac{\pi}{2} \quad \ldots\ldots\ldots\ldots\ldots\ldots \quad (31)$$

The remaining four of them were computed partly by numerical integration, and partly by approximating the integrand by its asymptotic values. The computation of $J_1\left(\frac{\pi}{2\lambda'}\right)$, $J_4(0)$ and $J_5\left(\frac{\pi}{2\lambda'}\right)$ was, in principle, similar to that of $J_2(x)$ shown before. The details of the computation of $J_0(0)$ are given in Appendix I. The results are presented in Table 2.

TABLE 2.—NUMERICAL VALUES OF INTEGRALS $J_0(0)$, $J_1\left(\frac{\pi}{2\lambda'}\right)$, $J_4(0)$ AND $J_5\left(\frac{\pi}{2\lambda'}\right)$

b/c	0.01	0.05	0.20	1.00
J_0 (0)	0.08765	0.24580	0.55595	1.31527
$J_1\left(\frac{\pi}{2\lambda'}\right)$	0.04992	0.09388	0.14828	0.23491
J_4 (0)	2.71914	1.99905	1.59923	1.32452
$J_5\left(\frac{\pi}{2\lambda'}\right)$	1.51816	0.69949	0.41172	0.28458

It was found that the following analytical expressions approximate the computed values of integrals, so that the maximum error in the interval $0.01 < b/c < 1.00$ remains of the order of 4% for $J_0(0)$, 5% for $J_1\left(\frac{\pi}{2\lambda'}\right)$, 3% for $J_4(0)$ and 10% for $J_5\left(\frac{\pi}{2\lambda'}\right)$:

$$J_0(0) = 1.370\left(\frac{b}{c}\right)^{0.587} \quad \ldots\ldots\ldots\ldots\ldots \quad (32)$$

$$J_1\left(\frac{\pi}{2\lambda'}\right) = 0.244\left(\frac{b}{c}\right)^{0.333} \quad \ldots\ldots\ldots\ldots \quad (33)$$

$$J_4(0) = 1.285\left(\frac{b}{c}\right)^{-0.155} \quad \ldots\ldots\ldots\ldots\ldots \quad (34)$$

and

$$J_5\left(\frac{\pi}{2\lambda'}\right) = 0.259\left(\frac{b}{c}\right)^{-0.360} \quad \ldots\ldots\ldots\ldots \quad (35)$$

Eqs. 21, 22, and 25 through 35 analytically define, with sufficient accurary, the integrals appearing in the general solution given by Eqs. 5 through 9, and 13 through 17 of the considered problem.

RELIABILITY OF THE CONVENTIONAL ANALYSIS

Footing and mat foundations, as well as grillage beams, resting on subgrades the behavior of which is usually well simulated by that of elastic solids, and frequently analyzed by the elementary theory of beams on elastic subgrade, are based on the assumption that the contact pressure at any point of the beam is proportional to the deflection of the beam at the same point (Winkler's hypothesis).

However, theoretical investigations mentioned earlier in this paper, as well as experiments made by De Beer[11] and others showed clearly that the pressure distribution at the contact between beams or slabs and subgrades may be quite different from that assumed by the conventional analysis. Winkler's hypothesis is, thus, generally not satisfied. And yet Biot has shown that it was possible, in solving a particular problem of bending of a beam of infinite length acted upon by a concentrated load, to choose a certain value of the coefficient of subgrade reaction k, which will give a bending moment diagram in reasonable agreement with that obtained by treating the subgrade as an elastic solid. His finding, as well as some of De Beer's and Ohde's analyses, imply that there must be some cases wereh the conventional analysis could be expected to give reasonably accurate results.

Therefore, the second part of this investigation was undertaken with the aim of clarifying the following questions:

1. Is Winkler's hypothesis ever satisfied for beams resting on an elastic-isotropic subgrade?
2. If the conventional analysis is found justified in some cases, what value should be assigned to the coefficient of subgrade reaction k?
3. What amount of error is to be expected if the analysis is made by the elementary theory based on Winkler's hypothesis?
4. Since the analysis by the conventional theory furnishes results which in some cases agree reasonably while in other cases deviate considerably from the results obtained by a more rigorous analysis, will it not be possible to establish a criterion for distinction of cases where reasonable accuracy can be expected?

VALIDITY OF WINKLER'S HYPOTHESIS

To answer the first question it is sufficient to compare Eqs. 26 and 27 with Eqs. 29 and 30, respectively. It can be seen that the ratio of the contact pressure and the deflection of the beam does not depend on x but on b/c only.

---

[11] "Tests for the Determination of the Distribution of Soil Reactions Underneath Beams Resting on Soil," by E. E. De Beer, Proceedings, Second Internatl. Conf. on Soil Mech. and Foundation Engrg., Vol. 2, Rotterdam, 1948, pp. 142-148.

Thus Winkler's hypothesis is practically satisfied for any determined beam of infinite length resting on a semi-infinite elastic subgrade. Any problem of bending of an infinite beam having a stiffness $E_b I$ and a width $B = 2b$ and resting on a semi-infinite subgrade defined by a Young's modulus E_s and a Poisson's ratio μ_s can be treated with reasonable accuracy by the conventional analysis using a coefficient of subgrade reaction k.

VALUE OF THE COEFFICIENT OF SUBGRADE REACTION

What value should be assigned to the coefficient k? The conventional analysis leads to solutions which contain, as it is well known, the same damped-wave functions as Eqs. 21 and 26 through 30, with a damping factor

$$\lambda = \sqrt[4]{\frac{K}{4 E_b I}} \quad \ldots\ldots\ldots\ldots\ldots\ldots \quad (36)$$

If this factor is equated to the factor λ' defined by Eq. 25 all the w, θ, M, V, and p-curves obtained by the conventional analysis will become congruent to the corresponding curves obtained by the rigorous solution of the same problem. Equating Eq. 25 to 36 and neglecting the small power of $C\left(1 - \mu_s^2\right)$ yields

$$K_\infty B = K_\infty = \frac{0.90}{C} \left[\frac{E_s b^4}{E_b I}\right]^{0.083} \frac{E_s}{1 - \mu_s^2} \quad \ldots\ldots\ldots \quad (37)$$

This expression differs somewhat from that found by Biot by simply equating the maximum bending moments (Eq. 4). Introducing B instead of 2b and taking $C = 1.10$ as a sufficiently correct value for any practical purpose, the following expression for K_∞ is obtained:

$$k_\infty B = K_\infty = 0.65 \sqrt[12]{\frac{E_s B^4}{E_b I}} \frac{E_s}{1 - \mu_s^2} \quad \ldots\ldots\ldots\ldots \quad (38)$$

From Eqs. 37 and 38 k_∞ can be computed if E_s is known. In some instances the value of the coefficient $\bar{k}$ for a square plate having a width B is known. Denoting $\bar{k} B = \bar{K}$ and knowing that, for a rigid square plate:

$$\frac{E_s}{1 - \mu_s^2} = 0.815 \frac{p B}{w} = 0.815 \bar{K} \quad \ldots\ldots\ldots\ldots\ldots \quad (39)$$

the following expression for K_∞ can be obtained:

$$k_\infty B = K_\infty = 0.52 \sqrt[12]{\frac{\bar{K} B^4}{E_b I}} \bar{K} \quad \ldots\ldots\ldots\ldots \quad (40)$$

It is interesting to compare this expression with the formulas presented by Karl Terzaghi,[12] Hon. M. ASCE and F. Vogt.[13] The Terzaghi formula gives $K_\infty = 0.67\ \overline{K}$ irrespective of the flexibility of the beam. Vogt formula gives $K_\infty = 0$; for beams of finite length L it gives again irrespective of the flexibility of the beam:

L/B	10	30	100	300	1000
$K/\overline{K}$	0.421	0.323	0.256	0.216	0.184

For the possible range of values of

$$\sqrt[12]{\frac{\overline{K}\,B^4}{E_b\,I}} = 0.40 - 1.25 \quad \ldots\ldots\ldots\ldots \quad (41)$$

Eq. 40 yields

$$K_\infty = 0.20 - 0.65\,\overline{K} \quad \ldots\ldots\ldots\ldots\ldots \quad (42)$$

where the lower limit is for very rigid beams and the upper limit is for very flexible beams.

ACCURACY OF THE CONVENTIONAL ANALYSIS

What amount of error is to be expected if beams of infinite length on an elastic-isotropic subgrade are analyzed by means of the elementary theory based on Winkler's Hypothesis?

Using the elementary theory with the value given in Eq. 25 for λ (or the value given in Eq. 37 for K), the maximum moment in a beam acted upon by a concentrated load is determined as

$$M(0) = \frac{P}{4\lambda} = 0.363\ Pc\left(\frac{b}{c}\right)^{0.187} \quad \ldots\ldots\ldots \quad (43)$$

This value may be compared with the exact value obtained from Eq. 7 and Table 1. The variation of the error induced by using the approximate value of Eq. 43, is given in Fig. 5.

In a similar manner, using the elementary theory the following values are found for maximum deflection and pressure under the load:

$$w(0) = \frac{P\lambda}{2K} = 0.381\,\frac{Pc^3}{E_b\,I}\left(\frac{b}{c}\right)^{0.563} \quad \ldots\ldots\ldots \quad (44)$$

and

$$p(0) = \frac{P\lambda}{2} = 0.3445\ \frac{P}{b}\ \left(\frac{b}{c}\right)^{0.813} \quad \ldots\ldots\ldots \quad (45)$$

---

12 "Evaluation of Coefficients of Subgrade Reaction," by Karl Terzaghi, Géotechnique, Vol. V, 1955, pp. 297-326.

13 "Uber Die Berechnung der Fundament-deformation," by F. Vogt, Avhandlinger, No. 2, Norske Videnskaps-Akademi, Math.-Naturv. Klasse, Oslo, 1925.

These values may be compared to the exact value obtained from Eqs. 5 and 9 with numerical values from Table 2. The errors induced by using approximate values of Eqs. 44 and 45 are shown in Fig. 5.

Examining Fig. 5 and bearing in mind that the "exact" values of integrals in Tables 1 and 2 were computed with an accuracy of $\pm$ 2%, the following conclusion may be reached:

1. When beams of infinite length on an elastic-isotropic semi-infinite subgrade are analyzed by means of the elementary theory based on Winkler's hypothesis with the value given by Eq. 25 for λ (or the value given in Eq. 37 for K), bending moments in the beam are overestimated; contact pressures and deflections of the beam are underestimated.

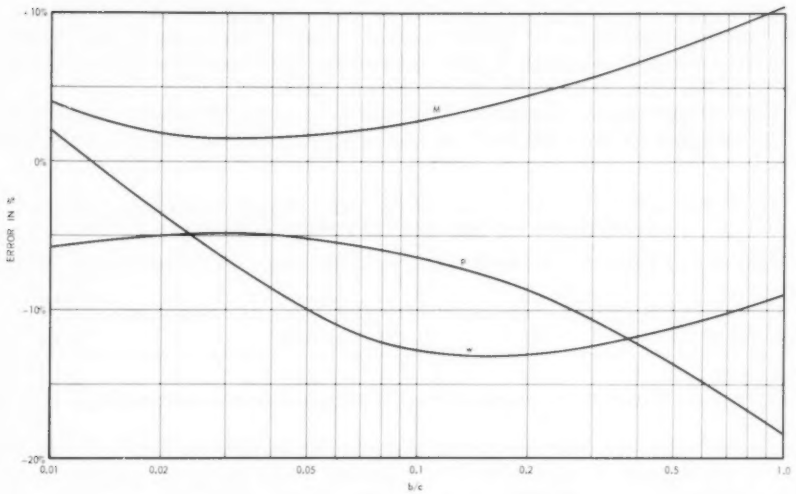

FIG. 5.—ERRORS IN THE MAXIMUM BENDING MOMENT M, DEFLECTION w, AND CONTACT PRESSURE

2. The amount of error depends on the relative stiffness of the beam. Table 3 gives the average and the maximum error for maximum bending moments, contact pressures and deflections of the beam.

CHOICE OF APPROPRIATE METHOD OF ANALYSIS

The preceding analysis has revealed the fact that the conventional analysis is reasonably accurate for beams of infinite length provided a proper value of coefficient k (Eq. 38) is chosen. However, earlier studies of beams of finite length have shown clearly that, depending on the flexibility of the beam, the conventional analysis may also furnish results which deviate considerably from those obtained by a more rigorous analysis. It seems reasonable, therefore,

to use the dimensionless length characteristics λL in establishing a criterion for distinction of cases where the application of the conventional analysis is justified.

According to λL-values, beams are usually classified into three groups:

1. long beams ($\lambda L > 5.00$)
2. beams of medium length ($0.80 < \lambda L < 5.00$)
3. short beams ($\lambda L < 0.80$)

Since the bending moments of a long beam can be computed with an error of less than 2% assuming that the length of the beam is infinite, it is not difficult to realize that the statements made on the validity of Winkler's hypothesis for beams of infinite length are valid without restrictions for long beams too.

Also, an analysis of different data available in the literature[2,3,4,5,6,7,8] clearly shows that Winkler's hypothesis is not satisfied for short beams. If an accurate analysis of such beams is to be made, procedures similar to those used by De Beer, Ohde, or others must be used. (Of course a very rough estimate of bending moments in such beams can be made assuming absolute rigidity of the beam and linear distribution of pressure.)

Concerning beams of medium length (a case of great practical interest due to the fact that most of the footings belong to this category) analyses made in-

TABLE 3.—ERROR IN ANALYSIS OF INFINITE BEAMS ON ELASTIC-ISOTROPIC SUBGRADES BY THE CONVENTIONAL k-METHOD.

Influence	M_{max}	w_{max}	p_{max}
Average error	+6%	-10%	-11%
Maximum error	+12%	-15%	-20%

dicate that, although Winkler's hypothesis is not strictly satisfied in this range of λL, reasonable accuracy may be expected using the conventional analysis, if the length characteristics λL stays within a certain limit.

To determine this limit, computations were made of bending moments in beams of different stiffnesses $E_b I$ resting on an elastic-isotropic subgrade, and acted upon by a concentrated load in the middle. Conventional analysis with K-values determined by means of Eq. 38 as well as a more rigorous analysis treating the subgrade as elastic-isotropic solid were used. Fig. 6 shows the amount of error in maximum bending moment involved by the use of Winkler's hypothesis. It is seen that with increase of characteristics λL, as defined by Eqs. 36 and 38, the error decreases, becoming practically negligible for $\lambda L > 2.25$.

Thus, in analyzing a beam of finite length under a concentrated load by the conventional analysis based on Winkler's hypothesis, reasonable accuracy is to be expected if the beam is sufficiently long ($\lambda L > 2.25$). It can be shown that the same criterion may be used when several loads are present on the beam with the total free length outside of the loads as L. The fundamental fallacy of the conventional computations of beams on elastic subgrade lies in application of the elementary theory to short beams. The "superposition meth-

ods" for beams of finite length are not applicable if the "end-conditioning forces" are not small enough compared to the loads acting on the beam.

These findings have been substantiated by large-scale tests performed recently at the Georgia Institute of Technology, Atlanta, with steel beams resting on a subgrade of compacted silt.[14,15]

CONCLUSIONS

1. A rigorous solution of the considered problem indicates that the ratio of pressures and deflections along the beam is practically constant if the beam has an infinite length. The approximate value of this constant ratio, defined in

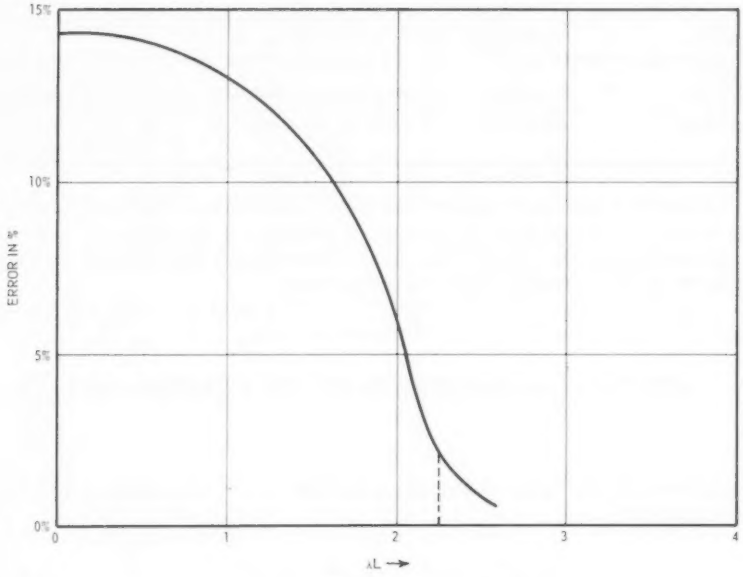

FIG. 6.—ERROR IN MAXIMUM MOMENT UNDER A CONCENTRATED LOAD IF THE COMPUTATION IS MADE BY THE CONVENTIONAL ANALYSIS

the elementary theory of beams on elastic subgrade as the coefficient of subgrade reaction k, can be computed by Eq. 38.

2. When beams of infinite length resting on an elastic-isotropic half-space are analyzed by means of the elementary theory based on coefficient of sub-

---

14 "Beams on Elastic Subgrade and the Winkler's Hypothesis," by A. B. Vesić, Proceedings, Fifth Internatl. Conf. on Soil Mech. and Foundation Engrg., Paris, 1961 (in press).

15 "Model Studies of Beams Resting on a Silt Subgrade," by A. B. Vesić and W. H. Johnson (in preparation, 1961).

grade reaction k, bending moments in the beam are overestimated, contact pressures and deflections underestimated. The amount of error, depending on the relative stiffness of the beam, is shown in Fig. 5 and Table 3.

TABLE 4.—RECOMMENDED PROCEDURES FOR ANALYSIS

Size of Beam (1)	Criterion for distinction (2)	Recommended Procedure	
		For Rough Estimates (3)	For Refined Analysis (4)
Long Beams	$\lambda L > 5.00$	Conventional analysis assuming infinite beam and estimating K by means of Eq. 38	
Moderately Long Beams	$2.25 < \lambda L < 5.00$	Conventional analysis as finite beam; K-value by means of Eq. 38	
Moderately Short Beams	$0.80 < \lambda L < 2.25$	conventional analysis	De Beer, Ohde, or similar methods
Short Beams	$\lambda L < 0.80$	treat as perfectly rigid	De Beer, Ohde, or similar methods

3. Concerning beams of finite length, it is shown that the conventional analysis based on the elementary theory is justified if the beam is sufficiently long. Depending on the value of the length characteristics λL, the procedures for analysis given in Table 4 are recommended.

APPENDIX I.—COMPUTATION OF THE INTEGRAL $J_0(0)$.

Due to the infinite value of the integrand for $\alpha = 0$, the integral was divided into three parts:

$$\left|J_0\right|_0^\infty = \left|J_0\right|_0^\epsilon + \left|J_0\right|_\epsilon^M + \left|J_0\right|_M^\infty \quad \ldots\ldots\ldots\ldots\ldots (46)$$

Here ϵ is an abscissa small enough that $\psi(\beta)$ can be approximated by its asymptotic value

$$\psi(\beta) = \frac{\pi}{2\beta}\left[\log\frac{1}{\beta} + 0.923\right]^{-1} \quad \ldots\ldots\ldots\ldots\ldots (47)$$

M is, as before, the abscissa of the point from where on the integrand can be approximated by a simpler analytical function representing its upper limit (Fig. 3). Both ϵ and M are chosen so as to assure an accuracy of $\pm$ 2% in the final value of the integral.

To compute $\left|J_0\right|_0^\epsilon$, it should be noted that, for small enough values of α, $\cos(\alpha x/c) \approx 1$ and α^4 becomes negligible compared with $\alpha\psi(\beta)$. Therefore:

$$\left|J_0\right|_0^\epsilon = \int_0^\epsilon \frac{\cos(\alpha x/c)\,d\alpha}{\alpha^3 + \psi(\beta)} \approx \int_0^\epsilon \frac{d\alpha}{\alpha\psi(\beta)} \quad \ldots\ldots\ldots (48)$$

Introducing for $\psi(\beta)$ its asymptotic value, Eq. 47, yields

$$\left|J_0\right|_0^{\epsilon} = \frac{2\,b}{\pi\,c} \int_0^{\epsilon} \left[0.923 - \log\left(\frac{b}{c}\,\alpha\right)\right] d\alpha \quad \ldots\ldots\ldots \quad (49)$$

which becomes, by integration,

$$\left|J_0\right|_0^{\epsilon} = \frac{b}{c}\,\epsilon\left[0.5876 + \frac{2}{\pi}\left(1 - \log_e \frac{b}{c}\,\epsilon\right)\right] \quad \ldots\ldots\ldots \quad (50)$$

The term $\left|J_0\right|_{\epsilon}^{M}$ is integrated using Simpson's rule and choosing the number of points for interpolation so as to assure an accuracy of 2%.

For $\left|J_0\right|_M^{\infty}$ M is chosen great enough so that $\psi(\beta)$ can be disregarded in comparison with α^3. Thus

$$\left|J_0\right|_M^{\infty} \approx \int_M^{\infty} \frac{\cos(\alpha\,x/c)\,d\alpha}{\alpha^4} \quad \ldots\ldots\ldots\ldots \quad (51)$$

This integral can be evaluated analytically, giving

$$\left|J_0\right|_M^{\infty} = \frac{1}{3}\,\frac{\cos\xi M}{3} - \frac{1}{6}\,\frac{\xi \sin\xi M}{M^2} - \frac{1}{6}\,\frac{\xi^2\cos\xi M}{M} + \frac{1}{6}\,\xi^3\left[\frac{\pi}{2} - \mathrm{Si}(\xi M)\right] \ldots (52)$$

in which $\xi = \frac{x}{c}$. Evidently for x = 0 this expression becomes

$$\left|J_0\right|_M^{\infty} = \frac{1}{3\,M^3} \quad \ldots\ldots\ldots\ldots\ldots\ldots \quad (53)$$

APPENDIX II.—NOTATIONS

The following symbols adopted for use in the paper and for the guidance of discussers, conform essentially with "American Standard Letter Symbols for Structural Analysis" (ASA Z10.8-1949), prepared by a committee of the American Standards Association with Society representation, and approved by the Association in 1949.

B = width of the beam = 2b, in inches

b = half-width of the beam, in inches

C = a function of β; C = 1.00 if the distribution of pressure across the beam is uniform; $1.00 < C < 1.13$ if the deflection across the beam is uniform

c = fundamental length of the beam = $\left[C\left(1-\mu_s{}^2\right) E_b\, I/E_s\right]^{1/3}$

E_b = Young's modulus for the beam, in pounds per square inch

E_s = Young's modulus for the subgrade, in pounds per square inch

e = 2.718

I = moment of inertia of the beam, in inches^4

J_0-J_5 = integrals defined in Eqs. 5 through 9 and Eqs. 13 through 17

K = modulus of subgrade reaction = kB, in pounds per square inch

K_∞ = modulus of subgrade reaction for an infinite beam, in pounds per square inch

$\overline{K}$ = modulus of subgrade reaction for a square plate, in pounds per square inch

k = coefficient of subgrade reaction, in pounds per cubic inch

k_∞ = value of coefficient of subgrade reaction for a beam of infinite length, in pounds per cubic inch

$\overline{k}$ = value of coefficient of subgrade reaction for a square plate, in pounds per cubic inch

L = length of the beam, in inches

M = Bending moment in the beam, in inches

M = a particular value of α

$\mathbf{M}$ = a couple acting on the beam, in pounds per inch

P = a concentrated load, in pounds

p = pressure at the contact between the beam and the subgrade, in pounds per inch

V = shearing force in the beam, in pounds

w = deflection of the beam, in inches

x = abscissa along the beam, in inches

Δx = increment of abscissa along the beams, in inches

x_0 = abscissa of the first zero of J_2, in inches

Z = any influence in the beam

Z_1 = influence in the beam due to a concentrated load P = 1

α = a dimensionless parameter

β = $b\alpha/c$

ϵ = a very small value of α

θ = slope of the elastic line of the beam

λ = damping factor-expression (36), in inches^{-1}

λ' = a parameter defined by (23) and (25), in inches^{-1}

μ_s = Poisson's ratio for the subgrade

ξ = x/c

π = 3.14

$\psi(\beta)$ = a function tabulated for $\beta > 0.1$ and given by an asymptotic expression for $\beta < 0.1$.

Journal of the
ENGINEERING MECHANICS DIVISION
Proceedings of the American Society of Civil Engineers

CONTINUOUS BEAM-COLUMNS ON ELASTIC FOUNDATION

By S. L. Lee,[1] M. ASCE, T. M. Wang,[2] and J. S. Kao[3]

SYNOPSIS

The analysis of continuous beam-columns on elastic foundation by means of the slope-deflection equations and related problems are presented. The application of the moment-distribution method to problems involving large numbers of spans is demonstrated by numerical example, and the computation of the critical axial force is illustrated by the treatment of a particular problem.

INTRODUCTION

Notation.—The letter symbols adopted for use in this paper are defined where they first appear, in the illustrations, or in the text, and are arranged alphabetically, for convenience of reference, in the Appendix.

General.—The differential equation of the elastic curve of a beam-column on an elastic foundation with uniform cross section[4] shown in Fig. 1 is

$$E\,I\,\frac{d^4y}{dx^4} + N\,\frac{d^2y}{dx^2} + k\,y = p(x) \quad \ldots\ldots\ldots\ldots\ldots (1)$$

Note.—Discussion open until September 1, 1961. To extend the closing date one month, a written request must be filed with the Executive Secretary, ASCE. This paper is part of the copyrighted Journal of the Engineering Mechanics Division, Proceedings of the American Society of Civil Engineers, Vol. 87, No. EM 2, April, 1961.

[1] Prof. of Civ. Engrg., Northwestern Univ., Evanston, Ill.
[2] Graduate Student, Civ. Engrg. Dept., Northwestern Univ., Evanston, Ill.
[3] Graduate Student, Civ. Engrg. Dept., Northwestern Univ., Evanston, Ill.

[4] "Beams on Elastic Foundation," by M. Héteyni, The University of Michigan Press, Ann Arbor, Mich., 1946, p. 135.

in which E I is the flexual rigidity, N denotes the axial force, k represents the foundation modulus and p(x) is the transverse load. The general solution of Eq. 1 may be written in the form

$$y(x) = \left(A_1\, e^{\beta x} + A_2\, e^{-\beta x}\right)\cos(\alpha x) + \left(A_3\, e^{\beta x} + A_4\, e^{-\beta x}\right)\sin(\alpha x) + y_p(x) \quad . . \quad (2)$$

in which $y_p(x)$ is a particular integral of Eq. 1 and

$$\alpha = \sqrt{\sqrt{\frac{k}{4\,E\,I}} + \frac{N}{4\,E\,I}} \quad \ldots\ldots\ldots\ldots\ldots \quad (3a)$$

and

$$\beta = \sqrt{\sqrt{\frac{k}{4\,E\,I}} - \frac{N}{4\,E\,I}} \quad \ldots\ldots\ldots\ldots\ldots \quad (3b)$$

Substituting Eq. 2 in the following boundary conditions

$$y(0) = y_a \quad \ldots\ldots\ldots\ldots\ldots\ldots \quad (4a)$$

$$y(1) = y_b \quad \ldots\ldots\ldots\ldots\ldots\ldots \quad (4b)$$

$$y''(0) = -\frac{M_{ab}}{E\,I} \quad \ldots\ldots\ldots\ldots\ldots \quad (4c)$$

and

$$y''(1) = \frac{M_{ba}}{E\,I} \quad \ldots\ldots\ldots\ldots\ldots \quad (4d)$$

leads to four equations, the solution of which yields the constants of integration A_1, A_2, A_3, and A_4. Substituting these constants in Eq. 2 and taking the particular solution in the form

$$y_p(x) = B_0\, p(x) + B_1\, p'(x) + B_2\, p''(x) \ldots\ldots\ldots\ldots \quad (5)$$

leads to the equation of the elastic curve

$$y(x) = C_1 \cos(h\beta x)\cos(\alpha x) + C_2 \cos(h\beta x)\sin(\alpha x) + C_3 \sin(h\beta x)\cos(\alpha x) + C_4 \sin(h\beta x)\sin(\alpha x) + y_p(x) \ldots\ldots\ldots\ldots\ldots\ldots\ldots \quad (6)$$

in which

$$y_p(x) = \frac{1}{k}\,p(x) - \frac{N}{k^2}\,p''(x) + \frac{1}{k^2}\left(\frac{N^2}{k} - K\,l\right)p^{IV}(x) - \frac{N}{k^3}\left(\frac{N^2}{k} - 2\,K\,l\right)p^{VI}(x) + \frac{1}{k^3}\left(\frac{N^4}{k^2} - \frac{3\,N^2\,K\,l}{k} + K^2\,l^2\right)p^{VIII}(x) \quad \ldots\ldots\ldots\ldots\ldots \quad (7)$$

and

$$C_1 = y_a - y_p(0) \quad \ldots\ldots\ldots\ldots\ldots \quad (8a)$$

$$C_2 = \zeta_{10}\left[\frac{M_{ab}\,l}{K} + l^2\,y_p''(0)\right] + \zeta_8\left[\frac{M_{ba}\,l}{K} - l^2\,y_p''(1)\right] - \zeta_{12}\left[y_a - y_p(0)\right] + \zeta_{13}\left[y_b - y_p(1)\right] \ldots\ldots\ldots\ldots\ldots\ldots\ldots\ldots \quad (8b)$$

$$C_3 = -\zeta_7\left[\frac{M_{ab}\,l}{K} + l^2\,y_p''(0)\right] - \zeta_9\left[\frac{M_{ba}}{K} - l^2\,y_p''(1)\right] + \zeta_{11}\left[y_a - y_p(0)\right] - \zeta_{14}\left[y_b - y_p(1)\right] \ldots\ldots\ldots\ldots\ldots\ldots\ldots\ldots \quad (8c)$$

$$C_4 = \zeta_1 \left[y_a - y_p(0) \right] - \zeta_2 \left[\frac{M_{ab}\, l}{K} + l^2\, y_p''(0) \right] \quad \ldots\ldots\ldots \quad (8d)$$

and

$$\zeta_1 = \frac{\phi^2 - \psi^2}{2\,\phi\,\psi} \quad \ldots\ldots\ldots\ldots\ldots\ldots \quad (9a)$$

$$\zeta_2 = \frac{1}{2\,\phi\,\psi} \quad \ldots\ldots\ldots\ldots\ldots\ldots \quad (9b)$$

$$\zeta_3 = \frac{\sin\phi \cos\psi}{\cos(h^2\,\psi) - \cos^2\phi} \quad \ldots\ldots\ldots\ldots \quad (9c)$$

$$\zeta_4 = \frac{\sin(h\,\psi) \cos\phi}{\cos(h^2\,\psi) - \cos^2\phi} \quad \ldots\ldots\ldots\ldots \quad (9d)$$

$$\zeta_5 = \frac{\cos(h\,\psi) \sin\phi}{\cos(h^2\,\psi) - \cos^2\phi} \quad \ldots\ldots\ldots\ldots \quad (9e)$$

$$\zeta_6 = \frac{\sin(h\,\psi) \cos(h\,\psi)}{\cos(h^2\,\psi) - \cos^2\phi} \quad \ldots\ldots\ldots\ldots \quad (9f)$$

$$\zeta_7 = \zeta_2\, \zeta_3 \quad \ldots\ldots\ldots\ldots\ldots\ldots \quad (9g)$$

$$\zeta_8 = \zeta_2\, \zeta_4 \quad \ldots\ldots\ldots\ldots\ldots\ldots \quad (9h)$$

$$\zeta_9 = \zeta_2\, \zeta_5 \quad \ldots\ldots\ldots\ldots\ldots\ldots \quad (9i)$$

$$\zeta_{10} = \zeta_2\, \zeta_6 \quad \ldots\ldots\ldots\ldots\ldots\ldots \quad (9j)$$

$$\zeta_{11} = \zeta_1\, \zeta_3 - \zeta_6 \quad \ldots\ldots\ldots\ldots\ldots\ldots \quad (9k)$$

$$\zeta_{12} = \zeta_1\, \zeta_6 + \zeta_3 \quad \ldots\ldots\ldots\ldots\ldots\ldots \quad (9l)$$

$$\zeta_{13} = \zeta_1\, \zeta_4 + \zeta_5 \quad \ldots\ldots\ldots\ldots\ldots\ldots \quad (9m)$$

$$\zeta_{14} = \zeta_1\, \zeta_5 - \zeta_4 \quad \ldots\ldots\ldots\ldots\ldots\ldots \quad (9n)$$

and

$$\phi = \alpha\, l \quad \ldots\ldots\ldots\ldots\ldots\ldots \quad (10a)$$

$$\psi = \beta\, l \quad \ldots\ldots\ldots\ldots\ldots\ldots \quad (10b)$$

and

$$K = \frac{E\, I}{l} \quad \ldots\ldots\ldots\ldots\ldots\ldots \quad (10c)$$

and l is the length of the beam-column.

Differentiating Eq. 6 with respect to x yields the slope

$$y'(x) = C_1' \cos(h\,\beta\,x) \cos(\alpha\,x) + C_2' \cos(h\,\beta\,x) \sin(\alpha\,x) + C_3' \sin(h\,\beta\,x) \cos(\alpha\,x) + C_4' \sin(h\,\beta\,x) \sin(\alpha\,x) + y_p'(x) \quad \ldots\ldots\ldots\ldots\ldots\ldots \quad (11)$$

in which

$$C_1' = \alpha\, C_2 + \beta\, C_3 \quad \ldots\ldots\ldots\ldots\ldots \quad (12a)$$

$$C_2' = -\alpha\, C_1 + \beta\, C_4 \quad \ldots\ldots\ldots\ldots\ldots \quad (12b)$$

$$C_3' = \alpha\, C_4 + \beta\, C_1 \quad \ldots\ldots\ldots\ldots\ldots\ldots (12c)$$

and

$$C_4' = -\alpha\, C_3 + \beta\, C_2 \quad \ldots\ldots\ldots\ldots\ldots\ldots (12d)$$

Differentiating Eq. 11 leads to the curvature

$$-\frac{M(x)}{E\,I} = y''(x) = C_1'' \cos(h\,\beta\,x)\cos(\alpha\,x) + C_2'' \cos(h\,\beta\,x)\sin(\alpha\,x) + C_3'' \sin(h\,\beta\,x)\cos(\alpha\,x) + C_4'' \sin(h\,\beta\,x)\sin(\alpha\,x) + y_p''(x) \quad \ldots\ldots (13)$$

in which $M(x)$ is the bending moment and

$$C_1'' = (\beta^2 - \alpha^2)\, C_1 + 2\,\alpha\,\beta\, C_4 \quad \ldots\ldots\ldots\ldots (14a)$$

$$C_2'' = (\beta^2 - \alpha^2)\, C_2 - 2\,\alpha\,\beta\, C_3 \quad \ldots\ldots\ldots\ldots (14b)$$

$$C_3'' = (\beta^2 - \alpha^2)\, C_3 + 2\,\alpha\,\beta\, C_2 \quad \ldots\ldots\ldots\ldots (14c)$$

and

$$C_4'' = (\beta^2 - \alpha^2)\, C_4 - 2\,\alpha\,\beta\, C_1 \quad \ldots\ldots\ldots\ldots (14d)$$

Differentiating Eq. 13 yields

$$-\frac{V(x)}{E\,I} = y'''(x) = C_1''' \cos(h\,\beta\,x)\cos(\alpha\,x) + C_2''' \cos(h\,\beta\,x)\sin(\alpha\,x) + C_3''' \sin(h\,\beta\,x)\cos(\alpha\,x) + C_4''' \sin(h\,\beta\,x)\sin(\alpha\,x) + y_p'''(x) \quad \ldots\ldots (15)$$

in which $V(x)$ is the shearing force and

$$C_1''' = (\beta^3 - 3\,\alpha^2\,\beta)\, C_3 - (\alpha^3 - 3\,\alpha\,\beta^2)\, C_2 \quad \ldots\ldots\ldots (16a)$$

$$C_2''' = (\beta^3 - 3\,\alpha^2\,\beta)\, C_4 + (\alpha^3 - 3\,\alpha\,\beta^2)\, C_1 \quad \ldots\ldots\ldots (16b)$$

$$C_3''' = (\beta^3 - 3\,\alpha^2\,\beta)\, C_1 - (\alpha^3 - 3\,\alpha\,\beta^2)\, C_4 \quad \ldots\ldots\ldots (16c)$$

and

$$C_4''' = (\beta^3 - 3\,\alpha^2\,\beta)\, C_2 + (\alpha^3 - 3\,\alpha\,\beta^2)\, C_3 \quad \ldots\ldots\ldots (16d)$$

It is obvious from Eqs. 8 that, under any loading condition, once the end moments M_{ab} and M_{ba} and the end deflections y_a and y_b are determined, the equation of the elastic curve is given by Eq. 5. The determination of the end moments and end deflections will be examined subsequently.

SLOPE-DEFLECTION EQUATIONS

Substituting Eq. 6 in the boundary conditions

$$y'(0) = \theta_a \quad \ldots\ldots\ldots\ldots\ldots\ldots (17a)$$

and

$$y'(1) = \theta_b \quad \ldots\ldots\ldots\ldots\ldots\ldots (17b)$$

and solving the resulting equations for M_{ab} and M_{ba} yield the slope-deflection equations[5]

[5] "Engineering Studies 1 (Slope Deflection Method)," by G. A. Maney, Univ. of Minnesota, Minneapolis, Minn., 1915.

$$M_{ab} = S_1 K \theta_a + S_2 K \theta_b + S_3 K \frac{y_a}{l} - S_4 K \frac{y_b}{l} + M_{Fab} \quad \ldots\ldots (18a)$$

and

$$M_{ba} = S_2 K \theta_a + S_1 K \theta_b + S_4 K \frac{y_a}{l} - S_3 K \frac{y_b}{l} + M_{Fba} \quad \ldots\ldots (18b)$$

in which

$$S_1 = \frac{\phi \psi \left[\phi \sin(h\, 2\psi) - \psi \sin(2\phi)\right]}{\phi^2 \sin(h^2 \psi) - \psi^2 \sin^2 \phi} \quad \ldots\ldots\ldots\ldots (19a)$$

$$S_2 = \frac{2 \phi \psi \left[\psi \sin\phi \cos(h\psi) - \phi \cos\phi \sin(h\psi)\right]}{\phi^2 \sin(h^2 \psi) - \psi^2 \sin^2 \phi} \quad \ldots\ldots (19b)$$

$$S_3 = \frac{(\phi^2 + \psi^2)\left[\phi^2 \sin h^2 \psi + \psi^2 \sin^2 \phi\right]}{\phi^2 \sin(h^2 \psi) - \psi^2 \sin^2 \phi} \quad \ldots\ldots\ldots (19c)$$

$$S_4 = \frac{\phi^2 + \psi^2 \left[2 \phi \psi \sin(h\psi) \sin\phi\right]}{\phi^2 \sin(h\psi) - \psi^2 \sin^2 \phi} \quad \ldots\ldots\ldots\ldots (19d)$$

and

$$M_{Fab} = -S_3 K \frac{y_p(0)}{l} + S_4 K \frac{y_p(1)}{l} - S_1 K y_p'(0) + S_2 K y_p'(1) - K l y_p''(0) \ldots (20a)$$

and

$$M_{Fba} = -S_4 K \frac{y_p(0)}{l} + S_3 K \frac{y_p(1)}{l} - S_2 K y_p'(0) + S_1 K y_p'(1) + K l y_p''(1) \ldots (20b)$$

In Eq. 18, M_{ab} and M_{ba} are positive if acting clockwise on the member, θ_a and θ_b are positive if clockwise and downward, y_a and y_b are positive (Fig. 1).

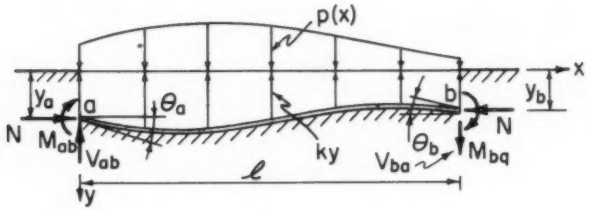

FIG. 1.—BEAM-COLUMN ON ELASTIC FOUNDATION

The fixed-end moments, M_{Fab} and M_{Fba}, are positive if acting clockwise on the member and the ratio

$$C = \frac{S_2}{S_1} = \frac{2\left[\psi \sin\phi \cos(h\psi) - \phi \cos\phi \sin(h\psi)\right]}{\phi \sin(h\, 2\psi) - \psi \sin(2\phi)} \quad \ldots\ldots (21)$$

is usually called the carry-over factor in the moment-distribution method[6] for analyzing continuous frames.

If end b (Fig. 1) is hinged, that is, $M_{ba} = 0$, Eq. 18(a) becomes

$$M'_{ab} = S_5 K \theta_a + S_6 K \frac{y_a}{l} - S_7 K \frac{y_b}{l} + M_{Fab} - C M_{Fba} \quad \ldots\ldots (22)$$

6 "Analysis of Continuous Frames by Distributing Fixed-End Moments," by H. Cross, Transactions, ASCE, Vol. 96, 1932.

in which

$$S_5 = \frac{4\,\phi\,\psi\left[\cos(h^2\,\psi) - \cos^2\phi\right]}{\phi\,\sin(h\,2\,\psi) - \psi\,\sin(2\,\phi)} \quad \ldots\ldots\ldots\ldots (23a)$$

$$S_6 = \frac{(\phi^2 + \psi^2)\left[\phi\,\sin(h\,2\,\psi) + \psi\,\sin(2\,\phi)\right]}{\phi\,\sin(h\,2\,\psi) - \psi\,\sin(2\,\phi)} \quad \ldots\ldots\ldots (23b)$$

and

$$S_7 = \frac{2(\phi^2 + \psi^2)\left[\psi\,\cos(h\,\psi)\,\sin\phi + \phi\,\sin(h\,\psi)\,\cos\phi\right]}{\phi\,\sin(h\,2\,\psi) - \psi\,\sin(2\,\phi)} \quad \ldots (23c)$$

The procedure for computing the end deflections and end moments by the use of the slope-deflection equations is best illustrated by means of numerical example.

EXAMPLE 1

Consider the continuous beam-columns on elastic foundation loaded as shown in Fig. 2(a). End a is fixed, end c is hinged while point b rests on a spring support, the spring constant being $30\,E\,I/l^3$.

For span ab, $\phi = 2.3186$ and $\psi = 2.1510$ and (5) yields

$$y_p(x) = \frac{w}{k} = 10^{-3}\,l \quad \ldots\ldots\ldots\ldots\ldots (24)$$

In this case Eqs. 18 give

$$M_{ab} = 2.8728\,K\,\theta_b - 6.5862\,K\,\frac{y_b}{l} - 14.478\times 10^{-3}\,K \quad \ldots\ldots (25a)$$

and

$$M_{ba} = 9.3010\,K\,\theta_b - 21.064\,K\,\frac{y_b}{l} + 14.478\times 10^{-3}\,K \quad \ldots\ldots (25b)$$

in which $K = E\,I/l$. Setting $x = l$ in Eq. 15 yields

$$V_{ab}(l) = -2\,E\,I\,y'''_{ab}(l) = -2\times 10^{-3}\,\frac{K}{l}\left(9032.9\,\theta_b - 44302\,\frac{y_b}{l} + 44.055\right) \ldots\ldots (26)$$

For span bc, $\psi = 3.0266$ and $\psi = 2.8566$ whereas $y_p(x) = 0$. In this case Eq. 22 gives

$$M_{bc} = 5.6684\,K\,\theta_b + 17.272\,K\,\frac{y_b}{l} \quad \ldots\ldots\ldots\ldots (27)$$

and setting $x = 0$ in Eq. 15 leads to

$$V_{bc}(0) = -\,E\,I\,y'''_{bc}(0) = -\,10^{-3}\,\frac{K}{l}\left(15270\,\theta_b + 99450\,\frac{y_b}{l}\right) \ldots\ldots (28)$$

The equilibrium conditions at support b require that

$$M_{ba} + M_{bc} = 0 \quad \ldots\ldots\ldots\ldots\ldots\ldots (29a)$$

and

$$V_{ab}(l) - V_{bc}(0) + 30\,\frac{E\,I}{l^3}\,y_b = 0 \quad \ldots\ldots\ldots\ldots (29b)$$

Substituting Eqs. 25, 26, 27 and 28 in Eqs. 29 leads to

$$14.969\,\theta_b - 3.7920\,\frac{y_b}{l} + 14.478\times 10^{-3} = 0 \quad \ldots\ldots\ldots (30a)$$

and

$$-\,3.7920\,\theta_b + 295.75\,\frac{y_b}{l} - 119.51\times 10^{-3} = 0 \quad \ldots\ldots\ldots (30b)$$

the solution of which yields $\theta_b = -0.86765 \times 10^{-3}$ and $y_b = 0.39294 \times 10^{-3}$ l. Substituting these values in Eqs. 25 and 27 gives

$$M_{ab} = -19.558 \times 10^{-3} \text{ K} \quad \ldots\ldots\ldots\ldots\ldots\ldots (31a)$$

and

$$-M_{ba} = M_{bc} = 1.8688 \times 10^{-3} \text{ K} \quad \ldots\ldots\ldots\ldots (31b)$$

Finally, substituting the end moments and end deflection of each span in Eq. 6 leads to

$$y_{ab}(x) = 10^{-3} l \left[-\cos(h\beta_1 x)\cos(\alpha_1 x) - 1.0132 \cos(h\beta_1 x)\sin(\alpha_1 x) + 1.0919 \sin(h\beta_1 x)\cos(\alpha_2 x) + 0.90525 \sin(h\beta_1 x)\sin(\alpha x) + 1 \right] \ldots (32a)$$

and

$$y_{bc}(x) = 10^{-3} l \left[0.39249 \cos(h\beta_2 x)\cos(\alpha_2 x) + 0.08646 \cos(h\beta_2 x)\sin(\alpha_2 x) - 0.39533 \sin(h\beta_2 x)\cos(\alpha_2 x) - 0.08534 \sin(h\beta_2 x)\sin(\alpha_2 x) \right] \ldots (32b)$$

in which $\alpha_1 = 2.3186/l$, $\beta_1 = 2.1510/l$, $\alpha_2 = 3.0266/l$ and $\beta_2 = 2.8566/l$.

The expressions for $y'(x)$, $M(x)$ and $V(x)$, if desired, may be obtained either by means of Eqs. 11, 13, and 15 or by successive differentiations of Eqs. 32.

MOMENT-DISTRIBUTION METHOD

When the number of spans increases, the number of unknown displacement components and equilibrium equations, such as Eqs. 30, increases accordingly. To avoid the solution of large number of simultaneous equations in such cases, the end moments and end deflections can be computed by means of the moment-distribution method.[6]

It can be seen from Eq. 18(a) that the bending stiffness of end a is S_1 K, that is, S_1 K is the value of M_{ab} required to cause $\theta_a = 1$ and $\theta_b = y_a = y_b = 0$, when $p(x) = 0$. Also, under these boundary conditions, Eq. 18(a) gives $M_{ba} = S_2$ K. Therefore, the carry-over factor is $C = M_{ba}/M_{ab} = S_2/S_1$, as defined by Eq. 21. For a beam-column with the far end hinged, the bending stiffness of the near end is S_5 K as indicated in Eq. 22.

The application of this method is best illustrated by means of a numerical example.

EXAMPLE 2

The values of the end moments and the deflection of point C in the continuous beam-column shown in Fig. 2(a) treated in Example 1 will now be computed by the moment-distribution method. This is done in two stages shown in Figs. 2(b) and (c), respectively. The bending stiffnesses of members ba and bc are 9.3010 k and 5.6684 k, respectively, as computed in Eqs. 25 and 27. Hence the distribution factors are

$$r_{ba} = \frac{9.3010 \text{ K}}{9.3010 \text{ K} + 5.6684 \text{ K}} = 0.62134$$

$$r_{bc} = \frac{5.6684 \text{ K}}{9.3010 \text{ K} + 5.6684 \text{ K}} = 0.37866$$

The carry-over factor from b to a is 0.30885 as given by Eq. 21 for $\phi = 2.3186$ and $\psi = 2.1510$. Since end c is hinged, the carry-over factor from b to c is of course zero.

In Fig. 2(b), an auxiliary force R'_b is introduced at point b so as to restrain point b from deflecting. The corresponding moment distribution operation is shown in Table 1. The distribution and carry-over factors are entered in row 1. The fixed-end moments due to the uniformly distributed load on span ab, shown in row 2, are computed by Eqs. 20 as in Eqs. 25. The distri-

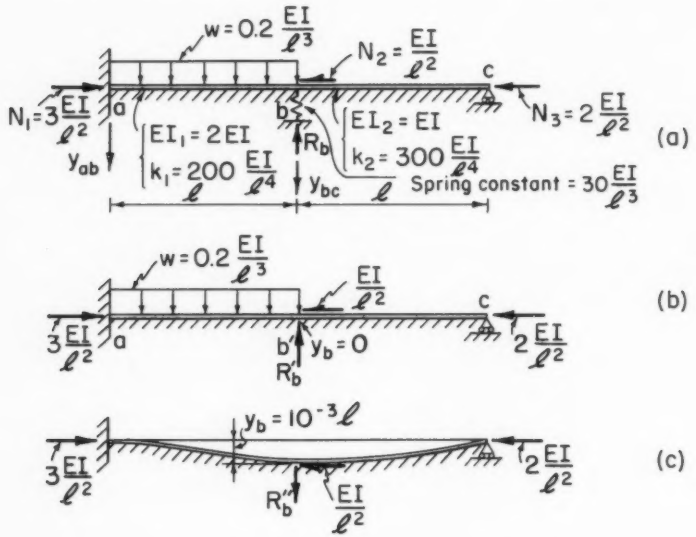

FIG. 2.—CONTINUOUS BEAM-COLUMN ON ELASTIC FOUNDATION

bution and carry-over operations are indicated in row 3 and the resulting end moments in row 4. The value of the auxiliary force at b is

$$R'_b = V_{bc}(0) - V_{ab}(1) = (14.769 + 70.632)\left(10^{-3}\frac{EI}{l^2}\right) = 85.401\times10^{-3}\frac{EI}{l^2} \quad \ldots (33)$$

in which $V_{bc}(0)$ and $V_{ab}(1)$ are computed by Eq. 15.

To allow for the deflection of the spring support, point b is arbitrarily deflected downward a distance $y_b = 10^{-3}\,l$ as shown in Fig. 2(c). The corresponding fixed-end moments are

$$M'_{Fab} = -\,6.5862\times10^{-3}\,K \quad \ldots (34a)$$

$$M'_{Fba} = -\,21.064\times10^{-3}\,K \quad \ldots (34b)$$

and

$$M'_{Fbc} = 17.272\times10^{-3}\,K \quad \ldots (34c)$$

and are entered in row 5 of Table 1. M'_{Fab} and M'_{Fba} are computed from Eq. 18(a) by setting $\theta_a = \theta_b = y_a = 0$ and $M_{Fab} = M_{Fba} = 0$, and M'_{Fba} is determined in a similar manner by Eq. 22. The distribution and carry-over operations are shown in row 6 and the resulting end moments in row 7. The corresponding value of R''_b is

$$R''_b = V_{ab}(1) - V_{bc}(0) = (83.914 + 103.32)\left(10^{-3}\frac{EI}{l^2}\right) = 187.23\times10^{-3}\frac{EI}{l^2} \quad \ldots (35)$$

The end moments and y_b of the system shown in Fig. 2(a) can now be determined by the superposition of the two systems shown in Figs. 2(b) and (c),

TABLE 1.—DISTRIBUTION TABLE FOR EXAMPLE 2

Row[a] (1)	M_{ab} (2)	C (3)	M_{ba} (4)	M_{bc} (5)
1	. . .	.30885	.62134	.37866
2	-14.478		14.478	
3	- 2.778	←	- 8.9958	- 5.4822
4	-17.256		5.4822	- 5.4822
5	- 6.5862		-21.064	17.272
6	0.7277	←	2.356	1.436
7	- 5.8585		-18.708	18.708

[a] All values in rows 2 to 7 to be multiplied by 10^{-3} K.

respectively. Let M, M′ and M″ denote, respectively, the end moments of the three systems. It is evident that they are related by

$$M = M' + \alpha M'' \quad \ldots\ldots\ldots\ldots\ldots\ldots \quad (36)$$

in which α is a proportional factor determined by the equilibrium condition

$$R_b = R'_b - \alpha R''_b \quad \ldots\ldots\ldots\ldots\ldots\ldots \quad (37)$$

or

$$\alpha\left(30\,\frac{E\,I}{l^3}\right)\left(10^{-3}\,l\right) = 85.401\times10^{-3}\,\frac{E\,I}{l^2} - \alpha\left(187.23\,\frac{E\,I}{l^2}\right) \quad \ldots \quad (38)$$

which yields $\alpha = 0.39314$. Hence, the deflection of point b is

$$y_b = \alpha\left(10^{-3}\,l\right) = 0.39314\times10^{-3}\,l \quad \ldots\ldots\ldots\ldots \quad (39)$$

and the end moments are

$$M_{ab} = \left[-17.256 + \alpha(-5.8585)\right]\left(10^{-3}\ \text{K}\right) = -19.559\times10^{-3}\ \text{K} \quad \ldots \quad (40a)$$

and

$$-M_{ba} = M_{bc} = \left[-5.4822 + \alpha(18.708)\right]\left(10^{-3}\ \text{K}\right) = 1.8727\times10^{-3}\ \text{K} \quad \ldots \quad (40b)$$

These values are in good agreement with the results of Example 1.

CRITICAL AXIAL FORCE

Use of slope-deflection equations in computing buckling loads of continuous beam-columns on elastic foundation.—Consider again the continuous beam-columns shown in Fig. 2(a). In the present instance, however, w = 0 and the loading consists of $N_1 = 1.5\,\rho\,E\,I/l^2$, $N_2 = 0.5\,\rho\,E\,I/l^2$ and $N_3 = \rho\,E\,I/l^2$ in which ρ is a parameter. The two equilibrium equations given by Eqs. 29 still apply in this case with the exception, of course, that M_{ba}, M_{bc}, $V_{ab}(1)$, and $V_{bc}(0)$ are changed. Expressing these end moments and end shearing forces in terms of θ_a and y_b by means of Eq. 18(b), Eq. 22 and Eq. 15, respectively,

and substituting the resulting expressions in Eqs. 29 lead to

$$\eta(\rho)\,\theta_b + \lambda(\rho)\,\frac{y_b}{l} = 0 \quad \ldots\ldots\ldots\ldots\ldots\ldots (41a)$$

and

$$\xi(\rho)\,\theta_b + \chi(\rho)\,\frac{y_b}{l} = 0 \quad \ldots\ldots\ldots\ldots\ldots\ldots (41b)$$

in which

$$\eta(\rho) = 2\,S_1' + S_5'' \quad \ldots\ldots\ldots\ldots\ldots\ldots (42a)$$

$$\lambda(\rho) = -\,2\,S_3' + S_6'' \quad \ldots\ldots\ldots\ldots\ldots\ldots (42b)$$

$$\begin{aligned}\xi(\rho) = 2\Big\{&\Big[\left(\psi_1^3 - 3\,\phi_1^2\,\psi_1\right)\left(\xi_7'\,S_2' + \xi_9'\,S_1'\right) + \left(\phi_1^3 - 3\,\phi_1\,\psi_1^2\right)\left(\xi_{10}'\,S_2'\right.\\ &\left.+\,\xi_8'\,S_1'\right)\Big]\cos(h\,\psi_1)\cos\phi_1 + \left(\psi_1^3 - 3\,\phi_1^3\,\psi_1\right)\xi_2'\,S_2'\cos(h\,\psi_1)\sin\phi_1\\ &-\left(\phi_1^3 - 3\,\phi_1\,\psi_1^2\right)\xi_2'\,S_2'\sin(h\,\psi_1)\cos\phi_1 - \Big[\left(\psi_1^3 - 3\,\phi_1^2\,\psi_1\right)\left(\xi_{10}'\,S_2'\right.\\ &\left.+\,\xi_8'\,S_1'\right) - \left(\phi_1^3 - 3\,\phi_1\,\psi_1^2\right)\left(\xi_7'\,S_2' + \xi_9'\,S_1'\right)\Big]\sin(h\,\psi_1)\sin\phi_1\Big\}\\ &-\left[\left(\psi_2^3 - 3\,\phi_2^2\,\psi_2\right)\xi_7'' + \left(\phi_2^3 - 3\,\phi_2\,\psi_2^2\right)\xi_{10}''\right]S_5'' \quad \ldots\ldots\ldots\ldots (42c)\end{aligned}$$

and

$$\begin{aligned}\chi(\rho) = -\,2\Big\{&\Big[\left(\psi_1^3 - 3\,\phi_1^2\,\psi_1\right)\left(\xi_7'\,S_4' + \xi_9'\,S_3' - \xi_{14}'\right) + \left(\phi_1^3 - 3\,\phi_1\,\psi_1^2\right)\\ &\left(\xi_{10}'\,S_4' + \xi_8'\,S_3' - \xi_{13}'\right)\Big]\cos(h\,\psi_1)\cos\phi_1 + \left(\psi_1^3 - 3\,\phi_1^2\,\psi_1\right)\xi_2'\,S_4'\\ &\cos(h\,\psi_1)\sin\phi_1 - \left(\phi_1^3 - 3\,\phi_1\,\psi_1^2\right)\xi_2'\,S_4'\sin(h\,\psi_1)\cos\phi_1\\ &+\Big[\left(\psi_1^3 - 3\,\phi_1^2\,\psi_1\right)\left(-\,\xi_{10}'\,S_4' - \xi_8'\,S_3' + \xi_{13}'\right) + \left(\phi_1^3 - 3\,\phi_1\,\psi_1^2\right)\\ &\left(\xi_7'\,S_4' + \xi_9'\,S_3' - \xi_{14}'\right)\sin(h\,\psi_1)\sin\phi_1\Big\} - \Big[\left(\psi_2^3 - 3\,\phi_2^2\,\psi_2\right)\xi_2''\\ &+\left(\phi_2^3 - 3\,\phi_2\,\psi_2^2\right)\xi_{10}''\Big]S_6'' + \left(\psi_2^3 - 3\,\phi_2^2\,\psi_2\right)\xi_{11}''\\ &+\left(\phi_2^3 - 3\,\phi_2\,\psi_2^2\right)\xi_{12}'' + 30 \quad \ldots\ldots\ldots\ldots\ldots\ldots (42d)\end{aligned}$$

In Eqs. 42, the subscript 1 and the superscript prime denote items for span ab, 2 and double primes refer to items for span bc and, by Eqs. 3 and 10,

$$\phi_1 = \sqrt{5 + \frac{3}{16}\,\rho} \quad \ldots\ldots\ldots\ldots\ldots\ldots (43a)$$

$$\psi_1 = \sqrt{5 - \frac{3}{16}\,\rho} \quad \ldots\ldots\ldots\ldots\ldots\ldots (43b)$$

$$\phi_2 = \sqrt{5\sqrt{3} + \frac{1}{4}\,\rho} \quad \ldots\ldots\ldots\ldots\ldots\ldots (43c)$$

and

$$\psi_2 = \sqrt{5\sqrt{3} - \frac{1}{4}\,\rho} \quad \ldots\ldots\ldots\ldots\ldots\ldots (43d)$$

For arbitrary values of the parameter ρ, the homogeneous equations (Eqs. 41) are satisfied only when $\theta_a = y_b = 0$, indicating that $y(x)$ is zero and the

continuous beam-columns remain straight. However, Eqs. 41 have non-zero solutions if the determinant of the coefficients vanishes, that is, if

$$D(\rho) = \begin{vmatrix} \eta(\rho) & \lambda(\rho) \\ \xi(\rho) & \chi(\rho) \end{vmatrix} = 0 \quad \ldots\ldots\ldots\ldots \quad (44)$$

With the expansion of $D(\rho)$, Eq. 44 furnishes an equation for the parameter ρ, the only unknown in this equation. The smallest value of ρ which satisfies Eq. 44 defines the critical axial force desired. This value can be determined approximately by the intersection of the D-ρ curve defined by Eq. 44 with the axis D = 0, the curve being plotted by computing at least three points in the vicinity of the intersection. Thus,

$$D(32.5) = 344.2$$

$$D(35.0) = 143.8$$

$$D(38.0) = -\ 87.0$$

The intersection of a smooth curve passing through these three points with D = 0 yields the critical value $\rho_c = 37.0$.

CANTILEVER BEAM-COLUMNS

Cantilever beam-columns on elastic foundation such as the one shown in Fig. 3 can be analyzed by the preceding method. In this case, the constants of

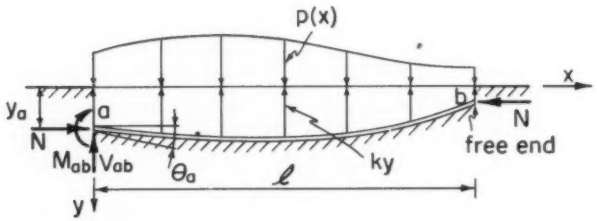

FIG. 3.—CANTILEVER BEAM-COLUMN ON ELASTIC FOUNDATION

integration A_1, A_2, A_3 and A_4 in Eq. 2 are determined by substituting Eq. 2 in the boundary conditions $y(0) = y_a$, $y''(0) = -\frac{M_{ab}}{EI}$, $y''(1) = 0$ and $y'''(1) = 0$. Substitution of the values of these constants in Eq. 2 yields

$$y(x) = C_1 \cos(h\beta x)\cos(\alpha x) + C_5 \cos(h\beta x)\sin(\alpha x) + C_6 \sin(h\beta x)\cos(\alpha x) + C_4 \sin(h\beta x)\sin(\alpha x) + y_p(x) \ldots \quad (45)$$

in which $y_p(x)$ is defined by Eq. 7, C_1 and C_4 by Eqs. 8(a) and 8(d), respectively, and

$$C_5 = \zeta_{24}\left[\frac{M_{ab}\,l}{K} + l^2\, y_p''(0)\right] + \zeta_{17}\left[y_a - y_p(0)\right] + \zeta_{26}\, l^2\, y_p''(1) + \zeta_{28}\, l^3\, y_p'''(1) \ldots (46a)$$

$$C_6 = \zeta_{25}\left[\frac{M_{ab}\,l}{K} + l^2\, y_p''(0)\right] - \zeta_{18}\left[y_a - y_p(0)\right] + \zeta_{27}\, l^2\, y''(1) + \zeta_{29}\, l^3\, y_p'''(1) \ldots (46b)$$

and

$$\zeta_{15} = \frac{1}{(\phi^2 + \psi^2)^2} \quad \ldots\ldots\ldots\ldots\ldots\ldots (47a)$$

$$\zeta_{16} = \frac{(\phi^2 - \psi^2)(\phi^2 - 3\psi^2)\sin(h^2\psi) - 2\psi^2(\psi^2 - 3\phi^2)\cos(h^2\psi)}{\phi\psi\sin(h\,2\psi) - \psi^2\sin(2\phi)} \quad \ldots (47b)$$

$$\zeta_{17} = \frac{(\psi^2 - \phi^2)\sin(h^2\psi) - 2\psi^2\sin^2\phi}{\phi\psi\sin(h\,2\psi) - \psi^2\sin(2\phi)} \quad \ldots\ldots\ldots (47c)$$

$$\zeta_{18} = \frac{2\phi^2\sin(h^2\psi) - (\psi^2 - \phi^2)\sin^2\phi}{\phi^2\sin(h\,2\psi) - \phi\psi\sin(2\phi)} \quad \ldots\ldots\ldots (47d)$$

$$\zeta_{19} = \frac{(\phi^2 - \psi^2)(\psi^2 - 3\phi^2)\sin^2\phi - 2\phi^2(\phi^2 - 3\psi^2)\cos^2\phi}{\phi^2\sin(h\,2\psi) - \phi\psi\sin(2\phi)} \quad \ldots\ldots (47e)$$

$$\zeta_{20} = \frac{2\psi(\psi^2 - 3\phi^2)\cos(h\psi)\cos\phi + 2\phi(\phi^2 - 3\psi^2)\sin(h\psi)\sin\phi}{\phi\sin(h\,2\psi) - \psi\sin(2\phi)} \ldots (47f)$$

$$\zeta_{21} = \frac{2\phi(\phi^2 - 3\psi^2)\cos(h\psi)\cos\phi - 2\psi(\psi^2 - 3\phi^2)\sin(h\psi)\sin\phi}{\phi\sin(h\,2\psi) - \psi\sin(2\phi)} \ldots (47g)$$

$$\zeta_{22} = \frac{4\phi\psi\cos(h\psi)\sin\phi + 2(\phi^2 - \psi^2)\sin(h\psi)\cos\phi}{\phi\sin(h\,2\psi) - \psi\sin(2\phi)} \quad \ldots\ldots (47h)$$

$$\zeta_{23} = \frac{4\phi\psi\sin(h\psi)\cos\phi - 2(\phi^2 - \psi^2)\cos(h\psi)\sin\phi}{\phi\sin(h\,2\psi) - \psi\sin(2\phi)} \quad \ldots\ldots (47i)$$

$$\zeta_{24} = \zeta_{15}\,\zeta_{16} \quad \ldots\ldots\ldots\ldots\ldots\ldots (47j)$$

$$\zeta_{25} = \zeta_{15}\,\zeta_{19} \quad \ldots\ldots\ldots\ldots\ldots\ldots (47k)$$

$$\zeta_{26} = \zeta_{15}\,\zeta_{20} \quad \ldots\ldots\ldots\ldots\ldots\ldots (47l)$$

$$\zeta_{27} = \zeta_{15}\,\zeta_{21} \quad \ldots\ldots\ldots\ldots\ldots\ldots (47m)$$

$$\zeta_{28} = \zeta_{15}\,\zeta_{22} \quad \ldots\ldots\ldots\ldots\ldots\ldots (47n)$$

and

$$\zeta_{29} = \zeta_{15}\,\zeta_{23} \quad \ldots\ldots\ldots\ldots\ldots\ldots (47o)$$

The expressions for $y'(x)$, $y''(x)$, and $y'''(x)$ are similar to those given by Eqs. 11, 13, and 15, and may be obtained by replacing the subscripts 2 and 3 by 5 and 6, respectively.

The slope-deflection equation for a cantilever beam-column on elastic foundation is obtained by setting $y'(0) = \theta_a$ in Eq. 45 which yields

$$M_{ab} = S_8\,K\,\theta_a + S_9\,K\,\frac{y_a}{l} + M''_{Fab} \quad \ldots\ldots\ldots\ldots (48)$$

in which

$$S_8 = \frac{\phi\psi}{\Omega}(\phi^2 + \psi^2)^2\left[\phi\sin(h\,2\psi) - \psi\sin(2\phi)\right] \quad \ldots\ldots (49a)$$

$$S_9 = \frac{1}{\Omega}(\phi^2 + \psi^2)^2\left[\phi^2(\psi^2 - \phi^2)\sin(h^2\psi) + \psi^2(3\phi^2 - \psi^2)\sin^2\phi\right]. \quad (49b)$$

$$\Omega = (\phi^2 + \psi^2)\left\{(\phi^2 + \psi^2)\left[\phi^2\sin(h^2\psi) - \psi^2\sin^2\phi\right] + 4\phi^2\psi^2\right\}. \quad (49c)$$

$$M''_{Fab} = -S_9 K \frac{y_p(0)}{l} - \sigma K l y''_p(1) - \tau K l^2 y'''_p(1) - K l y''_p(0) \quad (49d)$$

$$\sigma = \frac{2\phi\psi}{\Omega}(\phi^2 - \psi^2)\left[(\phi^2 + \psi^2)\sin(h\psi)\sin\phi - 2\phi\psi\cos(h\psi)\cos\phi\right]. \quad (49e)$$

and

$$\tau = \frac{2\phi\psi}{\Omega}(\phi^2 + \psi^2)\left[\psi\cos(h\psi)\sin\phi + \phi\sin(h\psi)\cos\phi\right]. \quad (49f)$$

Continuous beam-columns whose end spans are cantilevered can be treated in the manner illustrated in Examples 1 and 2 by using these expressions.

DISCONTINUOUS LOADS

The particular solution defined by Eq. 7 can be conveniently used in dealing with continuous loads extending over the entire span. In the treatment of discontinuous loads, however, $p(x)$ and $y_p(x)$ may be represented by trigonometric series of the type

$$p(x) = \sum_{n=1}^{\infty} a_n \sin\frac{n\pi x}{l} \quad (50a)$$

and

$$y_p(x) = \sum_{n=1}^{\infty} b_n \sin\frac{n\pi x}{l} \quad (50b)$$

Substituting Eq. 50b in Eq. 1 leads to the particular integral

$$y_p(x) = l^3 \sum_{n=1}^{\infty} \frac{a_n \sin\frac{n\pi x}{l}}{n^4\pi^4 K - n^2\pi^2 N l + k l^3} \quad (51)$$

Although Eq. 51 converges rapidly, the speed of convergence decreases with successive differentiations. It can be shown that Eq. 51 may be replaced by the more convenient form

$$y_p(x) = y_0(x) + \frac{l^4}{\pi^4 K}\sum_{n=1}^{\infty} \frac{a_n(n^2\pi^2 N - k l^2)\sin\frac{n\pi x}{l}}{n^4(n^4\pi^4 K - n^2\pi^2 N l + k l^3)} \quad (52)$$

in which $y_0(x)$ denotes the deflection of the same member with simply supported ends and subjected to the same load when $N = 0$ and $k = 0$, and

$$a_n = \frac{2}{l}\int_0^l p(x)\sin\frac{n\pi x}{l}\,dx \quad (53)$$

For a concentrated load P located at a distance s from the left end, for instance,[7]

---

7 "Analysis of Continuous Beams by Fourier Series," by S. L. Lee, Proceedings, ASCE, Vol. 83, No. EM 4, October, 1957; Transactions, ASCE, Vol. 124, 1959, p. 164.

$$a_n = \lim_{q \to 0} \frac{2}{l} \int_{s-q}^{s+q} \frac{P}{2q} \sin \frac{n \pi x}{l} \, dx = \frac{2P}{l} \sin \frac{n \pi s}{l} \quad \ldots\ldots (54)$$

Introducing $N = \rho E I/l^2$ and $k = \delta E I/l^4$ in Eq. 52 leads to the more compact form of the particular solution

$$y_p(x) = y_0(x) + \frac{l^3}{\pi^4 K} \sum_{n=1}^{\infty} \frac{a_n \left(n^2 \pi^2 \rho - \delta\right) \sin \frac{n \pi x}{l}}{n^4 \left(n^4 \pi^4 - n^2 \pi^2 \rho + \delta\right)} \quad \ldots\ldots (55)$$

In problems involving discontinuous loads, therefore, it is necessary only to replace Eq. 7 by Eq. 55.

CONCLUSIONS

In the preceding, N is assumed to be a compressive axial force. For the case in which N is a tensile axial force, the sign of the second term on the left side of Eq. 1 becomes negative, and the general solution of the resulting differential equation is obtained by interchanging α and β in Eq. 2, α and β being still defined by Eqs. 3. Therefore, all the expressions designated by numerals derived in the foregoing may be used in this case by simply interchanging ϕ and ψ with the exceptions of Eqs. 51, 52, and 55. In the last three expressions, the signs of the terms containing N or ρ should be changed.

Another analogous problem is that of a beam with uniformly distributed elastic restraint against both deflection and rotation. If the rotational restraint against both deflection and rotation. If the rotational restraint is proportional to $y'(x)$, that is, the restraining moment in an element dx is

$$dM_\gamma = \left(\gamma \frac{dy}{dx}\right) dx \quad \ldots\ldots\ldots\ldots\ldots (56)$$

the corresponding differential equation[8] is obtained by replacing N in Eq. 1 by $-\gamma$.

The present analysis can also be extended to the problem of the axisymmetrical bending of cylindrical shells subjected to radial and axial loads. In this instance, p(x) in Eq. 1 represents the radial load per unit length of a longitudinal strip of unit width of the cylinder, N the axial compressive force acting on the strip, E I should be replaced by $\frac{E h^3}{12\left(1 - \mu^2\right)}$ and k by $E h/r^2$. In the latter, μ is Poisson's ratio while h and r denote the thickness and the radius of the cylinder, respectively. In the analysis of cylinders with stiff transverse diaphragms, the latter may be treated as unyielding supports whereas ring stiffeners are analogous to the spring support of Examples 1 and 2. Cylinders with stepped wall thicknesses can be dealt with by considering the individual sections of constant thicknesses as separate spans.

With reference to Examples 1 and 2, the conclusion may be drawn that when the continuous beam-columns are composed of two or three spans, a solution may be conveniently obtained by applying the slope-deflection equations directly. When the number of spans increases, however, the moment-distribution

---

[8] "Beam on Elastic Foundation," by M. Hétenyni, The Univ. of Michigan Press, Ann Arbor, Mich., 1946, p. 139.

method is preferred since the successive approximation technique reduces the number of simultaneous equations needed to achieve a solution.

APPENDIX.—NOTATION

The following symbols are adopted for use in the paper and for the guidance of discussers.

A_1, A_2, A_3, A_4 = constants of integration;

a, b, c = subscripts denoting points;

a_n, b_n = Fourier coefficients defined by Eq. 53;

B_0, B_1, B_2 = undetermined coefficients;

C_1, C_2, C_3, C_4, C_5, C_6 = constants of integration defined by Eqs. 8 and 46;

C = carry-over factor defined by Eq. 21;

D = determinant;

E I = flexural rigidity;

h = thickness of cylindrical shells;

K = E I/l;

k = foundation modulus;

l = length of beam-column;

M, M′, M″ = bending moments;

M_{ab}, M_{ba} = end moments at a and b in member ab;

M_{Fab}, M_{Fba}, M''_{Fab} = fixed-end moments defined by Eqs. 20 and 49(d);

N = axial force;

P = concentrated load;

p(x) = load function;

R_b, R'_b, R''_b = reactions at point b;

r_{ba}, r_{bc} = distribution factors at joint b;

S_1, S_2, S_3, S_4, S_5 S_6, S_7, S_8, S_9 = stiffness factors defined by Eqs. 19, 23, 49(a) and 49(b);

s = distance of P from left end;

V_{ab}, V_{ba} = end shearing forces at a and b in member ab;

V(x) = shear function;

w = uniformly distributed load;

y_a, y_b = end deflections of member ab;

$y(x)$ = deflection function;

$y_0(x)$ = deflection of simply supported member when N = 0 and k = 0 defined by Eq. 52 or Eq. 55;

$y_p(x)$ = particular integral defined by Eq. 7 or Eq. 55;

α_1 β = defined by Eqs. 3;

γ = constant;

δ, ρ = parameters;

ξ_1 to ξ_{29} = constants in deflection functions defined by Eqs. 9 and 47;

η, λ, ξ, χ = coefficients which are functions of ρ;

θ_a, θ_b = end rotations;

μ = Poisson's ratio;

Ω, σ, τ = constants defined by Eq. 49(c), (e), and (f); and

ϕ, ψ = α l and β l, respectively.

Journal of the
ENGINEERING MECHANICS DIVISION
Proceedings of the American Society of Civil Engineers

DISCUSSION

Note.—This paper is part of the copyrighted Journal of the Engineering Mechanics Division, Proceedings of the American Society of Civil Engineers, Vol. 87, No. EM 2, April, 1961.

ANALYSIS OF FRAMES WITH NON-LINEAR BEHAVIOR[a]

Closure by Alfredo H.-S. Ang

ALFREDO H.-S. ANG,[10] A.M. ASCE.—It is reassuring to know that Mr. Wilson's independent results check closely the method presented by the writer.

Wilson points out the effect of vertical loads on the primary forces as a result of large lateral displacements. This point was purposely omitted in the original paper because theoretically, the moment-curvature relationship is a function of the ratio of the magnitude of vertical load to the critical buckling load of a given member.[11] The presence of vertical loads, therefore, is only partially considered when the effect of geometry alone is taken into account. However, if the vertical loads are small compared to the critical buckling loads of the columns, the moment-curvature relationship for pure bending can be used without appreciable error.

It was suggested in the paper that if simple relationships between the moments and the end slopes (for rigid joints),

$$\phi_{ji} = f(M_{ji}, M_{ij})$$

can be found, then the total rotations for each member can be expressed as in Eq. 3 and equations of continuity can be formed for each joint: Solution of these equations gives the end moments. Wilson's approach seems to be along the same general line. He assumes a continuous moment-curvature relationship, as given in Eq. 12, and obtains moment end-slope relationships given by Eq. 13.

For moment-curvature relationships with marked discontinuity, Eq. 12 does not give an accurate representation immediately following initial yielding. Eq. 12 with a = 3 and n= 7 gives too high a resisting moment for a given curvature in this region as may be seen in Fig. 13. The moment-curvature relationships presented as Figs. 3 and 4 are for pure bending. These agree closely with experimentally determined relationships, of members under bending and shear, for regions in which measured moment-curvature measurements are available.[12,13]

---

[10] Asst. Prof. of Civ. Engrg., Univ. of Illinois, Urbana, Ill.

[11] "Static and Dynamic Load-Deflection Tests of Steel Structures," by F. L. Howland, W. Egger, R. J. Mayerjak, and R. J. Munz, Univ. of Illinois Civ. Engrg. Studies, Structural Research Series No. 92, February, 1955.

[12] "Commentary on Plastic Design in Steel: General Provision and Experimental Verification," Progress Report No. 2 of the Joint WRC-ASCE Committee on Plasticity Related to Design, Proceedings, ASCE, Vol. 85, No. 3, July, 1959.

[13] "Shear Deflection of Wide-Flange Steel Beams in the Plastic Range," by W. J. Hall and N. M. Newmark, Transactions, ASCE, Vol. 122, 1957.

With the method proposed by the writer, it is not possible to determine directly or in a single computation the deformation corresponding to a given load. However, in certain problems related to structural dynamics, it is the resistance of a structure corresponding to given deformations that is of interest. It is in this type of problem that the method has greatest application. One advantage of computing for the load corresponding to a given deformation is that in most stress-strain or load-deformation relationships for structural materials, the slopes beyond the yield condition are small, and in certain cases, such as A-7 steel, this slope approaches zero immediately beyond the yield point. Thus, the strain or curvature corresponding to a given stress or moment is not uniquely defined in such regions. Such difficulties are not encountered with the writer's approach.

WIND STRESSES IN DOMES[a]

Discussion by Gerrit H. Toebes

GERRIT H. TOEBES,[16] A.M. ASCE.—The authors intend to furnish information concerning "stresses due to anti-symmetrical wind pressures in a hemispherical dome elastically built into a cylinder." The result would readily permit "their use by the designer." The solution is found "on the conservative side" and because the accuracy of the solution "improves very rapidly with decreasing thickness ratio, the solution is acceptable in all cases of practical significance."

The Static Wind Loading of Shells.—It appears that the previously cited aims are not quite fulfilled. The presented method of analysis is based on an anti-symmetrical distribution of the wind load. Although S. Timoshenko[3] adopted such a sinusoidally varying wind loading, a look at the potential flow net around a circular cylinder, together with the application of the Bernoulli equation would show that the wind load at the sides of the cylinder should be far from zero. In fact, the suction at the surface parallel to wind direction may exceed, in absolute magnitude, the stagnation pressure along the leading edge of the cylinder. An inspection of the streamline picture for the flow past a sphere would afford a similar conclusion. The top of the dome pictured in Fig. 1 would thus be subjected to a large suction loading.

The least that should be done to aid designers of large shells is to select a realistic loading based on wind-tunnel or water-tunnel tests. The paper by Placido Cicala[17] has recognized the uncertainty in regard to the loading. Aside from adopting a more realistic loading from French regulations Cicola's development of an analysis involving a truly general type of loading is a pertinent and an inherently fruitful approach to the problem.

In 1958 a series of six papers by a Committee on Wind Forces appeared in the Journal of the Structural Division. Based on Swiss experiments, loading distributions were presented[18] relevant to the discussed geometry. This information has been compared to the authors' anti-symmetrical loading in Figs. 8 through 11. The discrepancy is evident.

The Dynamic Wind Loading of Structures.—Even though building codes point the way in translating wind forces to static loads the designer should remain aware of the dynamic aspects of the problem. Utilizing static loads even if they correspond to winds of cyclonic or hurricane strength, may give

---

[a] October 1960, by P. Gondikas and M. G. Salvadori (Proc. Paper 2616).

[16] Asst. Prof. of Hydr. Engrg., Purdue Univ., Lafayette, Ind.

[17] "Membrane Stresses in Hyperboloid Shells of Revolution," by P. Cicala, Proceedings, ASCE, Vol. 86, No. 5, 1960.

[18] "Forces on Enclosed Structures," by T. W. Singell, Proceedings, ASCE, Vol. 84, No. 4, 1958.

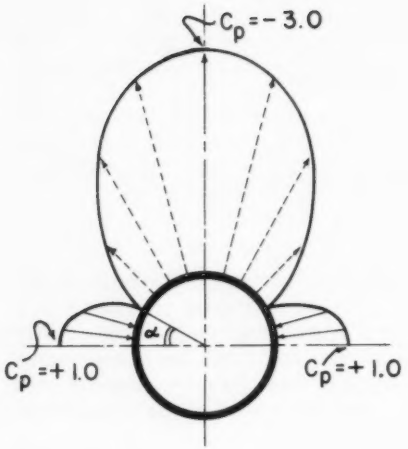

FIG. 8.—PRESSURE DISTRIBUTION AROUND INFINITE CYLINDER IN POTENTIAL FLOW ($C_p = 1 - 4\sin^2\alpha$)

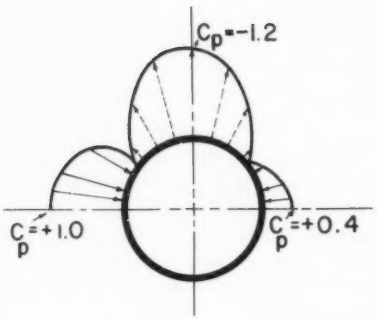

FIG. 9.—PRESSURE DISTRIBUTION OVER SPHERE (REFERENCE 17, FIGURE 2-24)

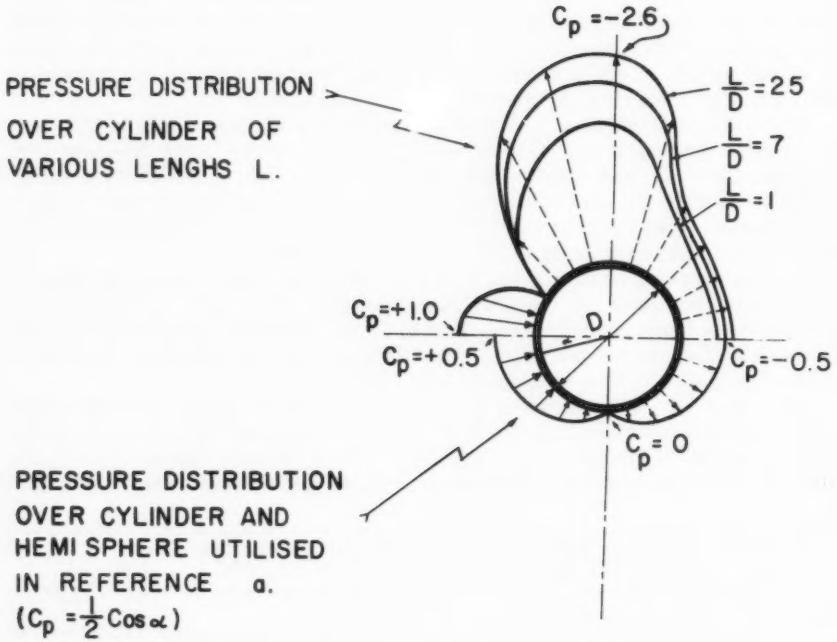

FIG. 10

a false sense of security. Perhaps the latest example that may be cited is the radar "Texas Tower" that was lost January 15, 1961 during a storm off the Atlantic coast near New York. Structures of novel configuration, of relative low mass and of larger dimension than previously contemplated should not be designed without some consideration of the turbulence characteristics of the wind or of the wake flow created by the structure.

Certainly this question constitutes a field of interest in itself. Despite considerable research efforts in many quarters[19,20] the picture is not entirely clear for even the well studied case of a circular cylinder. This is not too surprising. A mathematically reasonable description of turbulence must be a statistical one, so that securing experimental data, descriptive of a turbulent

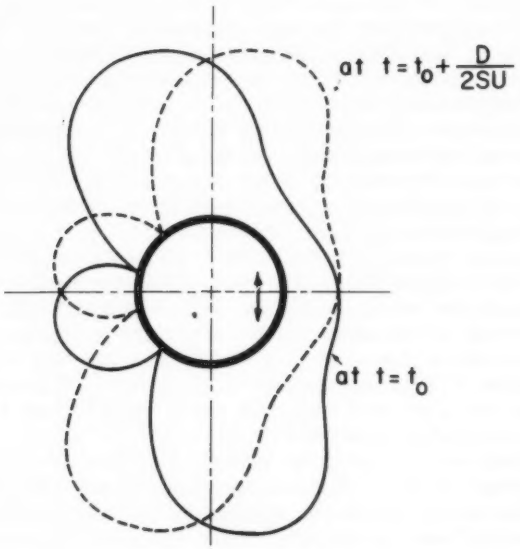

FIG. 11.—EXPECTED DYNAMIC PRESSURE DISTRIBUTION OVER CYLINDER IN TURBULENCE FREE WIND FOR $10^2 < R < 10^5$

flow around obstacles, requires very elaborate electronic equipment. Consequently, there exists a lack of basic data on "structured turbulence." Nevertheless, it may be useful to pursue the question when the adoption of a correctly distributed static (mean) windload might be unjustified. For the purpose of discussion four situations are distinguished below. In actuality these may not be found separately. For the structures considered, it is assumed that

19 "The Hydroelastic Behaviour of Flat Plates as Influenced by Trailing Edge Geometry," by A. T. Ippen, G. H. Toebes, and P. S. Eagleson, Hydrodynamics Lab., M.I.T., Technical Report No. 36, 1960.

20 "Fluctuating Lift and Drag Acting on a Cylinder in a Flow at Supercritical Reynolds Numbers," by Y. C. Fung, Journal of the Aerospace Sciences, Vol. 27, No. 11, 1960.

windloading is a primary consideration as it may be for thin shells, shells of light material, compositions of large panels, tall steel structures, and so on.

Structures Placed in a Turbulent Shear Flow.—At distances of more than 100 ft to 300 ft from the earth's surface the wind will resemble a homogeneously turbulent flow. Below this height at which turbulent mixing is influenced by the ground the flow will be a turbulent shear flow. The mixing process ("gustiness") will be intermittant ("squalliness"), but still entirely random. Both the scale relative to the structure and the intensity of the turbulence are to be known for a rational selection of design loads. Unfortunately, too little has been published of the work done in the field of micro-meteorology to permit such selection. Insight into the problem may be gained from a paper[21] by Robert H. Sherlock, F. ASCE. Analytical techniques to treat random loading are available. To mention a typical example: the case of structural panels located in a flow with random disturbances has been treated by J. C. Houbolt.[22]

In view of the random character of the loading it is probably adequate to adopt an equivalent static load. It should be realized, however, that the static loading suggested by building codes may need to be modified to account for local differences (geographically) in turbulence intensity or for the ratio of the scale of turbulence to that of the proposed structure. The recommendation[21] by R. H. Sherlock, F. ASCE, is a step in the correct direction. It is not felt that the adoption of a judiciously chosen static design loading would be inherently unsatisfactory.

Structures Placed in a Wake Flow.—Not all turbulence is entirely random in character. The wake behind blunt obstacles, whether this is a skyscraper or a ridge in the form of a long factory building will contain a certain amount of periodicity as well as turbulence of a larger scale than present in "natural" wind. Structures placed in such wake flows are said to be buffeted. The potential danger is of course that a predominant frequency component in the pressure spectrum of a wake flow would coincide with a natural frequency of the structure being buffeted.

Information concerning the pressure spectra of wake flows in addition to a knowledge of the natural frequencies of the proposed structure may be necessary for the design of stacks, shells, towers, and so on, located close to other structures. Analytically the problem would not be too involved[23] once sufficient information is available concerning the wake flow in question.

Fortunately it has been found[24] that going down stream the periodic component in wake flows degenerates into random turbulence quite rapidly. Except in cases of closely placed objects, such as a row of smoke stacks, it is felt that the danger of resonant buffeting will remain small. Further research data are needed, however, to substantiate the statement.

Structures Creating Marked Wake Flows.—Of greater consequence may be the periodic lift force, F_L, exerted on structures due to their own wake

---

21 "Wind Forces on Structures on Structures: Nature of the Wind," by R. H. Sherlock, Proceedings, ASCE, Vol. 84, No. 4, 1958.

22 "On the Response of Panels Subject to a Flow Field Containing Random Disturbances," by J. C. Houbolt, Shock and Vibration Bulletin Part II, Office of the U. S. Secy. of Defense, 1958.

23 "Design Criteria for Space Vehicles to Resist Wind Induced Vibrations," by A. A. Ezra and S. Birnbaum, Amer. Rocket Soc., Paper 1081, 1960.

24 "On the Development of Turbulent Wakes from Vortex Streets," by A. Roshko, NACA, Report 1191, 1954.

flows. The usual explanation for serious wind induced vibration is that von Karman vortices are shed periodically at a frequency given by the Strouhal number:

$$S = \frac{\omega_S D}{U} \quad \ldots\ldots\ldots\ldots\ldots\ldots \quad (66)$$

in which S is the Strouhal number, presumably constant for a given object; ω_S refers to the Strouhal frequency of vortex shedding, in radians per second; D denotes the characteristic transverse dimension of the structure, in feet; and U is the free stream velocity, in feet per second. When the frequency ω_S coincides with a natural frequency, ω_n, of the structure, resonance would ensue. Neither the magnitude of S nor the magnitude of the lift force, F_L, is considered predictable.

From a fluid mechanics point of view a few remarks can be made that may bring the problem into better focus. Th. von Karman's, Hon. M. ASCE,[25] analysis of the stability of a two-dimensional vortex array neither dealt with the mechanism of vortex shedding nor furnishes an adequate description of wakes for Reynolds numbers larger than (in the case of circular cylinders) $\mathbf{R} = U\ D/\nu = 300$ in which ν is the kinematic viscosity of the fluid. It is a matter of record, however, that the mechanism of vortex shedding persists up to the velocities at which the boundary layer becomes turbulent prior to separation (at the "critical reynolds number"). Therefore, even though the resulting wake periodicity becomes increasingly suppressed by general turbulence, von Karman's relationships are felt to describe the gross structure of the wake for subcritical **R**'s. If one adopts the relations as a convenient and idealized description of the wake structure it is readily shown[4] that:

$$S\ C_D = \text{constant} \quad \ldots\ldots\ldots\ldots\ldots\ldots \quad (67)$$

in which

$$C_D = \frac{2\,F_D}{\rho\,D\,U^2} = \text{drag coefficient} \quad \ldots\ldots\ldots\ldots \quad (68)$$

Experimental data for a circular cylinder verify reasonably the relation given in Eq. 67 with a value for the constant of 0.16 to 0.22. For non-circular cylinders[26] the constant appears to vary from 0.15 to 0.30. Eq. 67 may serve as a simple guide in considering geometric modification of a two-dimensional blunt cylindrical structure in order to avoid periodic lift forces of an undesirable frequency. Many drag data are either available or obtainable at small expense.

If an estimated Strouhal frequency, ω_S, appears nearly equal to a natural frequency, ω_n, of a design, there need not necessarily be reason for concern. As mentioned previously, with increasing Reynolds number the wake periodicity is increasingly suppressed by general turbulence leading to an increasingly random dynamic loading. The increase of general turbulence in the wake should associate with a break-up of the two-dimensional wake structure that exists at low flow velocities. The scale of the turbulence relative to the structure thus decreases with increasing **R**. What remains of the discreet vortex filaments along the trailing edge will be generated in a mutually random phase

25 "Uber den Mechanismus des Flusigkeitsund Luftwiderstandes," by Th. von Karman and H. Rubach, Phys. Zeit. No. 13, 1912, pp. 49-59.

26 "Low Speed Drag of Cylinders of Various Shape," by N. K. Delany and N. E. Sorensen, NACA Technical Note 3038, 1953.

relationship. Consequently, the net lift force will decrease with increasing wind velocity.

It thus appears that in judging the effect of a dynamic wind loading associated with the wake flow behind a structure, both the geometry of the structure and the scale of the wake turbulence constitute independent variables that must be considered. Unfortunately, little is known about the wake flow structure as a function of the Reynolds number to assess adequately the role of these variables.

Perhaps such detailed knowledge is not necessary. The random phase relation of lift forces along the trailing edge does not preclude the intermittant occurance of large lift forces. But their duration usually is too short to cause serious vibrations.

The design of structures creating marked wakes on the basis of an equivalent static wind load would appear acceptable as long as a non-periodic, turbulent wake may be anticipated. This must be qualified, however. A mechanical linear system may well be excited to vibration at its natural frequency by a random force. Only a small part of this force does effective work. But, if the force is large, this may yet lead to large stresses. Because lift forces increase with U^2, winds of cyclonic strength may conceivably impart sufficient kinetic energy to a structure to destroy it. This possibility depends on the elastic and internal damping characteristics of a structure.

Aeroelastic Vibrations of Structures Creating Marked Wake Flows.—In the discussion so far the tacit assumption was made that the elastic response does not influence the flow field. However, it is only by considering this response that a consistent description can be obtained for the many cases of really serious wind- or water-induced vibrations.

Detailed measurements and analyses of the resonant response of flat plates in a water tunnel[18] permitted the conclusion that, dependent on the geometry between the separating boundary layers, the effect of large amplitude motion (that necessarily occur at natural frequencies of the structure) is to restore a degree of two-dimensionality in the wake. The elastic response thus provides the aero-or hydroelastic effect of phasing the broken up vortex filaments. The net lift force increases, giving rise to larger amplitudes of vibration and again an increase in lift, F_L. The higher the wind velocity, U, the more dangerous this self-excitation becomes because $F \propto U^2$. The structural motion will govern the frequency of vortex formation over a limited to a wide range of free stream velocities mainly depending on the structural geometry near the trailing edge.[18]

These observations are made having in mind subcritical **R**'s and essentially two-dimensional structures such as the author's cylinder. For three-dimensional structures, such as the hemi-spherical dome proper treated by the authors, a dependency of the wake structure on the structural response must be assumed to exist. Factual knowledge about the wake dynamics of three-dimensional bodies is limited. It is known, however, that the base pressures just behind the trailing edge are higher than for two-dimensional configurations. From A. Roshko's interference tests[23] it may be deduced that low base pressures are essential to the formation of strong vortices. Hence, it is tentatively concluded that for three-dimensional structures the chances on aero- or hydroelastic vibrations is less than for two-dimensional geometries. For the supercritical Reynolds number region (that is different from one geometry to the other and for a circular cylinder is given by $\mathbf{R} > 5 \times 10^5$)

larger structural motions are likely to effect the turbulence, too. It probably arrests the trend to a smaller and smaller scale for the wake turbulence. If this happens, a further increase in wind velocity will bring increased excitation because $F_L \propto U^2$ and despite the fact that F_L remains a random force. The situation thus has the prerequisites for destructive self-excitation.

It is seen that the adoption of an equivalent static wind loading may be inconsistent with known facts. It makes a difference that structural materials are used. Larger deflections and lower internal damping make steel structures more prone to serious vibration than concrete structures. The natural frequencies of a structure can be as important a consideration as the computed static stress distribution. The permissible magnitude of deflections under loading may depend on considerations dealing with turbulent flow.

It is realized that the preceding remarks were not directed towards the analytical core of the authors' paper. Rather, the claim as to the immediate practical value of the analysis has been discussed.

Conclusions.

1. Analyses directed towards the determination of wind stresses in a structure should at least be based on experimentally obtained distributions of the mean aerodynamic pressure force. Fluid mechanics can not furnish entirely rational descriptions of the pressure distribution over two- or three-dimensional blunt objects.

2. Analyses directed towards the determination of wind stresses in a structure should attempt to incorporate as general a loading as is practical. Even for one and the same structural geometry the loading pattern may vary depending on surface irregularities or proximity of other structures.

3. The engineer should always realize that the translation of turbulent wind pressures to a static design load may constitute a dangerous simplification. That the real problem is a dynamic one may be of little consequence in some cases, but can be determinative in others.

4. Questions that require attention in the case of important or novel structures for which wind loading is an important consideration, include the following:

a. The turbulence characteristics of the oncoming air stream;

b. The amount and the frequency of discreet periodicity, as function of wind velocity, generated in the wake of the structure;

c. The ratio, as function of wind velocity, of the scale of the structure to the scale of the turbulence;

d. The structural natural frequencies, the internal damping and the magnitude of the elastic response during structural motions at natural frequency;

e. The influence of structural deflections on the wake structure.

These questions belong to the more difficult ones in the field of structural and fluid mechanics. Future structural designs will no doubt require answers.

BEARING CAPACITY OF FLOATING ICE SHEETS[a]

Discussion by L. W. Gold, R. H. Wood, N. C. Lind, D. T. Wright

L. W. GOLD.[5]—In 1957 a project that arose from the discussions that took place at the symposium sponsored by the National Research Council of Canada on the bearing capacity of ice was a survey among the pulp and paper companies of Canada on their field experience with the use of ice covers for storing logs. It is common practice in this industry to build up the thickness of the ice cover of selected lakes and rivers, and when this thickness is adequate, to transport the cut timber onto the cover by various types of trucks and sleighs. Many thousands of cords of wood are placed onto the ice in this way. Individual loads can be as large as 70 tons to 90 tons. Such extensive use of ice covers is certainly a rich source of field experience.

When Meyerhof prepared his paper, the records were available of ice failures obtained from the survey during the first winter. Some of these observations are shown in Fig. 8 along with observations on maximum and normal loads. Since that time, further information has been obtained, part of which has been published.[6] The additional observations on ice failures fall into the same region as those given by the author.

It was recognized early that many of the failures occurred for ice thicknesses that would normally have been considered adequate. Greater attention was then paid to the possible cause of the ice failure for each breakthrough. To date most of the breakthroughs that could not be attributed to thin ice were considered due to either (1) excessive vehicle speed, (2) repetitive use of the same road on the cover, or (3) the presence in the cover of a water layer between two ice layers.

With respect to the first point, it is the experience of men responsible for traffic on ice landings that an empty truck travelling at a speed between 15 mph and 20 mph will often cause more audible cracking of the cover than a fully loaded truck travelling at speeds not exceeding 5 mph. With respect to the second point, it is the practice of some companies to change the location of a regularly used road approximately every 2 hr. It is considered that this action has been beneficial in reducing the "fatigue" effect of the traffic.

Relative to the number of loaded vehicles that pulp and paper companies place onto ice covers, a breakthrough is not a common occurrence. During the winter of 1960-61, a daily record was kept at four large ice landings of the number and size of the loads placed onto the ice, along with the ice thick-

[a] October 1960, by G. G. Meyerhof (Proc. Paper 2627).

[5] Head, Snow and Ice Sect., Div. of Building Research, Natl. Research Council, Ottawa, Canada.

[6] "Field Study on the Load Bearing Capacity of Ice Covers," by L. W. Gold, Woodlands Review, Pulp and Paper Magazine of Canada, Vol. 61, No. 5, 1960, pp. 11-153.

ness. Only a part of these records are available as of March 1961. Those that were received showed that the average loads would lie between the lines $f_b = 50$ and $f_b = 100$ in Fig. 8. The maximum loads would extend into the region between $f_b = 100$ and $f_b = 200$. The weights of the loads, including the truck, were between 10 tons and 75 tons and the traffic density at times exceeded 150 trucks in 24 hr. No ice failure has been reported as yet in this survey of the traffic on these landings.

In the analysis of the observations obtained from the survey on ice failures, no attention has been paid to the influence of geometry of loading on the bearing capacity. It was considered that it would be unrealistic to take into account the load geometry in view of the lack of knowledge on the ice properties and the errors associated with estimating the load and measuring the ice thickness. The rectangular space defined by the wheels of a truck has an area of between 100 sq ft and 200 sq ft. This area is equivalent to a circle with radius "a" equal to about 7.5 ft. If the ice has a thickness between 25 in. and 30 in., the ratio of this radius to the characteristic length L would be about 0.15. For the majority of vehicles and ice thicknesses normally encountered, the equivalent a/L computed in this way would lie in the range $0.12 < a/L < 0.20$.

The author does state that the usual wheel spacing for a unit has no influence on the collapse load in practice. It would be appreciated if the author would enlarge on this opinion and in particular comment on whether it is sufficient under normal conditions to estimate the collapse load from an equivalent value for a/L obtained by letting "a" equal the radius of a circle enclosing the same area as defined by the wheels of the vehicle.

Some time ago, the writer made observations on the loads required to cause radial and circumferential cracking in thin ice sheets formed in a tank 72 in. in diameter.

The loads were applied at the center of the sheet over an area 0.5 in. in radius. The edges of the plates were frozen to the side of the tank. A hole was drilled in the sheet near the edge so that the water under the ice was not confined. The loads were applied fairly rapidly. For most of the tests the cracks formed within five minutes after loading was begun. The weight of water that came up through the drilled hole and onto the top of the plate was always less than about 2% of the applied load.

In Table 1 are given the thickness of the plates, their characteristic length L, the load required to form the radial and circumferential cracks and the radius of the circumferential crack. It was assumed that the ice was in the elastic state for each test. Eqs. 1 and 38 were used to compute the tensile stress, S_r, for the radial and the tensile stress f_b for the circumferential crack situation respectively. The ratios of the radius of the contact area of the load to the characteristic length of ice were in the range $0.013 < a/L < 0.033$, and the ratios of the radius of the tank to the characteristic length were in the range $0.95 < R/L < 2.4$.

It is realized that the values obtained for S_r and f_b are approximate only, and likely on the high side due to the finite size of the plate. The characteristic length L was computed from the expression $L = 40h^{3/4}$ obtained from field and laboratory observations (4).

In the preceding tests, the plate failed by punching, the radius of the punched hole being less than half the radius of the circumferential crack. In test number 6, the load was held at 17 lb for 15 min and then increased until

the circumferential cracks formed at 36 lb. For tests 7, 8, and 9 the load required to produce radial cracking was maintained until failure. For test number 7 this was 100 min, test number 8, 40 min and for test number 9 neither the circumferential cracking nor punching had occurred when the load was removed 120 min after it had been applied.

TABLE 1

Test	Thickness, in inches	L, in inches	Radial Crack		Circumferential Crack		
			P_r, in pounds	S_r, in pounds per square inch	P_b, in pounds	f_b, in pounds per square inch	radius, in inches
(1)	(2)	(3)	(4)	(5)	(6)	(7)	(8)
1	0.56	25.7	37.5	242	95.5	293	10
2	0.27	14.8	7.7	181	14.3	194	11
3	0.53	24.6	28.3	199	58.5	199	13
4	0.28	15.1	9.5	203	20.5	250	7
5	0.52	24.5	28.3	207			
6	0.42	20.9	17	181	36	194	6
7	0.63	28.2	30.9	159			
8	0.56	25.7	36	232			
9	0.91	37.2	59	161			
Average				196		226	

TABLE 2

Thickness in inches	L in inches	θ	P in pounds	f_b in pounds per square inch	Distance from load to crack	
					Along edge, in inches	Along bisector of wedge angle, in inches
(1)	(2)	(3)	(4)	(5)	(6)	(7)
0.42	20.9	$\pi/2$	10.4	233	9	
0.42	20.9	$\pi/2$	10.4	233	6 1/2	
0.42	20.9	π	27.0	291	10	7
0.73	31.6	$\pi/2$	25	180	13 1/2	
0.73	31.6	$\pi/2$	24	173	15 1/2	
0.73	31.6	π	59	212	[8 21]	[4 1/2 13]
Average				220		

For two tests, the plate was cut in half and one of the halves into quarters. The load was applied at the edge in the center of the half plate and at the tip of the 90° sector plates. The results are given in Table 2. Eq. 38 was used to compute f_b. For the last test in Table 2, the first radial crack occurred when the load was 49 lb. Using Eq. 14 gives for S_r a value of 250 psi.

The crack pattern for the edge loaded plate had the shape described by Meyerhof. The ratio of the distance along the edge from the load to the crack

to the same distance along the bisector was between 1.4 and 1.8. This compares quite well to the same ratio for the contours of constant deflection given in reference 4.

From the tables it is seen that the values obtained for S_r are about the same as those obtained for f_b. All the values are within the range previously reported for the tensile strength of ice (11). The experimental evidence supports the validity of the expressions developed by the author for estimating the collapse load of floating ice sheets under short time loading conditions.

The writer was on a lake on the first day that loads of wood were being placed onto the ice. Cracking could be heard near the truck as the trucks travelled over the ice at less than 5 mph. This cracking was probably radial only, no evidence of circumferential cracking was observed. The total load was about 40 tons and the ice thickness about 25 in. For the condition that no cracking occurs and assuming L to be 450 in. and a/L = 0.20, the value computed for S_r using Eq. 1 is about 365 psi and for f_b using Eq. 38 is about 120 psi. If the cracking that did occur was radial, the ultimate strength of the ice in the cover would, therefore, be between these two values and this is in agreement with the laboratory observations.

R. H. WOOD,[8] A.M.I.C.E.—The author's proposals to investigate the load-carrying capacity of large ice sheets by means of rigid-plastic theories of plate action is interesting and no doubt intended to be a first approximation. In point of fact the actual collapse loads are likely to be somewhere in between the predictions of breaking loads according to plastic and elastic theories respectively, and perhaps an interaction diagram could be plotted, after the style used by W. Merchant, M. ASCE,[9] and the writer[10] for predicting the collapse loads of building frames, if only more test results were available.

As discussed elsewhere by the writer[11] one of the main problems with plastic design of slabs is to discover a satisfactory yield criterion on which to base the mathematical treatises. It is perhaps surprising that Mr. Meyerhof has adopted the Tresca criterion for use with ice without further comment, not so much because there is any reliable evidence for or against the Tresca criterion in the case of ice, but if one intends to use approximate plastic theory, the Johansen criterion is much simpler, and a much more extensive list of known solutions is available.[12] In addition, the work of E. H. Mansfield[13] is appropriate to the use of the Johansen criterion, in predicting the worst patterns of collapse by variational methods, while the writer[11] has also found lower-bound solutions for collapse modes similar to that shown in Fig. 5. In this case the Johansen "square" criterion $(\pm M_o)$ results in a

---

[8] Principal Scientific Officer, Bldg. Research Sta., Dept. of Scientific and Industrial Research, Garston, Watford, Hertfordshire, England.

[9] "Frame Instability in the Plastic Range," by W. Merchant, Symposium on Plastic Theory of Structures; Cambridge, British Welding Journal, Vol. 3, 1956, p. 366.

[10] "The Stability of Tall Buildings," by R. H. Wood, Proceedings, I.C.E., London, Vol. 11, September, 1958, pp. 69-102; also Vol. 12, April, 1959, pp. 502-522.

[11] "Plastic and Elastic Design of Slabs and Plates," by R. H. Wood, Thames and Hudson, London. (In the press.)

[12] "Brudlinieteorier," by K. W. Johansen, Teknish Forlag, Kopenhagen, 1952.

[13] "Studies in Collapse Analysis of Rigid-Plastic Plates with a Square Yield Diagram," by E. H. Mansfield, Proceedings, Royal Soc., A., Vol. 241, 1957, pp. 311-338.

collapse load of $\left(2 + \pi\right) M_o$ in comparison with the author's $\left(2 + \frac{\pi}{2}\right) M_o$ based on Tresca's criterion. In the extreme case, there is the well known difference that a clamped plate should collapse under a point load when $P = 2\pi M_o$ by Tresca's criterion, but when $P = 4\pi M_o$ by Johansen's criterion. Such differences are, however, unusual.

It would appear doubtful whether the yield moment could be based on $f_o h^2/4$, that assumes equal yield strength and equal ductility in tension and compression. A. J. Ockleston[14] and the writer[11] have found considerable evidence of the strengthening effect of membrane compression, when the collapse mode is contained within a surrounding slab to prevent expansion in plan. For reinforced concrete slabs this can raise the collapse load to several times the Johansen load, by turning a no-tension-in-concrete theory into a kind of self-prestressed slab in which cracking is inhibited. There is then an instability ("pop-through") type of failure, but the highest moment that can be generated by membrane compression is of the order of $f_o h^2/12$. This suggests that one should be careful before adopting a criterion of maximum-plasticity-in-tension theory $\left(f_o h^2/4\right)$ in order to interpret the test results.

Both membrane action and elastic foundations have one thing in common—they invalidate to some extent the upper and lower bound theorems of Limit Analysis in that the load is now not constant but a function of the displacements. That being the case the author's inclusion of the upward water pressure is interesting but unnecessary. It was a foregone conclusion with rigid-plastic theories that the same starting collapse load would be given as for the standard proofs using the Tresca criterion, because at the start the deflection must be zero by plastic theories. As regards the evidence from elastic theory the writer would appreciate a helpful definition of the "characteristic" length L.

This interesting treatise by the author, taken together with information that is accumulating from other sources, seems to point to the conclusion that there is considerable scope in the future for plastic theories of failure that do not depend on a well defined yield point.

N. C. LIND,[15] and D. T. WRIGHT.[16]—It would be worthwhile to consider the deflections of floating ice sheets acting elastically and inelastically under the states of loading considered in the paper. It is important that the resisting moments in the ice sheet be developed at reasonably small deflections, and in any case before the state of loading is noticeably modified through submergence of the ice sheet. Although this requirement is most important for corner and edge loads, it should not be neglected for central loads of long duration, in which cracking of the ice from other causes is likely to occur. The following example serves to establish some approximate limits for the cases in which the deflections should be taken into account.

Consider a strip load of width $2a = 0.4L$ on the edge of a semi-infinite ice sheet. Assuming elastic action, Eqs. 18 and 19 give the maximum deflection

---

14 "Load Tests on a Three Story Reinforced Concrete Building in Johannesburg," by A. J. Ockleston, The Structural Engineer, Vol. 23, No. 10, October, 1955; also Vol. 24, No. 10, October, 1956.

15 Assoc. Prof. of Civ. Engrg., Univ. of Waterloo, Waterloo, Ontario, Canada.

16 Prof. of Civ. Engrg., Univ. of Waterloo, Waterloo, Ontario, Canada.

$w_o = -3.96\, M_r/kL^2$. Substituting $M_r = -f_b h^2/6$ and $L^2 = \sqrt{E'h^3}/\sqrt{12k}$ yields $w_o = 2.28\, f_b\sqrt{h}/\sqrt{E'k}$. With $k = 62.4$ pcf and $E' \approx 10^6$ psi

$$w_o \approx 0.012\, f_b \sqrt{h} \text{ in. } 5/2 \text{ lb}^{-1} \quad \ldots\ldots\ldots\ldots \quad (95)$$

The amount of deflection that would cause a noticeable degree of submergence in the active zone of the ice sheet is estimated at one fifth to one half of the thickness h of the ice sheet. Using $w_o < h/3$ as a criterion for negligible deflections, Eq. 1 yields $h > 10$ in. for relatively weak ice $(f_b = 100$ psi$)$ to $h > 21$ ft for strong ice $(f_b = 500$ psi$)$. Consequently, neglecting the influence of deflections in the elastic analysis for short-time loadings must be viewed with caution, especially for ice of high strength.

For long-duration loads, using a typical value of $f_b = 30$ psi, the preceding criterion indicates that the elastic deflections may be neglected in practice $(h > 1$ in.$)$. However, the inelastic deformations would presumably be many times the deflections indicated by Eq. 1. In the absence of data regarding these inelastic deformations, a reasonable first estimate would be approximately three times the elastic deformations. Then, with $f_b = (3)(30) \approx 100$ psi, Eq. 1 yields $h > 10$ in. This result indicates that deformations associated with the inelastic behaviour of ice are worthy of further study.

An unresolved matter of importance is the strength of natural ice. Analyses of behavior will induce little confidence without reliable knowledge of the basic strength of the material. As the author indicated, strength varies over wide ranges but not always consistently. The influence of factors such as structure, density, and solarity could be determined quite readily through load tests on small samples in the field.[17] Unfortunately, there is a marked scale effect in the strength of ice, and small sample tests cannot now be readily related to the strength of natural ice sheets. A theory for scale effect on ice strength thus appears to be sorely needed. V. V. Lavrov[18] has proposed such a theory, with hypotheses that are not entirely convincing.

Rational determination of the load capacity of floating ice sheets is thus seen to depend on procedures for determining strength in the field, a theory for scale influence, and analyses as developed by G. G. Meyerhof, F. ASCE.

---

17 "Recommended Standards for Small-Scale Ice Tests," by T. R. Butkovich, Transactions, Engrg. Inst. of Canada, Vol. 2, No. 3, p. 112, 1958.

18 "The Nature of The Scale Effect in Ice and The Strength of The Ice Sheet," by V. V. Lavrov, Soviet Physics - Doklady, Amer. Inst. of Physics Vol. 3, No. 5, p. 934, 1958.

ELASTO-PLASTIC ANALYSIS BY NUMERICAL PROCEDURES[a]

Discussion by Daniel Frederick

DANIEL FREDERICK,[6] A.M. ASCE.—The writer wishes to point out that the method used by the author for the elasto-plastic analysis of structures is practical and time-saving when compared with several other methods that might have been used. Dean T. Mook[7] considered the elasto-plastic analysis of bents by the complementary energy method taking a rectangular cross section and a material having a bilinear stress strain diagram with equal values in tension and compression and all other conditions the same as those used by the author. The complementary energy per unit length along the beam for the elasto-plastic cross section.

$$\frac{E_1 e_y I}{2 h^2}\left[\left(\frac{3}{\alpha} - \frac{2}{\alpha^2}\right)(1 - \mu) + \alpha \mu\right]$$

was integrated along the bent from one elastic zone to another. This with the usual expression for complementary energy in the elastic portions gave the total complementary energy. The usual methods based on complementary energy were then used to derive a set of non-linear algebraic equations involving the maximum value of α for each plastic zone. Although the method is exact, the solution of these equations is tedious and not readily amenable to high speed computers because programs for these complicated non-linear equations are not fully developed. Other methods, such as using transformed sections lead to the same difficulties. Based on this experience, it appears that the approximate method used by the author is one of the best for the analysis of bents also.

---

[a] December 1960, by Annabel L. Tong (Proc. Paper 2690).

[6] Prof. of Engrg. Mech. Virginia Polytechnic Inst., Blacksburg, Va.

[7] "Analysis of a Bent Constructed from a Strain-Hardening Material," by Dean T. Mook. Thesis submitted in partial fulfillment of the requirements for the degree of Master of Science at the Virginia Polytechnic Inst. at Blacksburg, Va., in 1960.

PROCEEDINGS PAPERS

The technical papers published in the past year are identified by number below. Technical-division sponsorship is indicated by an abbreviation at the end of each paper number, the symbols referring to: Air Transport (AT), City Planning (CP), Construction (CO), Engineering Mechanics (EM), Highway (HW), Hydraulics (HY), Irrigation and Drainage (IR), Pipeline (PL), Power (PO), Sanitary Engineering (SA), Soil Mechanics and Foundations (SM), Structural (ST), Surveying and Mapping (SU), and Waterways and Harbors (WW), divisions. Papers sponsored by the Department of Conditions of Practice are identified by the symbol (DP). For titles and order numbers, refer to the appropriate issue of "Civil Engineering." Beginning with Volume 26 (January 1956) papers were published in Sections of the various Technical Disciplines. To locate papers in the Journals, the symbols after the paper number are followed by a numeral designating the issue of a particular Journal in which the paper appeared. For example, Paper 2108 is identified as 2108(CO3) which indicates that the paper is published in the third issue of the Journal of the Structural Division, for 1961.

VOLUME 86 (1960)

APRIL: 2426(ST4), 2428(ST4), 2430(PO2), 2431(EM2), 2432(PO2), 2433(ST4), 2434(EM2), 2435(PO2), 2436(ST4), 2437(ST4), 2438(ST4), 2439(EM2), 2440(EM2), 2441(ST4), 2442(ST4), 2443(EM2), 2444(ST4), 2445(ST4), 2446(EM2), 2447(EM2), 2448(EM2), 2449(HY4), 2450(ST4), 2451(HY4), 2452(ST4), 2453(HY4), 2454(EM2), 2455(ST4), 2456(HY4), 2457(PO2), 2458(SA2), 2459(SM2).

MAY: 2460(AT1), 2461(ST5), 2462(AT1), 2463(AT1), 2464(CP1), 2465(CP1), 2466(CO1), 2467(AT1), 2468(SA3), 2469(HY5), 2470(ST5), 2471(SA3), 2472(SA3), 2473(ST5), 2474(SA3), 2475(ST5), 2476(SA3), 2477(ST5), 2478(HY5), 2479(ST5), 2480(ST5), 2481(SA3), 2482(CO2), 2483(CO2), 2484(HY5), 2485(HY5), 2486(AT2), 2487(CP1), 2488(CO2), 2489(HY5), 2490(CO2), 2491(ST5), 2492(CO2).

JUNE: 2493(EM3), 2494(EM3), 2495(ST6), 2496(EM3), 2497(EM3), 2498(EM3), 2499(EM3), 2500(EM3), 2501(EM3), 2502(EM3), 2503(EM3), 2504(EM3), 2505(EM3), 2506(HY6), 2507(ST6), 2508(EM3), 2509(EM3), 2510(EM3), 2511(EM3), 2512(ST6), 2513(HW2), 2514(CP2), 2515(PO3), 2516(EM3), 2517(WW2), 2518(WW2), 2519(EM3), 2520(PO3), 2521(EM3), 2522(EM3), 2523(ST6), 2524(EM3), 2525(HY6), 2526(CP2), 2527(HW2), 2528(ST6), 2529(HW2), 2530(HW2), 2531(HY6), 2532(EM3), 2533(EM3), 2534(EM3), 2535(EM3), 2536(EM3), 2537(EM3), 2538(EM3), 2539(EM3), 2540(EM3), 2541(EM3), 2542(EM3), 2543(EM3), 2544(EM3), 2545(EM3), 2546(EM3), 2547(EM3), 2548(EM3), 2549(EM3), 2550(EM3), 2551(EM3), 2552(EM3), 2553(EM3), 2554(EM3), 2555(EM3), 2556(EM3), 2557(EM3), 2558(EM3), 2559(EM3), 2560(EM3), 2561(EM3), 2562(EM3), 2563(EM3), 2564(EM3), 2565(EM3), 2566(EM3), 2567(EM3), 2568(EM3), 2569(EM3), 2570(EM3), 2571(EM3), 2572(EM3), 2573(EM3), 2574(EM3), 2575(EM3), 2576(EM3), 2577(HY6), 2578(EM3), 2579(EM3), 2580(EM3), 2581(ST6), 2582(EM3), 2583(ST6), 2584(EM3), 2585(EM3), 2586(EM3), 2587(EM3), 2588(EM3), 2589(EM3), 2590(WW2), 2591(EM3), 2592(HY6), 2593(HY6), 2594(HY6), 2595(HY6), 2596(HY6), 2597(WW2), 2598(HY6), 2599(WW2), 2600(WW2), 2601(WW2), 2602(WW2), 2603(WW2), 2604(WW2), 2605(SA5), 2606(WW2), 2607(SA5), 2608(ST6), 2609(SA5), 2610(HY6), 2611(WW2), 2612(ST6), 2613(HY6), 2614(WW2).

OCTOBER: 2615(EM4), 2616(EM4), 2617(PP1), 2618(EM4), 2619(EM4), 2620(EM4), 2621(ST10), 2622(ST6), 2623(EM4), 2624(EM4), 2625(EM4), 2626(EM4), 2627(EM4), 2628(EM4), 2629(ST10), 2630(ST10), 2631(PO4), 2632(EM4), 2633(ST10), 2634(ST10), 2635(ST10), 2636(ST10), 2637(ST10), 2638(EM4).

NOVEMBER: 2639(ST11), 2640(ST11), 2641(CO3), 2642(ST11), 2643(SA4), 2644(WW4), 2645(ST11), 2646(HY8), 2647(ST11), 2648(WW4), 2649(WW4), 2650(ST11), 2651(CO3), 2652(HY8), 2653(HY8), 2654(ST11), 2655(HY8), 2656(HY8), 2657(SA4), 2658(WW4), 2659(HY8), 2660(SA4), 2661(CO3), 2662(CO3), 2663(SA4), 2664(CO3), 2665(HY8), 2666(SA4), 2667(ST11).

DECEMBER: 2668(ST12), 2669(EM5), 2670(EM5), 2671(EM5), 2672(EM5), 2673(EM5), 2674(ST12), 2675(EM5), 2676(EM5), 2677(HW4), 2678(ST12), 2679(EM5), 2680(ST12), 2681(EM5), 2682(EM5), 2683(EM5), 2684(EM5), 2685(EM5), 2686(EM5), 2687(CO4), 2688(ST12), 2689(EM5), 2690(EM5), 2691(EM5), 2692(ST12), 2693(EM5), 2694(HW4), 2695(EM5), 2696(EM5), 2697(HW4).

VOLUME 87 (1961)

JANUARY: 2698(PP1), 2699(PP1), 2700(HY1), 2701(SA1), 2702(SU1), 2703(ST1), 2704(ST1), 2705(EM1), 2706(EM1), 2707(ST1), 2708(HW1), 2709(PO1), 2710(ST1), 2711(HY1), 2712(ST1), 2713(HY1), 2714(PO1), 2715(ST1), 2716(HY1), 2717(SA1), 2718(SA1), 2719(SU1), 2720(ST1), 2721(HY1), 2722(ST1), 2723(PP1), 2724(HY1), 2725(ST1).

FEBRUARY: 2726(PP2), 2727(EM2), 2728(EM2), 2729(EM2), 2730(WW1), 2731(EM2), 2732(EM2), 2733(PP1), 2734(EM2), 2735(EM2), 2736(EM2), 2737(PL1), 2738(PL1), 2739(PL1), 2740(EM2), 2741(ST2), 2742(EM2), 2743(ST2), 2744(WW1), 2745(WW1), 2746(EM2), 2747(WW1), 2748(EM2), 2749(WW1), 2750(EM2), 2751(EM2), 2752(ST2), 2753(PL1), 2754(ST2), 2755(PL1), 2756(ST2), 2757(PL1).

MARCH: 2758(HY2), 2759(HW1), 2760(AT1), 2761(CO1), 2762(ST3), 2763(EM3), 2764(HY2), 2765(HY2), 2766(HY2), 2767(HW1), 2768(CO1), 2769(EM3), 2770(HY2), 2771(HY2), 2772(HW1), 2773(AT1), 2774(AT1), 2775(EM3), 2776(HY2), 2777(HY2), 2778(HY2), 2779(HY2), 2780(HY2), 2781(HY2), 2782(HW1), 2783(SA2), 2784(CO1), 2785(EM3), 2786(HY2), 2787(AT1), 2788(ST3), 2789(EM3), 2790(HW1).

APRIL: 2791(EM4), 2792(EM4), 2793(EM4), 2794(EM4), 2795(EM4), 2796(EM4), 2797(EM4), 2798(EM4), 2799(EM4), 2800(EM4), 2801(EM4), 2802(EM4), 2803(EM4), 2804(EM4), 2805(EM4), 2806(EM4), 2807(EM4), 2808(EM4), 2809(EM4), 2810(EM4), 2811(EM4), 2812(EM4), 2813(EM4), 2814(EM4), 2815(EM4), 2816(EM4), 2817(EM4), 2818(EM4), 2819(EM4), 2820(EM4), 2821(EM4), 2822(EM4), 2823(EM4), 2824(EM4), 2825(EM4), 2826(EM4), 2827(EM4), 2828(EM4), 2829(EM4), 2830(EM4),